GL01313

DOE/ID/12079-16
ESL-44

GM3D: INTERACTIVE THREE-DIMENSIONAL GRAVITY AND MAGNETIC MODELING PROGRAM (GM3D.REV1 USER'S GUIDE)

J. Maurer

and

J. W. Atwood

October, 1980

Work performed under contract No. DOE/ID12079

DOE/ID/12079-16
ESL-44

GM3D: INTERACTIVE THREE-DIMENSIONAL GRAVITY AND MAGNETIC MODELING PROGRAM

(GM3D.REV1 USER'S GUIDE)

J. Maurer

and

J. W. Atwood

October, 1980

EARTH SCIENCE LABORATORY
UNIVERSITY OF UTAH RESEARCH INSTITUTE
420 Chipeta Way, Suite 120
Salt Lake City, UT 84108

Prepared for the
U. S. DEPARTMENT OF ENERGY
DIVISION OF GEOTHERMAL ENERGY
Under Contract No. DOE/ID12079

NOTICE

This report was prepared to document work sponsored by the United States Government. Neither the United States nor its agent, the United States Department of Energy, nor any Federal employees, nor any of their contractors, subcontractors or their employees, makes any warranty, express or implied, or assumes any legal liability or responsibility for the accuracy, completeness, or usefulness of any information, apparatus, product or process disclosed, or represents that its use would not infringe privately owned rights.

NOTICE

Reference to a company or product name does not imply approval or recommendation of the product by the University of Utah Research Institute or the U.S. Department of Energy to the exclusion of others that may be suitable.

TABLE OF CONTENTS

ABSTRACT

GM3D has been developed for computing the gravity or magnetic anomaly due to a three-dimensional body, and for plotting the resulting contour map. A complex body may be constructed from several right-rectilinear vertical-sided prisms. The program allows the input and editing of the prism data which are then used to calculate the anomaly map for plotting. Plotting is done on either a Tekronix 4014 graphics terminal, a Statos electrostatic plotter, or a CalComp pen plotter. A terminal plot is also available which can be printed on any terminal and on a line printer.

The program is written in FORTRAN IV code and operates on a PRIME 400 computer system. Adaptation of the program to other systems is relatively straightforward.

INTRODUCTION AND PURPOSE OF THE GM3D PROGRAM

This publication has been written to document, and as a user's guide to, GM3D. GM3D is an interactive program developed to compute and plot gravity or magnetic anomalies created by three-dimensional right-rectilinear prism models. The program can produce continuous contour anomaly maps on a Tektronix 4014 graphics terminal or a hard copy plot on a Statos electrostatic plotter. Discrete contour maps are also available on a line printer and on terminals without graphics capabilities.

The program was originally developed on the University of Utah's UNIVAC 1108 by D. T. Purvance. Jim Maurer converted the program to the University of Utah Research Institute's (UURI) Prime 400 computer. GM3D uses the methodology described by Goodacre (1973) to compute the vertical component of the gravity or magnetic fields.

PROGRAM DESCRIPTION

Introduction

The GM3D program uses a prism-modeling system to compute the anomalies, and then plots the computed anomaly map on the desired plot device. An option system allows the user to systematically input, edit, compute, and plot the computed models. The user can also save a model to a large merge file, or retrieve a desired model from the merge file, by using the proper option. The option system and file formats are described below.

The GM3D Option System

An option system permits easy use of the program and subroutines. At certain times in the program the user is asked for an option number which directs the program to the desired operation or function. The program assumes that the user is familiar with the option choices. If this is not the case, the user can produce an option list at the terminal for any specific option request simply by pressing the carriage return key. An invalid option number will also produce a listing of the available options.

The user performs the desired operation when appropriate by entering the correct option number when prompted by the program to do so. The options in the main program start execution of the major program operations. These options include input and editing of the model prisms, computation of the model, printing and/or plotting the model and computed map, and execution of the file maintenance routines. The various options may sometimes

lead to another option list; for example, the file maintenance routine (FMAIN option) allows the saving or reading of the merge file, the deletion of unwanted files, initialization of a new merge file, and production of a merge file directory listing. For a more complete description of the program options, see the User's Guide section.

Program File Structures

GM3D uses two files to store and manipulate data: a work file (GM3D-WORK), and a merge file (GM3D-MERGE). These files are direct-access files which can be read and written dynamically by the program. They are created and/or opened automatically when the program starts execution and are closed automatically when the program is exited through normal channels.

The work file contains one set of data at a time. The data consists of descriptive headers, model parameters, the computed models, and the prism parameters. There are two descriptive headers, one to describe the project and one to describe the particular model stored in the work file. The model parameters are the grid spacing, and, for the magnetic model, the Earth's total field intensity and angles of inclination and declination. Each work file can also store the most recent computed gravity and magnetic models as well as the prism parameters. If a model is to be kept, the user saves the work file by writing it to the merge file before changing the parameters for computing a new model. Once a change has been made to the work file, any computed model contained in the work file would have the wrong parameters associated with it.

The merge file is a collection of data sets which have been saved from the work file at various times. The data sets, or subfiles, are numbered in sequence as they are stored to facilitate access by the user. These numbers can be specified to restore a subfile from the merge file to the work file where it can be manipulated by the other portions of the program. A more detailed description of the work and merge files can be found in Appendix A.

Model Prism Format

The GM3D program uses a model consisting of up to 25 right-rectilinear prisms to compute the anomaly map. A prism is defined by the top corners (X1, X2, Y1, Y2), depth to the top (Z1), and depth to the bottom (Z2). These coordinates are given in relation to the origin (0,0) which is located at the center of the grid on the earth's surface. Each prism is also assigned a magnetic susceptibility contrast SC (for magnetic model) or a density contrast DC (for gravity model). The magnetic model also

associates three additional parameters with each prism in the model: the remanent magnetization angle of inclination, the remanent magnetization angle of declination, and the Koenigsberger ratio.

The units which are used in the model are feet (length), grams/cc (density), cgs x 10E-6 (magnetic suseptibility), degrees (angles), milligals (gravity), and gammas (magnetic intensity).

GM3D USER'S GUIDE

Introduction

Use of the GM3D program consists entirely of responding to questions and choices presented to the user by the program. The program tells the user what information it is seeking, and also the format of the data expected. There are three types of data that the program requests, and these are designated by the letters (I), (F), and (A) as printed by the request prompt. (I) tells the user that the data requested should be an integer, (F) that the data should be a floating point value, and (A) that the data should be alphanumeric.

Execution of the Program

Upon entering the GM3D program the user is asked to specify whether the model is to be a magnetic or gravity model. Switching model selection at any time can be done within the program simply by choosing the appropriate option within GM3D. The first set of options which the user encounters is the GM3D option list.

GM3D Options:

```
GM3D options are:
        1 - Stop
        2 - Input prisms
        3 - Edit
        4 - List prisms and model
        5 - Plan view of model
        6 - Compute model
        7 - Map output
        8 - Change model type
        9 - File maintenance
```

Option 1 causes termination of the program. The work and

merge files are automatically closed before the program returns control to the operating system.

Option 2 passes control to the data input routine where another option selection is made. (See Input Options)

Option 3 passes control to the data editing routine where there is also another option selection to be made.

Option 4 presents the user with a listing of the prism and model parameters at the terminal or line printer.

Option 5 produces a plan view of the prism model on the terminal for checking.

Option 6 computes the anomaly and stores it in the work file. This computation may take several minutes to complete if the model is large. Option 6 automatically passes control to Option 7.

Option 7 produces the contour maps. The user must specify if a discrete-valued contour map (terminal plot) is wanted. If the user wishes to continue, the program asks for the number of contour levels to plot. The user can then either specify the contour values or allow the program to calculate them. The user is also asked to specify a contour interval. If a negative interval is given, the program will compute one. The user is then asked for a map title.

The program then produces a prism and model list followed by the contour map. The user is then asked if a continuous contour map is wanted. If the answer is yes, the program asks if the contour values are whole numbers. Control is then passed to the section of the program which asks for a scaling option.

Option 8 allows the user to switch between the gravity and magnetic modeling routines.

Option 9 passes control to the file maintenance routines.

Input Options:

Input options are:
1 - Return to master level
2 - Initial input
3 - Add prisms

Option 1 returns control to the main program.

Option 2 prompts the user for the information necessary for describing the model.

Option 3 allows the user to add prisms to an existing model.

Edit Options:

Edit options are:

1 - Return to master program
2 - Edit project name
3 - Edit model description
4 - Change grid spacing
5 - Edit Earth"s field
6 - Change angle of inclination
7 - Change angle of declination
8 - Change prism parameters
9 - Delete and pack prisms

Option 1 returns control to the main program.

Options 2 through 7 allow the user to change the specified value.

Option 8 passes control to another option list for changing the prism parameters.

Option 9 allows the user to delete unwanted prisms from the model.

Prism Editing Options:

The prism parameters are:

1 - X1
2 - X2
3 - Y1
4 - Y2
5 - Z1
6 - Z2
7 - Remanent magnetization inclination
8 - Remanent magnetization declination
9 - Koenigsberger ratio
10 - Magnetic susceptibility
11 - Density contrast

Options 1 through 11 allow the user to change the indicated prism parameter.

Scaling Options:

```
SCALE   OPTION # (I)=
      1  1:12,000
      2  1:24,000
      3  1:62,500
      4  1:125,000
      5  1:250,000
```

Options 1 through 5 are the scaling options for the map. After giving the desired scale option the user is asked if a grid is wanted. If the answer is yes, the user is asked to supply a grid interval. This interval must be an integral divisor of the floating point number given in the inquiry. For example, if the number given by the program inquiry were 28000.0, the user could obtain a grid of 4 sectors (2 x 2) by entering a 14000.0, a grid of 16 sectors by entering a 7000.0, or a grid of 49 sectors by entering a 4000.0, etc.

The user also is given the option of having the prisms drawn on the map. The user is asked to give the user's name and the date, and control is passed to the plotting portion of the program which asks for the plot device option.

Plot Device Options:

```
Enter device number:
        1 - Tektronix 4014
        2 - Statos plotter
        3 - Calcomp plotter
```

Option 1 produces a plot on the Tektronix graphics terminal. This option should not be used with any other terminal.

Option 2 produces a plot on a file which is then used to plot on the Statos electrostatic plotter.

Option 3 produces a plot on a file which can then be used to create a plot on the Calcomp plotter.

File Maintenance Options:

```
FMAIN---OPTION # (I)=
      1  Return to master program
      2  List merge file directory
      3  Save work file on merge file
      4  Restore work file from merge file
```

5 Delete and pack merge file
6 Initialize merge file

Option 1 returns control to the main program.

Option 2 produces a directory of the merge file contents. This is sent to either the terminal or line printer.

Option 3 writes the contents of the work file to a new subfile within the merge file.

Option 4 reads a specified subfile from the merge file into the work file.

Option 5 allows the user to delete unwanted subfiles from the merge file by placing a "Y" directly beneath the subfile number as printed by the computer. For example if there were 16 subfiles in the merge file:

The computer would print: 123456789*123456
User response : Y Y Y YY

The above reponse would delete subfiles 2, 4, 10, 13, and 14.

Option 6 initializes the merge file. The merge file needs to be (and should be) initialized only once prior to saving the first work file. Any furthur initialization will result in the destruction of any previously saved data.

PROGRAM CONVERSION

GM3D was originally designed to run on a UNIVAC 1108 computer and has been converted and expanded by the Earth Science Laboratory to run on a PRIME 400 computer. Conversion of the program to another system should be fairly straightforward. The program requires approximately 32K four-byte words of storage; a byte consists of 8 bits. The program requires no special software capabilities with the exception of direct-access file handlers. Some bit manipulation functions are desirable for use in the continuous contour map routine.

GM3D utilizes an "industry standard" plotting library which must be supplied by the user.

REFERENCES

Baranov, V., 1957, A new method for the interpretation of aeromagnetic maps: pseudogravimetric anomalies: Geophysics 22, p. 359-383.

Botezatu, R., Visarion, M., Scurtu, F., and Cucu, G., 1971, Approximation of the gravitational attraction of geological bodies: Geophysical Prospecting 19, p. 218-227.

Goodacre, A. K., 1973, Some comments on the calculation of the gravitational and magnetic attraction of a homogeneous rectangular prism: Geophysical Prospecting 21, p. 66-69.

Kellogg. O. D., 1929, Foundations of potential theory: Berlin, Julius Springer, 384 p.

Nagy, D., 1966a, The gravitational attraction of a right rectilinear prism: Geophysics 31, p. 362-371.

Nagy, D., 1966b, Reply by author to discussions by J. Cl. de Bremaecker and Charles E. Corbato: Geophysics 31, p. 987.

APPENDIX A

GM3D File Formats

GM3D Work File Format

Record length is 17 words of 4 bytes each.

Record 1 -

NR = (Integer) Number of records (32 + NP). (1 word)

NAME1 = (Alphanumeric) (8 words)

NAME2 = (Alphanumeric) (8 words)

Record 2 -

NP = (Integer) Number of prisms. (1 word)

GMESH = (Real) (1 word)

RTHFLD = (Real) (1 word)

ANGINC = (Real) (1 word)

ANGDEC = (Real) (1 word)

MODEL = (Alphanumeric) (12 words)

Records 3 through 17 - (I = 1 through 15)

IMAG = (Integer) (1 word)

M = (Integer) (1 word)

F(I,J) = (Real) J = 1 through 15 (15 words)

Records 18 through 32 - (I = 1 through 15)

IGRAV = (Integer) (1 word)

M = (Integer) (1 word)

F(I,J) = (Real) J = 1 through 15 (15 words)

Records 34 through (32 + NP) - (I = 1 through NP)

XP(1,I) = (Real) (1 word)

XP(2,I) = (Real) (1 word)

YP(1,I) = (Real) (1 word)

YP(2,I) = (Real) (1 word)

ZP(1,I) = (Real) (1 word)

ZP(2,I) = (Real) (1 word)

REMINC = (Real) (1 word)

REMDEC = (Real) (1 word)

QF = (Real) (1 word)

SC = (Real) (1 word)

DC = (Real) (1 word)

GM3D Merge File Format

Record length is 17 words of 4 bytes each.

Record 1 -

LR = (Integer) Record length (= 17). (1 word)

NSF = (Integer) Number of subfiles. (1 word)

TITLE = (Alphanumeric) Merge file title. (15 words)

Record 2 -

NR(1) = (Integer) Number of records in subfile 1.

(1 word)

NAME1 = (Alphanumeric) (8 words)

NAME2 = (Alphanumeric) (8 words)

Record 3 through (NR(1) + 1) - Subfile records

Record (NR(1) + 2) -

NR(2) = (Integer) Number of records in subfile 2.

(1 word)

NAME1 = (Alphanumeric) (8 words)

NAME2 = (Alphanumeric) (8 words)

Record (NR(1) + 3) through (NR(1) + NR(2) + 1) - Subfile records.

ETC.

APPENDIX B

Sample Sessions

```
OK, GM3D
GO

          ***** GM3D MODELING PROGRAM *****

 Please enter the model type (I):
          1 - Magnetic model
          2 - Gravity model
1

 Enter GM3D option (I):


 GM3D options are:
          1 - Stop
          2 - Input prisms
          3 - Edit
          4 - List prisms and model
          5 - Plan view of model
          6 - Compute model
          7 - Map output
          8 - Change model type
          9 - File maintenance

 Enter GM3D option (I):
9
*FILE MAINTENENCE*


      FMAIN---OPTION # (I)=
            1  Return to master program
            2  List merge file directory
            3  Save work file on merge file
            4  Restore work file from merge file
            5  Delete and pack merge file
            6  Initialize merge file

      FMAIN---OPTION # (I)=   2
TEST MERGE FILE FOR GM3D.

There are  3 subfiles in the merge file.

Project: SAMPLE MERGE FILE                FOR THE USER'S GUIDE.
    Model: THIS IS THE FIRST MODEL.                              4 prisms.

Project: SAMPLE MERGE FILE                FOR THE USER'S GUIDE.
    Model: THIS IS THE SECOND MODEL.                             6 prisms.

Project: SAMPLE MERGE FILE                FOR THE USER'S GUIDE.
    Model: THIS IS THE THIRD MODEL.                              3 prisms.
```

```
     FMAIN---OPTION # (I)=    1

 Enter GM3D option (I):
2

 Enter input option (I):


 Input options are:
         1 - Return to master level
         2 - Initial input
         3 - Add prisms

 Enter input option (I):
2

 Enter the project name on two lines, max. 32 chars. each (A):
SAMPLE MERGE FILE
FOR THE USER'S GUIDE.

 Enter the model description, max. 48 chars. (A):
THIS IS THE FOURTH MODEL.

 Enter the number of prisms in the model (25 max.) (I):
3

 Enter the grid spacing in feet (F):
500.

 Enter the Earth"s field in gammas (F):
50000.

 Enter the angles of inclination and declination in degrees (F):
12.,35.

 Enter X1 and X2 for prism #  1 (F,F):
250.,1250.

 Enter Y1 and Y2 for prism #  1 (F,F):
-1250.,250.

 Enter Z1 and Z2 for prism #  1 (F,F):
300.,600.

 Enter the remanent inclination and declination for prism #  1 (F,F):
0.0,0.0
```

```
 Enter the Koenigsberger ratio and the magnetic susceptibility
 for prism #  1 (F,F):
0.0,-100.

 Enter X1 and X2 for prism #  2 (F,F):
-1500.,-750.

 Enter Y1 and Y2 for prism #  2 (F,F):
-750.,0.

 Enter Z1 and Z2 for prism #  2 (F,F):
300.,1300.

 Enter the remanent inclination and declination for prism #  2 (F,F):
0.0,2.0

 Enter the Koenigsberger ratio and the magnetic susceptibility
 for prism #  2 (F,F):
0.0,-1000.

 Enter X1 and X2 for prism #  3 (F,F):
-1250.,-250.

 Enter Y1 and Y2 for prism #  3 (F,F):
1000.,1500.

 Enter Z1 and Z2 for prism #  3 (F,F):
300.,600.

 Enter the remanent inclination and declination for prism #  3 (F,F):
0.0,0.0

 Enter the Koenigsberger ratio and the magnetic susceptibility
 for prism #  3 (F,F):
0.0,-1000.

 Data stored.

 Enter input option (I):
1

 Enter GM3D option (I):
5
```

```
PLAN VIEW OF PRISM MODEL   + Y ACROSS PAGE,   + X  UP PAGE

      1   2   3   4   5   6   7   8   9  10  11  12  13  14
15    .   .   .   .   .   .   .   .   .   .   .   .   .   .
14    .   .   .   .   .   .   .   .   .   .   .   .   .   .
13    .   .   .   .   .   .   .   .   .   .   .   .   .   .
12    .   .   .   .   .   .   .   .   .   .   .   .   .   .
11    .   .   .   .   .   .   .   .   .   .   .   .   .   .
                          1               1
10    .   .   .   .   .   .   .   .   .   .   .   .   .   .
9     .   .   .   .   .   .   .   .   .   .   .   .   .   .
                          1               1
8     .   .   .   .   .   .   .   .   .   .   .   .   .   .
                                          3   3
7     .   .   .   .   .   .   .   .   .   .   .   .   .   .
                              2       2
6     .   .   .   .   .   .   .   .   .   .   .   .   .   .
                                          3   3
5     .   .   .   .   .   .   .   2   .   2   .   .   .   .   .
4     .   .   .   .   .   .   .   .   .   .   .   .   .   .
3     .   .   .   .   .   .   .   .   .   .   .   .   .   .
2     .   .   .   .   .   .   .   .   .   .   .   .   .   .
1     .   .   .   .   .   .   .   .   .   .   .   .   .   .

 Enter GM3D option (I):
6

    DATA RANGE  =        -20.56        50.20
```

```
 Would you like a contour map? (Y,N) - (A)
Y

 Do you want a line printer listing? (Y/N) - (A)
N

 How many contour levels would you like? (I)
10

 Do you want to specify the 10 contour levels? (Y - N) (A)
N

 Contour interval? (neg. for prog. comp.) - (F)
7.0

 Area name? (max 35 char) - (A)
FOR THE USER'S GUIDE.
```

Project name: SAMPLE MERGE FILE
FOR THE USER'S GUIDE.
Model: THIS IS THE FOURTH MODEL.

MAGNETIC PRISM MODEL
Earth"s field: 50000. gammas.
Inclination = 12. degrees Declination = 35. degrees.

Grid spacing = 500.00 feet.

PRISM	X1	X2	Y1	Y2	Z1	Z2	SC
1	250.	1250.	-1250.	250.	300.	600.	-100.
2	-1500.	-750.	-750.	0.	300.	1300.	-1000.
	Rem. incl. = 0.			Rem. decl. = 2.		Q =	0.00
3	-1250.	-250.	1000.	1500.	300.	600.	-1000.

FOR THE USER'S GUIDE.

TRUE VALUES FOR ISOLINES

(L) = 0.560E 02 (M) = 0.490E 02 (N) = 0.420E 02 (O) = 0.35

(P) = 0.280E 02 (Q) = 0.210E 02 (R) = 0.140E 02 (S) = 0.700

(T) = 0.000E 00 (U) = -0.700E 01 (V) = -0.140E 02 (W) = -0.210

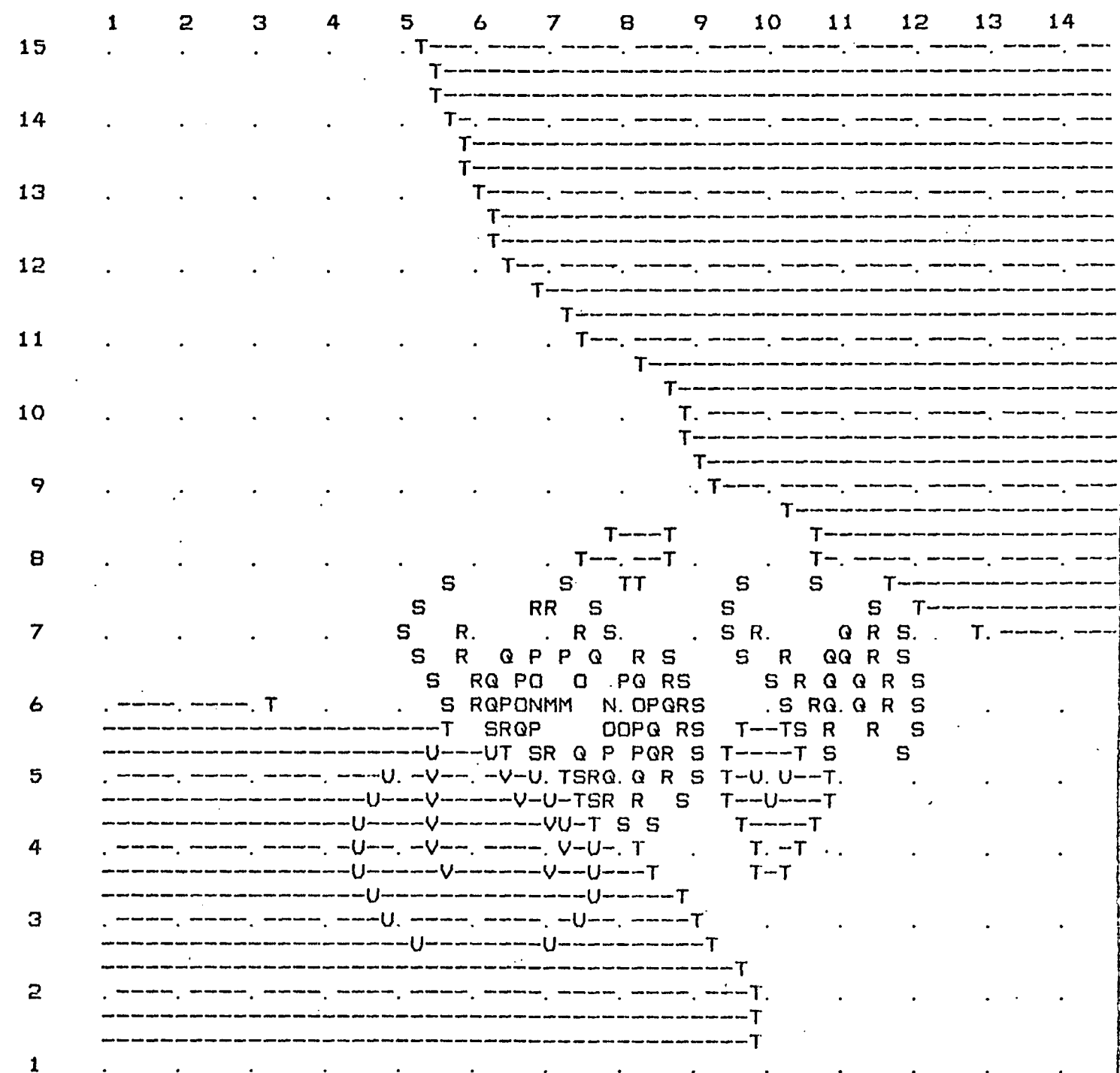

FOR THE USER'S GUIDE.
GRID VALUE SCALE FACTOR 1.E 01

2	2	2	1	0	-1	-2	-4	-4	-5	-5	-5	-5	-4
2	2	2	2	1	-1	-3	-5	-6	-7	-7	-7	-6	-5
3	4	4	4	3	0	-4	-8	-10	-10	-10	-9	-8	-6
4	5	6	7	7	3	-5	-12	-15	-14	-13	-12	-10	-8
5	6	9	12	18	19	6	-10	-20	-19	-19	-17	-13	-10
5	8	11	15	22	47	43	26	-9	-21	-27	-25	-18	-12
6	8	12	16	14	29	27	20	3	-16	-42	-38	-23	-12
5	8	13	22	31	40	15	-22	10	66	-33	-46	-21	-10
3	5	10	24	63	168	209	34	6	174	212	12	-2	-2
-1	-1	-1	2	18	119	502	400	39	8	255	75	21	8
-4	-8	-15	-33	-82	-206	-49	268	67	-105	41	58	26	12
-7	-13	-24	-49	-105	-195	-177	-6	28	-8	10	25	19	12
-9	-15	-26	-45	-74	-102	-88	-32	1	6	10	14	13	9
-9	-14	-22	-33	-46	-53	-45	-24	-6	3	7	8	8	7
-8	-12	-17	-23	-28	-30	-25	-16	-6	0	4	5	5	5

MAP VALUES IN GAMMAS
POINT (8,8) ON MAP CORRESPONDS TO COORDINATE (0,0)
GRID SPACING = 500.0 FT

Would you like a continuous contour map? (Y,N) - (A)
N

```
 Enter GM3D option (I):
3

 Enter edit option (I):


 Edit options are:
         1 - Return to master program
         2 - Edit project name
         3 - Edit model description
         4 - Change grid spacing
         5 - Edit Earth"s field
         6 - Change angle of inclination
         7 - Change angle of declination
         8 - Change prism parameters
         9 - Delete and pack prisms

 Enter edit option (I):
8

 There are currently  3 prisms in the model.
 Which prism do you wish to edit (I)?
1

 Enter the parameter of prism #  1 to be edited (I):


 The prism parameters are:
         1 - X1
         2 - X2
         3 - Y1
         4 - Y2
         5 - Z1
         6 - Z2
         7 - Remanent magnetization inclination
         8 - Remanent magnetization declination
         9 - Koenigsberger ratio
        10 - Magnetic susceptibility
        11 - Density contrast

 Enter the parameter of prism #  1 to be edited (I):
10

 The current magnetic susceptibility is   -100.00 .
 Enter the new value (F):
-1000.

 Do you want to make another parameter change (Y/N)?
N

 Changes saved.

 Enter edit option (I):
1
```

```
 Enter GM3D option (I):
7

 The stored model is obsolete. Please use option 6 to re-compute the model.

 Enter GM3D option (I):
6

    DATA RANGE  =        -22.94        46.67

 Would you like a contour map? (Y,N) - (A)
Y

 Do you want a line printer listing? (Y/N) - (A)
Y

 How many contour levels would you like? (I)
10

 Do you want to specify the 10 contour levels? (Y - N) (A)
N

 Contour interval? (neg. for prog. comp.) - (F)
6.6

 Area name? (max 35 char) - (A)
USER'S GUIDE AGAIN.
```

```
 Project name:  SAMPLE MERGE FILE
                FOR THE USER'S GUIDE.
 Model:  THIS IS THE FOURTH MODEL.

 MAGNETIC PRISM MODEL
 Earth"s field:   50000. gammas.
 Inclination =  12.  degrees          Declination =  35.  degrees.

 Grid spacing =      500.00 feet.
```

PRISM	X1	X2	Y1	Y2	Z1	Z2	SC
1	250.	1250.	-1250.	250.	300.	600.	-1000.
2	-1500.	-750.	-750.	0.	300.	1300.	-1000.
	Rem. incl. = 0.			Rem. decl. = 2.		Q = 0.00	
3	-1250.	-250.	1000.	1500.	300.	600.	-1000.

USER'S GUIDE AGAIN.
TRUE VALUES FOR ISOLINES

(L) =	0.528E 02	(M) =	0.462E 02	(N) =	0.396E 02	(O) =	0.33
(P) =	0.264E 02	(Q) =	0.198E 02	(R) =	0.132E 02	(S) =	0.660
(T) =	0.000E 00	(U) =	-0.660E 01	(V) =	-0.132E 02	(W) =	-0.198
(X) =	-0.264E 02	(					

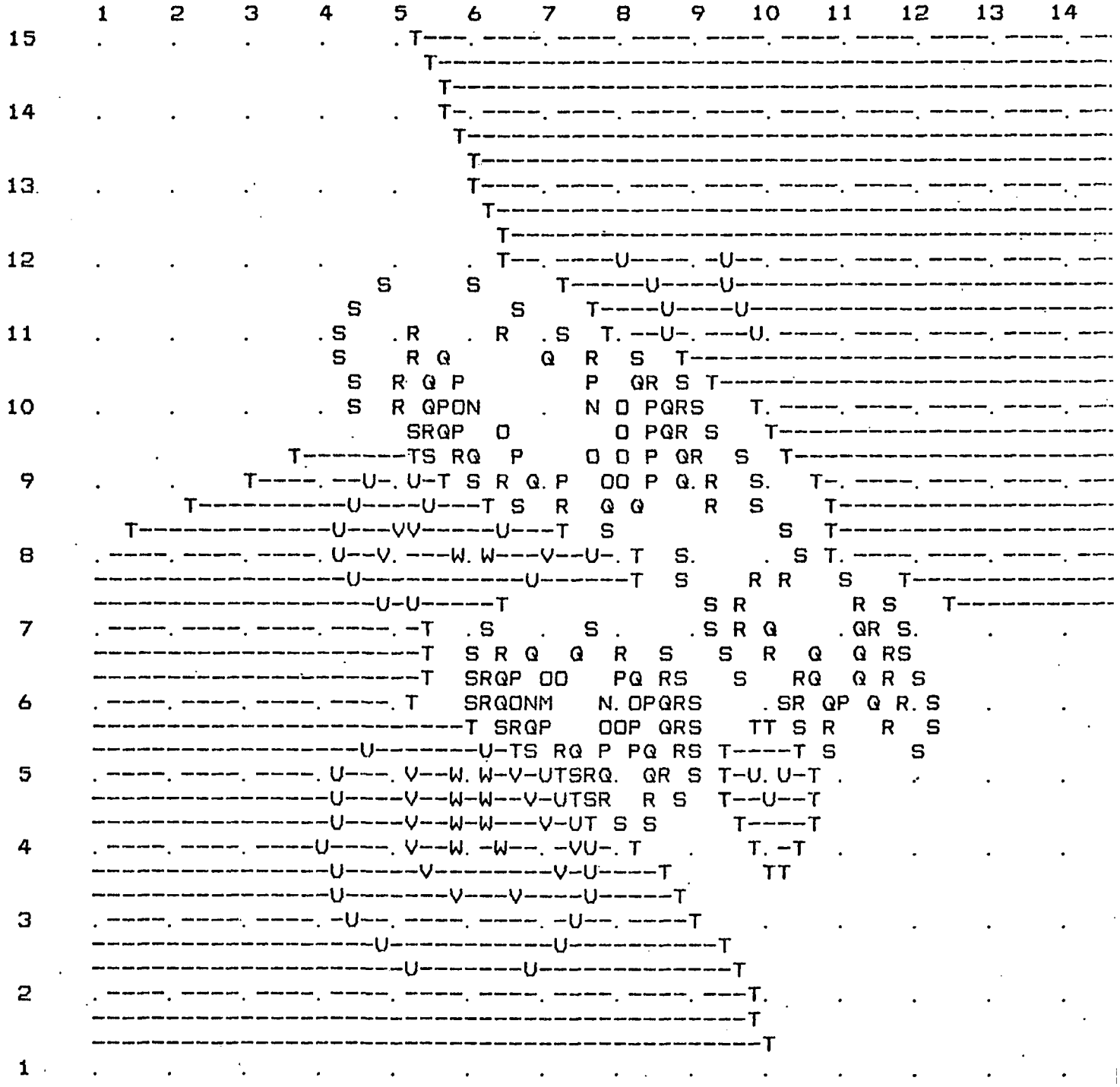

```
USER'S GUIDE AGAIN.
GRID VALUE SCALE FACTOR    1.E 01

    5    5    5    4    1   -3   -9  -13  -15  -15  -14  -11   -9   -7
    6    8    9    9    5   -3  -14  -22  -25  -23  -19  -15  -11   -9
    8   11   14   17   15    0  -22  -39  -42  -35  -26  -19  -14  -10
    9   14   22   34   43   21  -29  -70  -73  -50  -32  -22  -15  -11
    9   14   26   54  125  161   81  -27  -92  -55  -34  -24  -17  -12
    7   11   18   36  109  395  440  358   56  -21  -28  -25  -18  -12
    3    3    0  -22  -99   83  240  341  174   28  -27  -32  -20  -11
   -1   -3  -13  -46 -153 -210 -140  -26  100  112  -13  -36  -16   -7
   -5   -8  -16  -29  -32   53  127   14   28  199  228   21    3    2
   -8  -13  -21  -31  -28   70  467  387   45   19  265   82   26   11
  -11  -18  -30  -53 -106 -229  -67  260   68 -100   46   63   30   15
  -13  -21  -35  -62 -119 -208 -186  -11   27   -6   13   29   22   14
  -14  -21  -33  -53  -83 -110  -94  -36    0    6   12   16   15   11
  -13  -18  -27  -39  -52  -58  -49  -26   -7    3    7   10   10    8
  -11  -15  -21  -27  -32  -33  -28  -18   -7    0    4    6    6    6

MAP VALUES IN GAMMAS
   POINT (8,8) ON MAP CORRESPONDS TO COORDINATE (0,0)
   GRID SPACING  =      500.0 FT

PRINT FILE PRT001

  The contour map has been listed as GM3D-LIST.
```

```
 Would you like a continuous contour map? (Y,N) - (A)
Y

 Did you enter contour values as whole numbers? (Y,N) - (A)
Y

 Do you want high/low centers printed? (Y,N) - (A)
N
SCALE   OPTION # (I)=
      1  1:12,000
      2  1:24,000
      3  1:62,500
      4  1:125,000
      5  1:250,000

SCALE   OPTION # (I)=   1

 Would you like a grid overlay? (Y,N) - (A)
Y

 Grid interval in ft.? (must be an integral divisor of   7000.0) - (F)
1000.

 Draw prisms on map? (Y,N) - (A)
Y

 Your name? (max 15 char) - (A)
JIM

 Todays date? (max 8 char) - (A)
TODAY

 Enter device number:
              1 - Tektronix 4014
              2 - Statos plotter
              3 - Calcomp plotter
2
# OF VECTORS=      1363

 Plot completed.

 Enter GM3D option (I):
9
*FILE MAINTENENCE*


     FMAIN---OPTION # (I)=   3
*SAVE WORK FILE*
WORK FILE SAVED AS SUBFILE#  4
```

```
     FMAIN---OPTION # (I)=    2
TEST MERGE FILE FOR GM3D.

There are  4 subfiles in the merge file.

Project: SAMPLE MERGE FILE                    FOR THE USER'S GUIDE.
    Model: THIS IS THE FIRST MODEL.                                  4 prisms.

Project: SAMPLE MERGE FILE                    FOR THE USER'S GUIDE.
    Model: THIS IS THE SECOND MODEL.                                 6 prisms.

Project: SAMPLE MERGE FILE                    FOR THE USER'S GUIDE.
    Model: THIS IS THE THIRD MODEL.                                  3 prisms.

Project: SAMPLE MERGE FILE                    FOR THE USER'S GUIDE.
    Model: THIS IS THE FOURTH MODEL.                                 3 prisms.


     FMAIN---OPTION # (I)=    1

 Enter GM3D option (I):
1

 Program stopped.

OK,
```

$$\begin{vmatrix} a_1 & b_1 & c_1 \\ a_2 & b_2 & c_2 \\ a_3 & b_3 & c_3 \end{vmatrix} = a_1b_2c_3 + b_1c_2a_3 + c_1a_2b_3 - a_3b_2c_1 - b_3c_2a_1 - c_3a_2b_1$$

LBCADETR

RCL 14
RCL 15
X
RCL 19
X
$a_1b_2c_3$

RCL 14
RCL 18
X
RCL 13
X
$b_1c_2a_3$

+
RCL 17
RCL 12
X
RCL 16
X
$c_1a_2b_3$

+
RCL 13
RCL 15
X
RCL 17
X
$a_3b_2c_1$

−
RCL 16
RCL 18
X
RCL 11
X
$b_3c_2a_1$

−
RCL 19
RCL 12
X
RCL 14
X
$c_3a_2b_1$

−

1 2 3
1 2
1

11
15

4 2 4
3 1 4
2 15 1
1 15 225

144

$y = Ax^2 + bx + c$

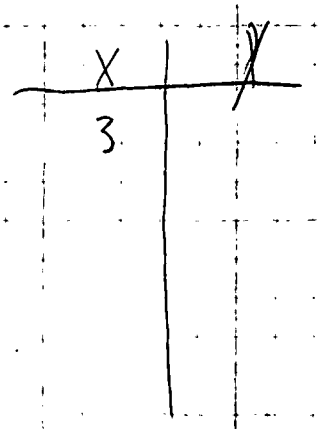

.71
.67
-8.38

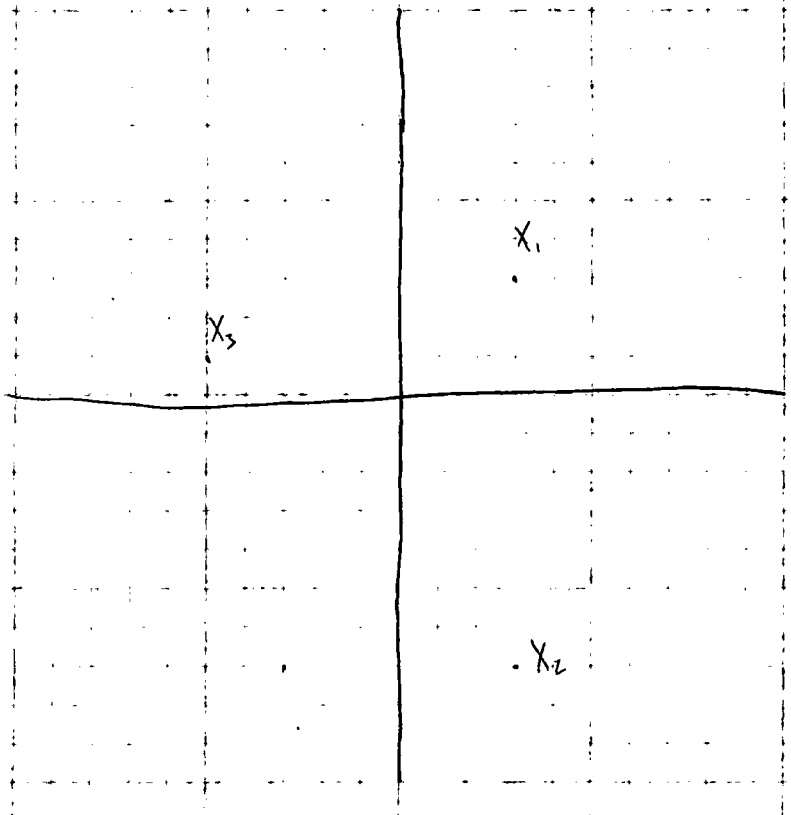

$dx^2+ex+f=y$

$dx_1^2+ex_1+f=y_1$

$dx_2^2+ex_2+f=y_2$

$dx_3^2+ex_3+f=y_3$

(1,14) x_1, y_1 ②

(3,15) x_2, y_2 ④

(5,16) x_3, y_3 ⑥

a =

b =

c =

```
LBL QUADFIT          "X1 = ?"
STO 1   X1   STO14   PROMPT
 R/S          X^2
              STO 11
STO 2   Y1
 R/S
STO 3   X2   STO15
 R/S          X^2
              STO 12
STO 4   Y2
 R/S
STO 5   X3   STO16
 R/S          X^2
              STO 13
STO 6   Y3
 1
STO
 17
 1
STO 18
 1
STO 19
XEQ A DET A
STO 7
RCL 2
STO 11
RCL 4
STO 12
RCL 6
STO 13
XEQ A DET A
STO 8
RCL 1
 X^2
STO 11
RCL 3
 X2
STO 12
RCL 5
 X2
STO 13
RCL 2
STO 14
RCL 4
STO 15
RCL 6
STO 16
```

DELTA

```
XEQ A DET A
STO 9
RCL 1
STO 14
RCL 3
STO 15
RCL 5
STO 16
RCL 2
STO 17
RCL 4
STO 18
RCL 6
STO 19
XEQ A DET A
STO 10
RCL 8
RCL 7
 ÷          "A a ="
 PSE
RCL 9
RCL 7
 ÷
 PSE
RCL 10
RCL 7
 ÷
 PSE
END
```

RCL 2
STO 11

A	0.17
B	-0.83
C	3.00

.27
2.0
2.80

-.83

3
3

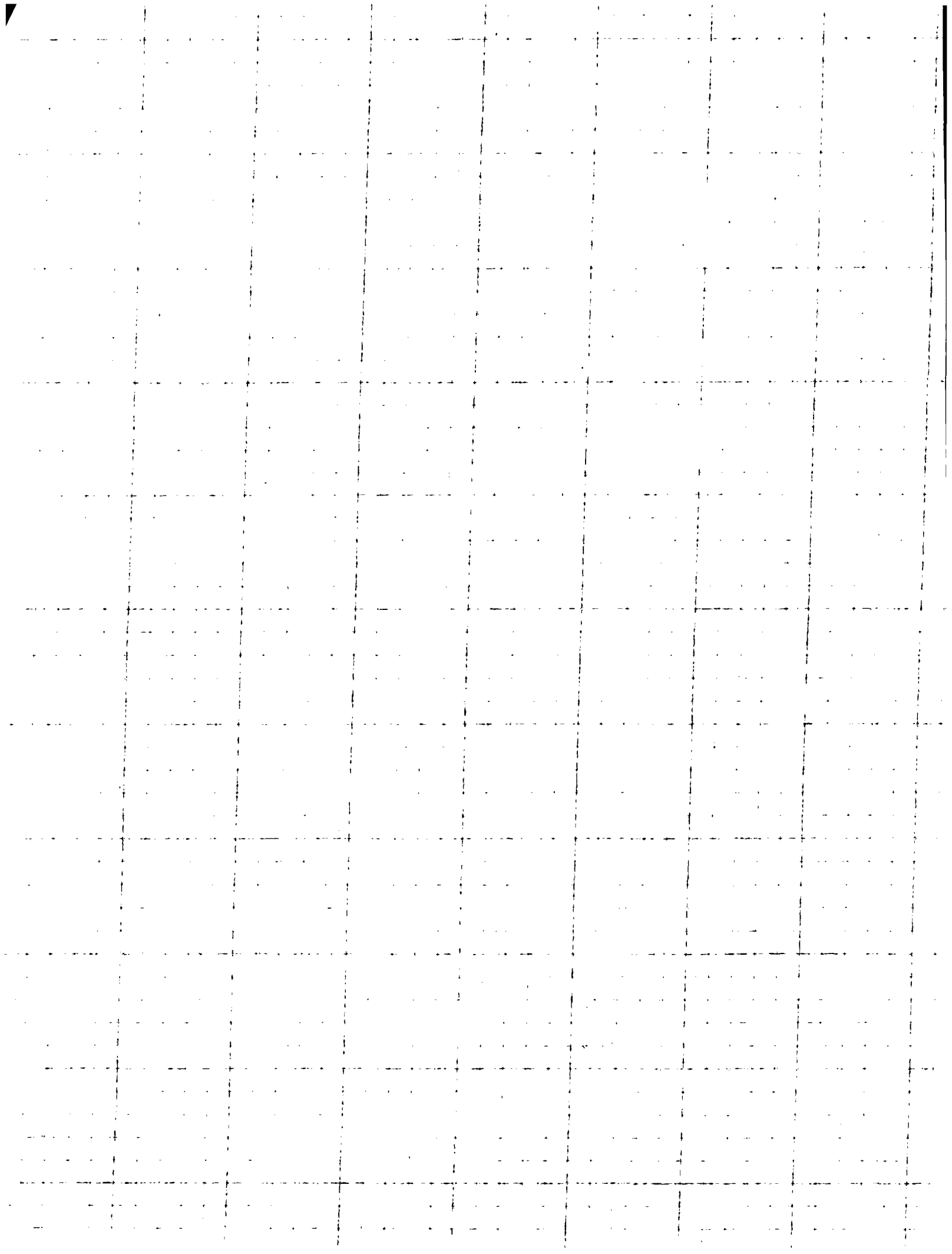

$H_r = \frac{2M\cos\theta}{r^3}$ $\quad H_\theta = \frac{M\sin\theta}{r^3}$

now for the earth H_θ = max at equator, value = 900

and $M/r^3 = 32000\gamma$, i.e. $M = 32000 r^3\ \gamma\,cm$

$r = 3963$ miles $= 6.3778 \times 10^8$ CM $= 6378$ KM

so $M = 8.302 \times 10^{25}\ \gamma - cm^3$ =

θ = colatitude, so $\alpha = 90 - \theta$ = geographic latitude

$V = H_r$ = vertical field $\quad H = H_\theta$ = horizontal field

$T = \sqrt{H_r^2 + H_\theta^2}$ = total field

$I = \tan^{-1} H_r/H_\theta$ = inclination relative to horizontal

$= \tan^{-1} 2\cos\theta/\sin\theta$

Rob

FIX 0

STO 03

1/1/1111

RCL 3

```
01 LBL A MAGDPL A
02 8.30 2 E15
03 A RAD = ? A
04 PROMPT
05 - 3
06 y^x
07 ÷
08 STO 00
09 LBL 01
10 A LAT = ? A
11 PROMPT
12 CGS
13 90
14 +
15 STO 01
16 COS
17 2
18 *
19 RCL 00
20 *
21 A V =
22 ARCL X
23 AVIEW
24 PSE
25 RCL 01
26 SIN
27 RCL 00
28 *
29 A H =
30 ARCL X
31 AVIEW
32 PSE
33 x^2
34 ⇄
35 x^2
36 +
37 SQRT
38 A T =
39 ARCL X
40 AVIEW
41 PSE
42 RCL 01
43 COS
44 2
45 - *
46 RCL 01
47 SCN
48 X≠0 ?
49 GTO 02
   E-80 ÷
   1
   ⇄
   LBL 02
   ÷
53 ATAN
54 A I =
55 ARCL Y
56 AVIEW
57 PSE
58 FS?C 01
59 GTO MAGDPL
60 GTO 01
61 END
```

DIST MOON
386,253 KM

TABLE I

Form	Effect	Amplitude Constant*	Variation Formula	Curve No.	Fig.
Sphere	Gravity	$8.52\sigma R^3/z^2$	$f_1(x/z)=[1+(x/z)^2]^{-2}/^2$	1	1
Sphere	Magnetism	$8.38\times10^5 I(R/z)^3$	$f_2(x/z)=[1-x^2/(2z^2)][1+(x/z)^2]^{-5}/^2$	2	1
Horizontal Cylinder	Gravity	$12.77\sigma R^2/z$	$f_3(x/z)=[1+(x/z)^2]^{-1}$	3	1
Horizontal Cylinder	Magnetism	$6.28\times10^5 I(R/z)^2$	$f_4(x/z)=[1-(x/z)^2][1+(x/z)^2]^{-3}$	4	1
Vertical Cylinder	Gravity	$6.39\sigma R^2/z$	$f_5(x/z)=[1+(x/z)^2]^{-1/2}$	5	1
Vertical Cylinder	Magnetism	$3.14\times10^5 I(R/z)^2$	$f_1(x/z)=[1+(x/z)^2]^{-3/2}$	1	1
Fault	Gravity	$12.77\sigma t$	$f_6(x/z)=\frac{1}{2}+(1/\pi)\tan^{-1}(x/z)$	6	2
Fault	Magnetism	$2\times10^5 It/z$	$f_7(x/z)=(x/z)[1+(x/z)^2]^{-1}$	7	1
Vertical Sheet	Gravity	$9.36\sigma t$	$f_8(x/z)=\log\sqrt{1+(z/x)^2}$	8	3
Vertical Sheet	Magnetism	$2\times10^5 It/z$	$f_3(x/z)=[1+(x/z)^2]^{-1}$	3	1
Horizontal Circular Lamina	Gravity	$2.03\omega\sigma t$	Solid angle chart	—	4
Vertical Circular Cylinder	Magnetism	$10^5 I\omega$	Solid angle chart	—	4
Two-dimensional slab	Gravity	$4.07\sigma t$	θ(=subtended angle)	—	—
Two-dimensional slab	Magnetism	$2\times10^5 I$	$\theta_1-\theta_2$	—	—

* Values of the amplitude constant, for gravity formulas, give g in milligals when R, z and t are in units of kilo-feet and σ is the density contrast in c.g.s. units (i.e., grams per cc. or specific gravity). For the magnetic formulas, values give V in gamma for the polarization, I, in c.g.s. units (magnetic moment per unit volume). If the susceptibility, k, is given and the body is magnetized in the earth's field of H oersteds, (value, in the U. S. around 0.6), then $I=kH$. Since the linear dimensions (R, z and t) enter the magnetic equations as ratios, their units do not affect the amplitude constants.

For each of the first three shapes considered, the ratio of the magnetic to the gravity amplitude factors[3] is

$$\frac{V}{g}=\frac{I}{\sigma}\cdot\frac{C}{z}; \qquad \frac{zV}{g}=\frac{I}{\sigma}C$$

[3] This relation was first pointed out to the writer by L. H. Bailey.

GRAVITY PROGRAMS

Common Data Input

```
LBL 'GDAT
FIX 3
Ω RAD = ? KFT
XEQ PROMPT
STO 00
Ω DPTH = ? KFT
XEQ PROMPT
STO 01
Δ RHO = ?
XEQ PROMPT
STO 02
END
```

```
LBL 'GDATA
FIX 3
Ω T = ? KFT
XEQ PROMPT
STO 00
Ω DPTH = ? KFT
XEQ PROMPT
STO 01
Δ RHO = ?
XEQ PROMPT
STO 02
END
```

Common Output

```
LBL 'GOUT
Δ G =
ARCL X
AVIEW
XEQ PSE
XEQ PSE
END
```

Sphere

$g = 8.520\,R^3/z^2\left[1+\frac{x^2}{z^2}\right]^{-3/2}$

```
LBL 'GSPH
XEQ GDAT
LBL 01
Ω X = ? KFT
XEQ PROMPT
RCL 01
÷
↑
X
1
+
-1.5
y^x
RCL 00
3
y^x
X
RCL 01
↑
X
÷
RCL 02
X
8.52
X
XEQ GOUT
FS? 01
GTO GSPH
GTO 01
END
```

Horiz Cylinder

$g = 12.770\,R^2/z\left[1+\frac{x^2}{z^2}\right]^{-1}$

```
LBL 'GHCYL
XEQ GDAT
LBL 01
Δ X = ? KFT
XEQ PROMPT
RCL 01
÷
↑
X
1
+
1/X
RCL 00
↑
X
RCL 01
÷
RCL 02
X
12.77
X
XEQ GOUT
FS? 01
GTO GHCYL
GTO 01
END
```

Vert Line Mount

$g = 6.390\,R^2/z\left[1+\frac{x^2}{z^2}\right]^{-1/2}$

```
LBL 'GVLIN
XEQ GDAT
LBL 01
Δ X = ? KFT
XEQ PROMPT
RCL 01
÷
↑
Y
1
+
SQRT
1/X
RCL 00
↑
X
X
RCL 01
÷
RCL 02
X
6.39
Y
XEQ GOUT
FS? 01
GTO GVLIN
GTO 01
END
```

Vert Sheet

$g = 9.36\pi t \log\sqrt{1+\left(\frac{z}{x}\right)^2}$

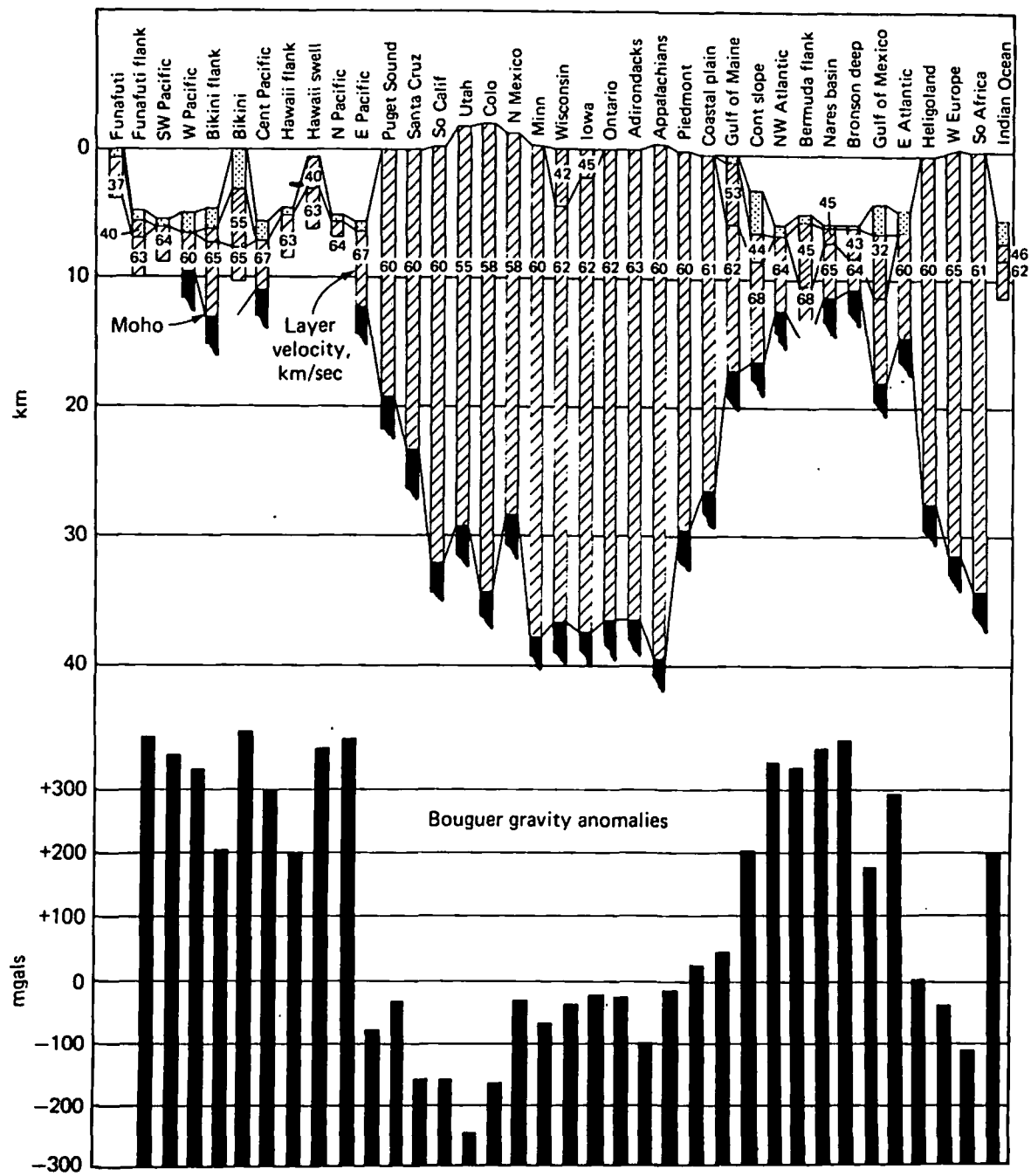

FIGURE 9-3
Relation of crustal thickness obtained from seismic measurements to Bouguer gravity anomalies. (*From Woollard, 1959, p. 1526; by permission of the American Geophysical Union.*)

of isostasy is very real and that it is adequately explained, in broad terms, by variations in the depth of the Moho. Very extensive studies of the relations of gravity to topography have been carried out since about 1960 as worldwide gravity data have become available, particularly over the oceans. They have shown that there are many departures from ideal compensation.

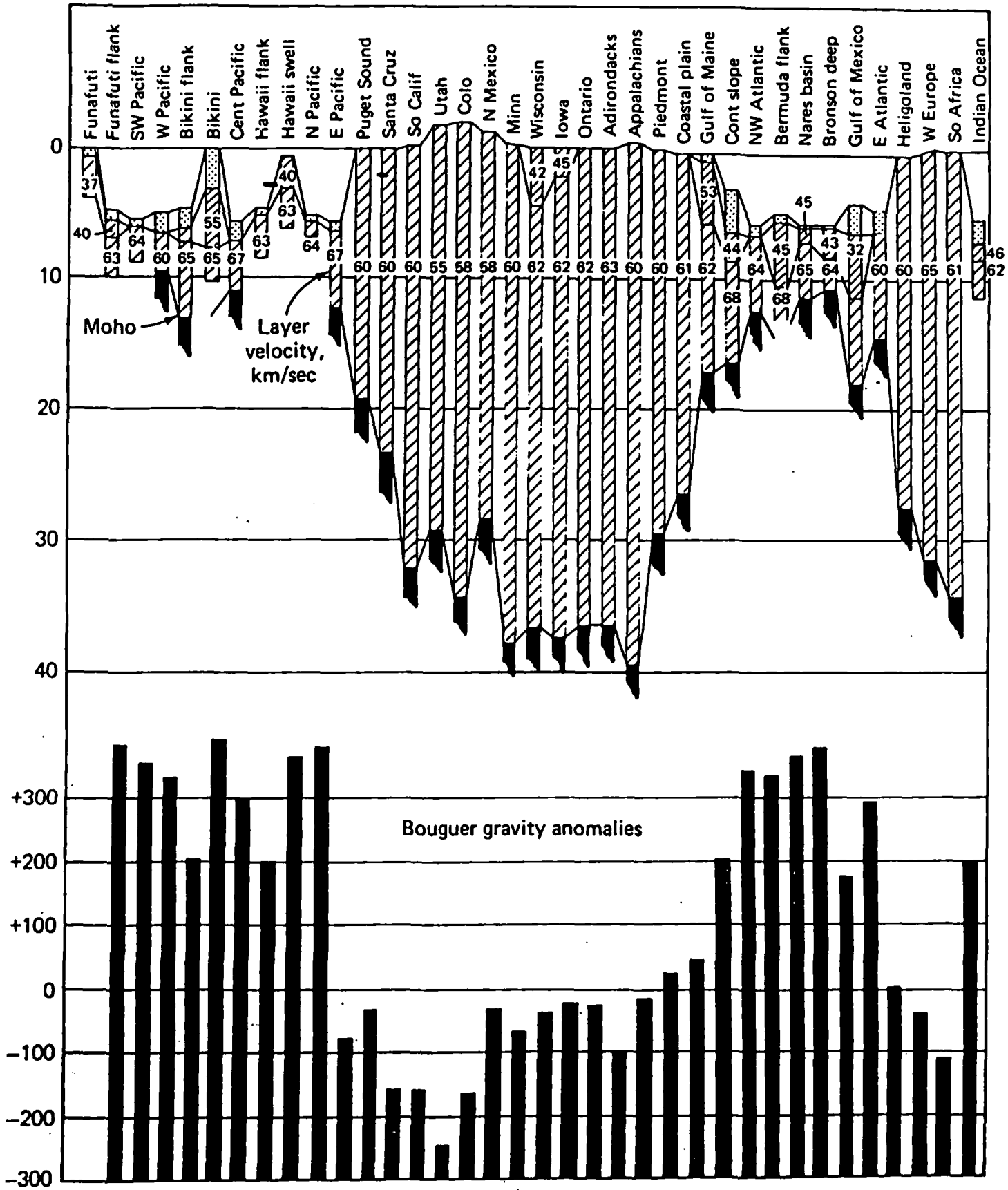

FIGURE 9-3
Relation of crustal thickness obtained from seismic measurements to Bouguer gravity anomalies. (*From Woollard, 1959, p. 1526; by permission of the American Geophysical Union.*)

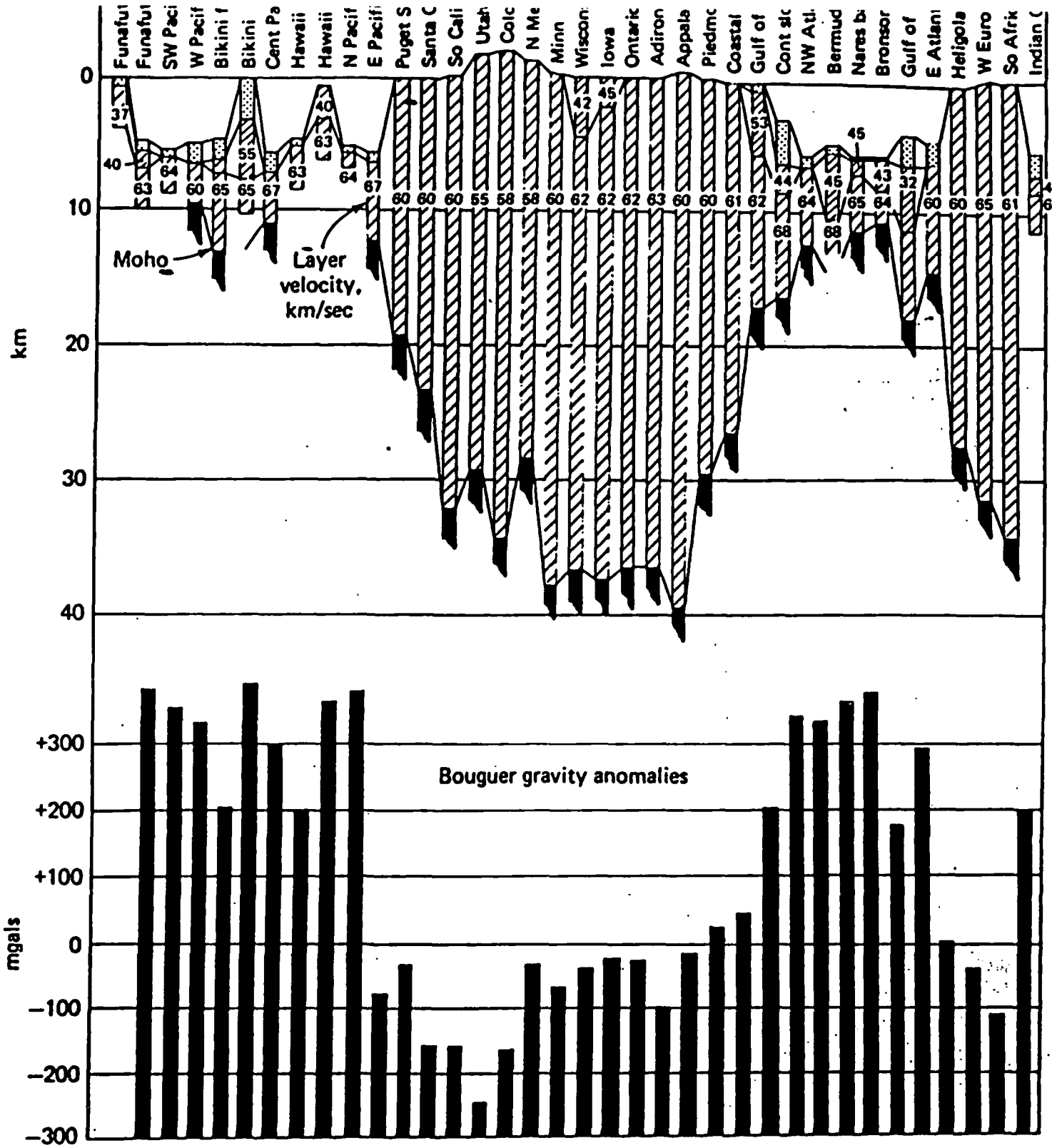

FIGURE 9-3
Relation of crustal thickness obtained from seismic measurements to Bouguer gravity anomalies. (*From Woollard, 1959, p. 1526; by permission of the American Geophysical Union.*)

REVIEWS OF GEOPHYSICS VOL. 5, NO. 4 NOVEMBER 1967

Measurement of Gravity at Sea and in the Air

LUCIEN J. B. LACOSTE

LaCoste and Romberg, Inc., Austin, Texas

Abstract. General problems of gravity measurement at sea are discussed. A treatment of the effects of vertical accelerations shows that gravity meter nonlinearities cause errors that ordinarily are proportional to the square of the vertical acceleration. In a treatment of horizontal accelerations, similarities and differences that exist between gimbal supported and stabilized platform gravity meters are pointed out. It is shown that optimization of the parameters of a stabilized reference can reduce gravity meter errors by two or more orders of magnitude at long periods. A method for correcting for inadequate period of a stabilized reference is given. The Schuler-tuned stabilized platform is briefly described. The theory of inherent type cross coupling and examples of imperfection type cross coupling are given.

Theory and significant details of construction are given for the LaCoste and Romberg (L&R) gravity meter and stabilized platform. Tests on L&R air-Sea gravity meters made during the last decade are discussed. The largest error in earlier work is shown to have been due to vertical accelerations. A method of correcting for these errors is described. Tests indicate that presently attainable accuracy of L&R gravity meters is appreciably better than 1 mgal.

INTRODUCTION

Gravity has been measured at sea with underwater gravity meters (operated on the ocean bottom), with Vening-Meinesz pendulums, and with shipboard gravity meters. Underwater gravity meters are well adapted to shallow water operation. They also give greater detail than the other types of instrumentation because they have higher accuracy and because underwater gravity data are taken closer to the anomalies. Underwater gravity meter accuracy falls off as the water depth increases because of increasing errors in measuring water depth and because of uncertainty in the position of the gravity meter relative to the ship. Furthermore, underwater gravity meters can detect detail that is lost in the averaging procedures inherent in instruments operating on moving ships. Until recently nearly all sea gravity work for oil exploration was done with underwater gravity meters. They can be modified for use at any desired water depth, but operation at great depths is slow and expensive.

From the 1920's Vening-Meinesz pendulums have been used in submarines to measure gravity [*Vening Meinesz*, 1929, 1932, 1941; *Browne*, 1937; *Browne and Cooper*, 1950, 1952; *Worzel and Ewing*, 1950; *Worzel et al.*, 1955; *Harrison*, 1960]. For many years they were the only instruments used for measuring gravity in deep water. They have an accuracy of 1–2 mgal, but they are complicated to operate and computation of the data is laborious. They handle very well the small-amplitude, long-period accelerations encountered in a submarine, but they do not handle the larger-amplitude, short-period accelerations present on a sur-

face ship. The preceding difficulties might have been overcome, but the advent of submarine and surface ship gravity meters discouraged work in that direction. At present few if any Vening-Meinesz pendulums are still in use. Consequently, they will not be considered further in this review; they are well described in the references mentioned.

Since the end of World War II several gravity meters have been designed for use in submarines and on surface ships. *Gilbert* [1949] made a vibrating string gravity meter and later B. J. Electronics and *Tsuboi et al.* [1961] made similar instruments. In these gravity meters the vibrating string supported a mass whose changes in weight affected the frequency of vibration. Very recently Worden, Bell Aircraft, and Texas Instruments have designed instruments that employ the 'force-balance' principle that is used in some accelerometers. In this method changes in the gravitational pull on the mass are balanced by electromagnetic or electrostatic forces controlled by a very fast acting servo. The Bell instrument has given good results at sea. The type of shipboard gravity meter that has so far been the most successful is, however, a highly overdamped spring type of gravity meter. The Graf and the LaCoste and Romberg shipboard gravity meters are both of this type.

Originally these highly overdamped gravity meters were designed for operation in submarines. Their accuracy and their ability to withstand accelerations were soon improved, however, to such an extent that they were capable of operating on a surface ship. Recently their accuracy has been further improved so as to make them valuable in oil exploration. Although their accuracy does not equal that of underwater gravity meters in shallow water, it is comparable in deep water because their results are not so much affected by errors in depth measurements. Furthermore, shipboard gravity surveys are much faster and cheaper than underwater gravity surveys. Shipboard gravity meters can also be used on the same ship with magnetometers and sparkers, which reduces costs.

UNDERWATER GRAVITY METERS

Underwater gravity meters are essentially remote controlled land gravity meters, although underwater work involves some substantial additional problems. The electronic requirements for remote operation are well within the state of the art; thus, it is hardly worth while in this review to give electronic details. A recent improvement was to reduce the number of conductors in the controlling cable. This improvement makes it economically feasible to use an armored cable with larger conductors, which is important because cable failures are the greatest source of trouble at sea. Cable conductor breakage near the submersible gravity unit occurs regularly because of continual flexure in this region. The standard operating procedure is to cut off a few feet of cable near the gravity meter every few weeks and reterminate the cable. Broken cable conductors are often very troublesome because electrical conductivity at the break is often restored when the load on the cable is removed. Cable trouble could be reduced by a further reduction in the number of cable conductors, and research is being done to implement this change.

Unlike land gravity meters, underwater gravity meters must withstand very rough treatment. They usually receive a substantial bump when they hit the ocean floor; they are sometimes accidentally dragged on the ocean bottom; and they sometimes hit the side of the ship when they are being raised out of the water. Also, poor hoist operators often bump gravity meters when raising them into their cages on the hoist. The rough treatment makes the errors in sea surveys greater than the errors encountered in a land survey, but the gravity meters are made rugged enough that the errors are only about 0.1 mgal. Rough treatment can also knock gas bubbles in the column of the mercury thermostat which has up to now been used to regulate the temperature of the gravity meters. This trouble has been eliminated in recent gravity meters by replacing the mercury thermostat with a thermistor-transistor circuit.

Seismic motion problems. Seismic motion of the ocean bottom has been a considerable problem in making underwater gravity surveys. This seismic motion is caused by wave action and is particularly troublesome on muddy bottoms at depths less than about 50 feet. The vertical motion in this seismic action is often greater than the motion that can be tolerated in the gravity meter beam without introducing errors caused by mechanical hysteresis in the gravity meter spring. Two methods have been used to overcome this problem.

The first method was to put the gravity meter unit on a servo-controlled elevator to approximately counteract the vertical seismic motion [*LaCoste*, 1952*a*, *b*]; a diagram showing this operation is given in Figure 1. Obviously the acceleration of the servo can be controlled so that the gravity meter beam or weight can be held (for a while) at any point on its scale regardless of the seismic motion. This can not generally be done for an indefinitely long time because the elevator will usually reach a limit of its travel. Although the elevator operation described will counteract vertical seismic motion, it will not in itself

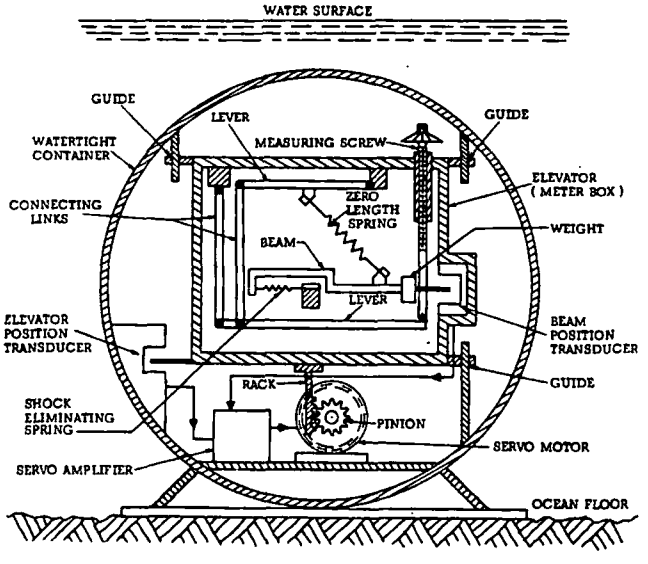

Fig. 1. Elevator for seismic compensation of underwater gravity meter.

permit a measurement of gravity because an unknown acceleration (that of the elevator) has been introduced.

To measure gravity, an additional feature is added that makes the acceleration of the elevator average out to zero. As shown in Figure 1, this is done by feeding to the servo an error signal that is a combination of the beam position and the elevator position. The combination is chosen so as to make the servo null the beam above its center position when the elevator is above its center position, and vice versa. Thus, a stability is given to the elevator operation, as can be seen from the following considerations. As the elevator moves up, the servo nulls the beam closer to the top stop. This beam position reduces the spring tension, which causes the beam to be accelerated down. This downward acceleration is equivalent to a restoring force on the elevator and results in an equilibrum position for the elevator provided that the gravity meter is not too far out of balance.

The elevator system just described would give an undamped oscillatory motion to the elevator. To damp it, some dead space is provided in the servo. More damping can be provided if desired by modifying the electrical circuit. When the servo is first turned on, initial conditions can be troublesome. To damp them out before the elevator reaches a limit of its range, the operator is provided with two controls that apply an electrostatic force to the beam in either an upward or a downward direction. Efficient operation of these controls requires some training.

The elevator system was developed about 1948 and is still in use, but many operators do not take full advantage of its capabilities. It has an advantage over other systems in that the elevator almost completely eliminates vertical accelerations that would otherwise be experienced by the gravity meter unit; this makes it unnecessary for the gravity meter to respond to accelerations linearly.

The second method for overcoming the problem of vertical accelerations of the ocean bottom is to highly overdamp the gravity meter beam or weight. This method is used in most present day shipboard gravity meters. It will be described in detail later, but a few comments about it will be made now. It would be thought that high damping would make a gravity meter very slow to read. This difficulty can be avoided, however, by reading the gravity meter before it has come to rest, which can be accomplished by observing the *velocity* of the beam. If the velocity is zero, the beam has come to rest. If the velocity is not zero, a correction can be made for the observed velocity. By using this method an overdamped gravity meter can be read as fast as an ordinary gravity meter. The overdamped gravity meter is simpler to operate than the elevator type.

Accuracy. The accuracy of underwater gravity meter results depends to a considerable extent on how the gravity meter is handled. The inherent precision of the gravity meter is about 0.01 mgal. In actual sea operations under normal conditions, base station checks indicate an accuracy of about 0.1 mgal [*Beyer et al.*, 1966], although many carefully controlled surveys have been made with an appreciably higher accuracy. An accuracy of 0.1 mgal is generally adequate because uncertainties in water depth and latitude often given larger errors. Water depth is usually measured with pressure gages whose accuracy is not much better than ½%. A 2-foot error in depth corresponds to about 0.1 mgal. Also, a 500-

foot error in the north–south direction corresponds to about 0.1 mgal at a latitude of 30°. An over-all accuracy of about 0.2 mgal is considered good in a survey in water 500 feet deep.

Much gravity exploration for oil has been done in water up to 600 feet deep, but not much has been done at greater depths because of increased costs and lower accuracies of the measurements in deeper water. In exploration for oil, accurate electronic navigation systems such as Raydist and Shoran are used.

Recently some experimental gravity work has been done at depths up to 2900 feet [*Beyer et al.*, 1966]. In this work an over-all accuracy of 0.24 mgal was achieved, but it was necessary to make very precise depth measurements to achieve this accuracy. The depth was measured in several ways. One transponder was mounted on the ship, and it gave good results when the bottom was flat. A second transponder was mounted on the gravity meter, and travel times to the ship were measured. It gave good results when the gravity meter was directly below the ship. This position was found by looking for the shortest travel time. Furthermore, the actual velocity of sound in the water was measured as the gravity meter was lowered, thereby eliminating errors caused by using an incorrect value of sound velocity. The measurements were made with an instrument fixed to the gravity meter. Depth was also measured by a pressure gage (accuracy ¼%), but the depth values obtained in this way were not considered to be as accurate as the other values.

Other uses of underwater gravity meters. Underwater gravity meters have also been used in swamps, on muskegs, and on frozen lakes and ice islands. In such places there is often so much seismic motion that a land gravity meter would not operate satisfactorily. An underwater gravity meter with a light fiberglass container is then used. Either the elevator type gravity meter or the overdamped model can handle the long-period seismic motion and is usually satisfactory. Trouble is sometimes experienced however, by short-period motions caused by the wind blowing the trees in a swamp or by the movement of the operator if he is too close to the gravity meter. In some cases it is desired to hover a helicopter over the gravity meter while taking a reading. Tests indicate that this can be done even in a soft peat bog if the helicopter is more than about 100 feet off the ground. Efforts are now being made to suitably shock-mount the gravity meter so that it will be possible for the helicopter to hover closer to the gravity meter.

SHIPBOARD AND AIRPLANE GRAVITY METERS

Eotvos Effect

Before considering any details of shipboard or airplane gravity meters, it is desirable to discuss some problems that are common to all types of moving instruments. One problem is caused by the motion of the ship or airplane over a curved rotating earth. This motion results in a centripetal acceleration, which must be corrected for. This correction, known as the Eotvos correction, is [*Thompson and LaCoste*, 1960; *Nettleton et al.*, 1960].

$$E = (R_\varphi + h)(2V_\varphi V_\cdot + V^2)/R_\varphi^2 \qquad (1)$$

where R_φ is the earth's radius at latitude φ, h is the height above sea level, V_φ is the speed of rotation of the earth's surface at latitude φ, and V_e is the easterly component of V, the total speed of the vehicle. At speeds less than 15 knots the Eotvos correction can be approximated by 7.5 cos φ milligals per knot of east–west speed to be added to the observed gravity values for eastward velocities. The Eotvos correction is typically in the range of -50 to $+50$ mgal for measurements at sea and of the order of 1000 mgal for airplane observations.

It is therefore apparent that navigational errors are often the most serious limitation in the accuracy of gravity measurements made on moving platforms. If there is a 1-knot error in the east–west speed of a ship, it will introduce a 7.5-mgal error in the Eotvos correction at the equator and a somewhat smaller error at higher latitudes. Errors in ship velocity of 1 knot can easily occur if a ship is out of range of land and accurate electronic aids to navigation and must depend on astronomical sights. The use of satellite and inertial navigation will reduce navigational errors in the future.

In (1) the term, containing V^2 as a factor would occur even if the earth were not rotating. However, the term containing $V_\varphi V_e$ as a factor is present because of the rotation of the earth. This term is actually the vertical component of the Coriolis force $2\,\Omega \times \mathbf{V}$, where Ω is the vector representing the angular rotation of the earth and V is the vector representing velocity relative to the earth. The horizontal component of the Coriolis force is directed in the east–west direction; it is produced by north–south motion over the earth. Since the horizontal component is at right angles to gravity, its effect on gravity is generally negligible. It can always be disregarded in ship measurements and is only of the order of a milligal in airplane measurements.

Vertical Accelerations

The biggest problem in the measurement of gravity on a moving platform is caused by vertical accelerations. Since no instrument can distinguish between gravity and acceleration, any gravity measurement made on a moving platform will actually be a meaurement of gravity plus vertical acceleration or $g + z''$. Furthermore, instantaneous vertical accelerations are generally 10,000 to 100,000 times greater than the desired gravity meter accuracy. It is therefore necessary to do some averaging or filtering of the data. If a simple averaging process is used over the time interval T, the data give

$$\frac{1}{T}\int_0^T (g + z'')\,dt = \langle g \rangle + [z']_0^T/T \tag{2}$$

where the angle brackets denote an average value.

Equation 2 shows that averaged gravity measurements must be corrected by an amount equal to the change in vertical velocity during observation divided by the time duration of the observation. The precise method used to make the correction depends on the circumstances of the measurement. In a shipboard measurement the vertical ship accelerations are large, but there can be no long-term change in z', since the vertical accelerations of the ocean surface due to tides are negligible. In this case, therefore, it is merely necessary to filter out the wave

frequencies. In submarine measurements filtering can be used also, but an additional correction must be made for long-term changes in depth. In making measurements in aircraft, however, there is no such easy division by period. In this case it is necessary to measure and correct continuously for variations in height, making sure that the corrections are filtered the same way that the gravity data are.

Vertical accelerations also make it necessary for the gravity meter and filter responses to be extremely linear in order to avoid errors in averaged gravity indications [*Harrison and LaCoste*, 1968]. To study the effect of nonlinearities the differential equation for a spring-type gravity meter will be needed. Although the equation to be derived does not apply to any particular spring-type gravity meter, it might be helpful to refer to Figure 2. If horizontal accelerations are negelected, the equation is

$$g + z'' + bB'' + fB' + kB - cS = 0 \qquad (3)$$

where z'' is the vertical acceleration of the gravity meter case, B is the displacement of the gravity meter mass relative to a null position in the gravity meter case, and b, f, k, and c are constants if the gravity meter is linear. The first three terms in (3) result from the gravitational and acceleration forces on the mass. If the mass is constrained to move in an approximately straight line, b will be very nearly constant. It will be assumed constant. The term fB' results from damping, and kB is due to the restoring force of the spring. The term cS represents the vertical force per unit mass exerted at the center of mass by the spring acting through the various links in the gravity meter when the mass is nulled. S can be adjusted by moving the point of attachment (A in Figure 2) of the spring on the gravity meter case.

The coefficients f, k, and c will be taken, respectively, as the sum of constants f_0, k_0, and c_0 and variables f_v, k_v, and c_v. Equation 3 then becomes

$$g + z'' + bB'' + (f_0 + f_v)B' + (k_0 + k_v)B - (c_0 + c_v)S = 0 \qquad (4)$$

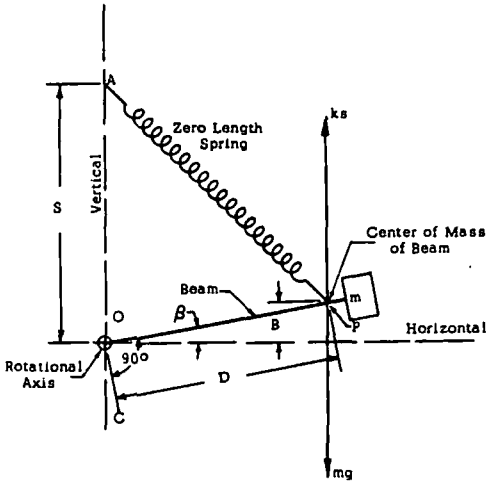

Fig. 2. Diagram of LaCoste and Romberg gravity meter.

Gravity can be determined correctly from (4) provided that z'', S, and B and its derivatives are known; however, if f_v, k_v, and c_v are neglected, an erroneous value g_e of gravity will be obtained. g_e is given by

$$g_e + z'' + bB'' + f_0B' + k_0B - c_0S = 0 \tag{5}$$

Combining (4) and (5) gives the error e in g_e as

$$e = g_e - g = f_eB' + k_eB - c_eS \tag{6}$$

To evaluate (6) the coefficients must be known. They all can have a term proportional to z'' because the forces caused by vertical acceleration can alter the geometry of the gravity meter. The coefficient f can also contain terms proportional to B and B' because the damping can depend on the position of the damping device and its velocity relative to the gravity meter case. k_v can include a term proportional to B but it is not likely to include a term proportional to B', although such a term could easily be included and would be found to have no effect on the average error. c_v can include a term proportional to S. For convenience S will be expressed as the sum of its average value $\langle S\rangle$ plus a variable term S_v, whose average value is zero. Equation 6 then becomes

$$e = (f_1z'' + f_2B + f_3B')B' + (k_1z'' + k_2B)B - (c_1z'' + c_2\langle S\rangle + c_2S_v)(\langle S\rangle + S_v) = 0 \tag{7}$$

Some of the terms of (7) can be neglected. For instance, the average value of f_2BB' can be shown to be negligible. Consider B to be expressed as a Fourier series. Then for each frequency B and B' will differ in phase by 90°, and therefore the average value of the product will be zero. Also the average value of the products of different frequencies will be zero. The average value of $\langle S\rangle z''$ will be zero on a ship because $\langle S\rangle$ is a constant and the average value of z'' must be zero. The average value of $\langle S\rangle S_v$ is zero because $\langle S_v\rangle$ is zero. The term $c_2\langle S^2\rangle$ will be dropped because it does not involve z'', and therefore it is presumably taken care of in the static calibration of the gravity meter. Equation 7 then gives for the average error

$$\langle e\rangle = \langle (f_1z'' + f_3B')B'\rangle + \langle (k_1z'' + k_2B)B\rangle - \langle (c_1z'' + c_2S_v)S_v\rangle = 0 \tag{8}$$

For particular types of gravity meters, (8) can be simplified as follows. If S is not varied while a reading is taken, the terms involving S_v will of course be zero. If S is varied by means of a servo, S_v will be approximately proportional to z'', or $S_v = S_2\, z''$. Also, if the gravity meter is highly damped, B' will be approximately proportional to z'', or $B' = K\, z''$. The preceding relation is accurately satisfied if the gravity meter has infinite sensitivity; i.e., $k = 0$. If the preceding relations are introduced into (8) and it is noted that $\langle z'\, z''\rangle$ is zero because z' and z'' are 90° out of phase (as was shown for $\langle B'\, B\rangle$), then (8) gives

$$\langle e\rangle = (f_1K + f_3K^2 - c_1S_2 - c_2S_2^2)\langle z''^2\rangle + k_2K^2\langle z'^2\rangle \tag{9}$$

For a LaCoste and Romberg shipboard gravity meter some further simplifications can be made. In this gravity meter the servo controlling S is so slow

that it varies S only a few milligals in response to wave accelerations; therefore, the constant S_2 can be taken as zero. Also, the coefficient k is so close to a constant that the term kB in (3) contributes less than 1 mgal over the entire range of B; therefore, k_2 can be taken as zero. Equation 9 for a LaCoste and Romberg meter then becomes

$$\langle e \rangle = (f_1 K + f_3 K^3)\langle z''^2 \rangle \tag{10}$$

Equation 10 was determined empirically in the laboratory for LaCoste and Romberg gravity meters before it was derived theoretically. It was found to hold accurately. Of course the attempt is made to adjust each gravity meter so that the vertical acceleration error is zero before the gravity meter is put into operation, but (10) shows that it is possible to correct data for vertical acceleration error even if the adjustment has not been made accurately enough. More will be said about such corrections later.

It is probably worth while to consider an example of nonlinearity in order to see how much is required to cause a 1-mgal error at 0.1-g rms vertical acceleration. In this example k will be taken as zero, cS will be taken equal to g, and B'' will be neglected. It is permissible to neglect B'' in actual overdamped gravity meters unless readings are taken in times much shorter than 1 sec. If f is taken equal to $f_0 + f_3 B'$, equations 3 and 7 give, respectively,

$$\langle (f_0 + f_3 B')B' \rangle = \langle -z'' \rangle = 100{,}000 \text{ mgal} \tag{11}$$

and

$$\langle e \rangle = f_3 \langle B'^2 \rangle = 1 \text{ mgal} \tag{12}$$

Combining (11) and (12) gives

$$f_3 \langle B' \rangle / f_0 = 1/99{,}999 \tag{13}$$

This equation states that the damping coefficient can not vary more than one part in 99,999 over a damper velocity range corresponding to a vertical acceleration range of 0 to 0.1 g. This is a very high linearity. Also, for a 0.2-g vertical acceleration, the permissible variation would be only half as much over twice the range; this corresponds to reducing the nonlinearity constant f_3 to one-fourth.

Another effect of large vertical accelerations is that they tend to cause the moving element of the gravity meter to exceed its permissible range, which is determined by mechanical hysteresis errors in the spring. Methods of reducing the motion of the gravity responsive element will be discussed later when describing the different types of gravity meters.

Horizontal Accelerations

Introduction. Since gravity meters operating on moving platforms are subjected to horizontal accelerations as well as to vertical accelerations, their effect must also be taken into account. Two methods have been used in the past: one method is to suspend the gravity meter from a gimbal joint and to correct for the swinging; the second method is to mount the gravity meter on a stabilized platform. The gimbal method was first put into practice by *Vening Meinesz*

[1941]. Until 1965 this method was used on LaCoste and Romberg gravity meters. It now appears that the stabilized platform method is considerably better, but, since so much work has been done and is still being done with gimbal suspensions, it seems worth while to discuss the principle in detail and to make comparisons between it and the stabilized platform method. There are striking similarities and some basic differences.

Gimbal suspension. A gravity meter suspended from a gimbal joint is shown in Figure 3. The gimbal joint is at 0; the center of gravity of the suspended system is at G; and the sensing element of the gravity meter (the mass) is at P. For long-period accelerations it can be seen that the gravity meter measures the vector sum of gravity plus the negative of the horizontal acceleration as indicated in the vector diagram in Figure 3. A solution of the vector triangle gives the gravity meter measurement as

$$g_a \doteq g + g\theta^2/2 \tag{14}$$

where g = gravity. This equation is known as the Browne correction [*Browne*, 1937] or the horizontal acceleration correction, and it has been found to be adequate for the motions encountered in submerged submarines. For motions occurring on a surface ship, *LaCoste and Harrison* [1961*a*] have made a more comprehensive analysis in which simultaneous horizontal and vertical accelerations were considered. The analysis included fourth-order terms, and it showed that (14) was correct up to the fourth order provided that the distance l is the length of a simple pendulum having the same period as the gimbal supported gravity meter. The mathematics is as follows.

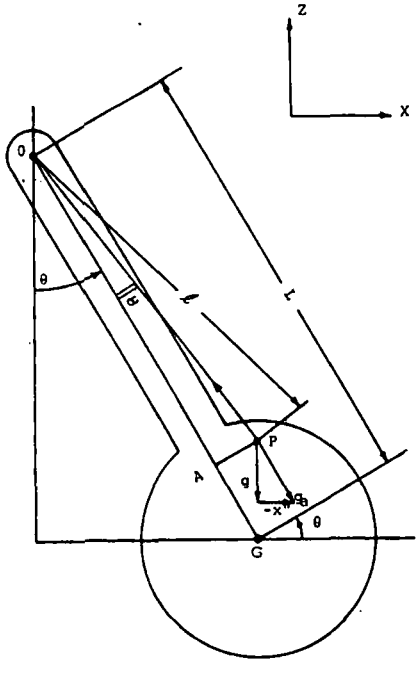

Fig. 3. Gimbal suspended gravity meter.

In Figure 3 we will let $0P = l$, $\angle\ 0AP = 90°$, and the free period of the gimbal system be $T_G = 2\pi/w_G$. The point 0 is subjected to periodic horizontal and vertical accelerations x'' and z''. Then the equation of motion of the gimbal system is

$$\theta'' + F\theta' + w_G^2(1 + z''/g) \sin \theta + w_G^2(x''/g) \cos \theta = 0 \tag{15}$$

where F is a damping coefficient. The force per unit mass at P parallel to 0G is

$$g_a = l\theta'^2 \cos \alpha - x'' \sin \theta + (g + z'') \cos \theta + l\theta'' \sin \alpha \tag{16}$$

and the force per unit mass at P perpendicular to G0 is

$$a_a = l\theta'^2 \sin \alpha - x'' \cos \theta - (g + z'') \sin \theta - l\theta'' \cos \alpha \tag{17}$$

If (15) is solved for x'' and the result is substituted into (16) and (17), we obtain

$$g_a = l\theta'^2 \cos \alpha + l\theta'' \sin \alpha + (g/w_G^2) \tan \theta[\theta'' + F\theta' + w_G^2(1 + z''/g) \sin \theta] + (g + z'') \cos \theta \tag{18}$$

and

$$a_a = l\theta'^2 \sin \alpha - l\theta'' \cos \alpha + (g/w_G^2)(\theta'' + F\theta') \tag{19}$$

Expanding (18) in powers of θ, we obtain

$$g_a = l(\theta'^2 \cos \alpha + \theta'' \sin \alpha) + (g/w_G^2)(\theta\theta'' + \theta^3\theta''/3 + F\theta\theta' + F\theta^3\theta'/3) + g(1 + \theta^2/2 + 5\theta^4/24) + z''(1 + \theta^2/2) \tag{20}$$

neglecting fifth-order terms in θ, its derivatives, and z''.

Since we are interested in obtaining average gravity values over several minutes, we can take θ in (12) as the Fourier series

$$\theta = \sum_i B_{s,i} \sin w_i t + \sum_i B_{c,i} \cos w_i t. \tag{21}$$

If we then take averages over a length of time that is long compared with the periods in the Fourier series and if we note that $\langle z'' \rangle = 0$ on a ship and that $\langle \theta\theta'' \rangle = \langle -\theta'^2 \rangle$, we obtain from (20)

$$\langle g \rangle = \langle g_a \rangle - \tfrac{1}{2}g\langle \theta^2 \rangle - (l \cos \alpha - g/w_G^2)\langle \theta'^2 \rangle - \tfrac{5}{24}\langle g\theta^4 \rangle - \tfrac{1}{3}(g/w_G^2)\langle \theta^3\theta'' \rangle - \tfrac{1}{2}\langle z''\theta^2 \rangle \tag{22}$$

In (22) we note that there is a second-order correction term in $\langle \theta^2 \rangle$ and another in $\langle \theta'^2 \rangle$. The latter can be eliminated by taking $l \cos \alpha = g/w_G^2$, which is the length of a simple pendulum having the same period as the gimbal suspended system. Equation 22 then becomes

$$\langle g \rangle = \langle g_a \rangle - \tfrac{1}{2}\langle g\theta^2 \rangle - \tfrac{5}{24}\langle g\theta^4 \rangle - \tfrac{1}{3}(g/w_G^2)\langle \theta^3\theta'' \rangle - \tfrac{1}{2}\langle z''\theta^2 \rangle \tag{23}$$

The second-order correction term is the same as the Browne correction term given in (14). It is the only term that is normally used, but to make this possible, the distance $l \cos \alpha$ is carefully adjusted to equal g/w_G^2. This adjustment is made

by carefully testing the gimbal-supported gravity meter while it is being subjected to controlled horizontal accelerations. The final results must be independent of $\langle\theta'^2\rangle$ or independent of the period of the accelerations.

LaCoste and Harrison [1961a] have investigated the effect of the fourth-order terms is (23) for x'' and z'' equal to 50 gals and found that these terms contributed about 3 mgal. Therefore, fourth-order terms should be taken into account even below this acceleration if very high accuracy is desired. The fourth-order terms plus the need for high accuracy in computing large second-order terms make analog computers unsatisfactory at high accelerations. Replacing analog computors with digital computers would solve the problem but would unduly complicate the system.

It should be noted that (23) is independent of F, the damping in the gimbal suspension. It will appear later, however, that such damping will cause an error due to cross coupling between horizontal and vertical accelerations. For this reason the gimbals are always undamped, and resonance is avoided by the scheme shown in Figure 4. There the undamped gimbal suspension is shown supported at b by a *damped* gimbal, which is supported on the ship at a. The motion at b is not quite the same as that of the ship at a, but the corrected gravity reading is independent of any differences. On the other hand, the damping in the upper support absorbs energy from both pendulums and thereby limits resonant motion.

An important feature of the gimbal supported gravity meter is that the suspension can be made so that no forces are exerted on the gravity meter weight except along the sensitive axis of the gravity meter regardless of the motion of the gimbal support. This requires that $l \cos \alpha$ be made equal to g/w_G^2, which is always done. Then (19) becomes

$$a_n = (g/w_G^2)(\theta'^2 \tan \alpha + F\theta') \tag{24}$$

By making $\alpha = 0$ and $F = 0$, the acceleration a_n normal to the sensitive axis of the gravity meter becomes identically zero. This parameter choice simplifies the gravity meter design by eliminating any need to make the meter capable of withstanding such forces; it is a distinct advantage of the system. A second ad-

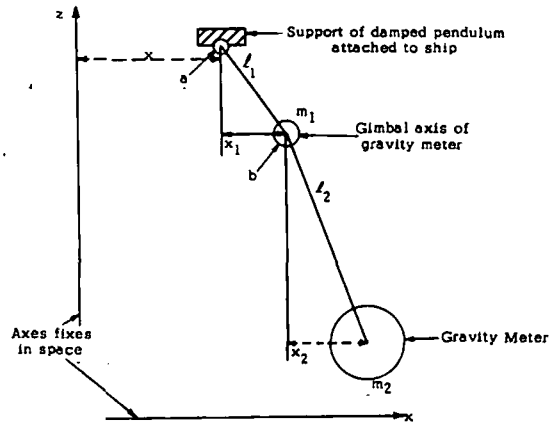

Fig. 4. Damping scheme for gimbal suspended gravity meter.

vantage of making a_n identically equal to zero is that it eliminates cross-coupling errors, which will be considered later. Actually cross-coupling errors can be made negligible by merely making $F = 0$.

To determine the Browne correction given in (14) or the correction given in (23), it is necessary to measure θ; this measurement requires a stabilized reference. The stabilized reference used by *Vening Meinesz* [1941] consisted of an approximately horizontal inertia bar supported for oscillation on knife edges very close to its center of gravity. The inertia bar had a 25- to 30-sec oscillation period, which was long enough to serve as a stabilized reference in a submarine where the accelerations were small. The LaCoste and Romberg gimbal-type gravity meters have used a refined version of this long-period pendulum [*LaCoste* 1960]. In it the knife edges are replaced by a fine wire suspension, as indicated in Figure 5. The restoring forces exerted by the fine wire suspension are approximately counterbalanced by the labilizing spring shown. Also, the box supporting the horizontal bar is rotated by a servo to almost eliminate relative motion between the box and the inertia bar. This further reduces the restoring forces exterted by the wires suspending the bar. The servo support is fixed to the swinging gravity meter, and therefore the angular rotation of the servo is a measure of θ.

Obviously, gyros can also be used for stabilized references. The main reason that they have not been used with gimbal-supported gravity meters is that until a few years ago the estimated lives of good gyros was only 1000 hours. Because good gyros with estimated lives of 1½ years are now available, they should be used with either gimbal or stabilized platform gravity meters because they have more than adequate accuracy, whereas the performance of long-period pendulums is marginal.

The main disadvantages of the long-period pendulums are that vibration or large accelerations can cause interference between moving and fixed parts and

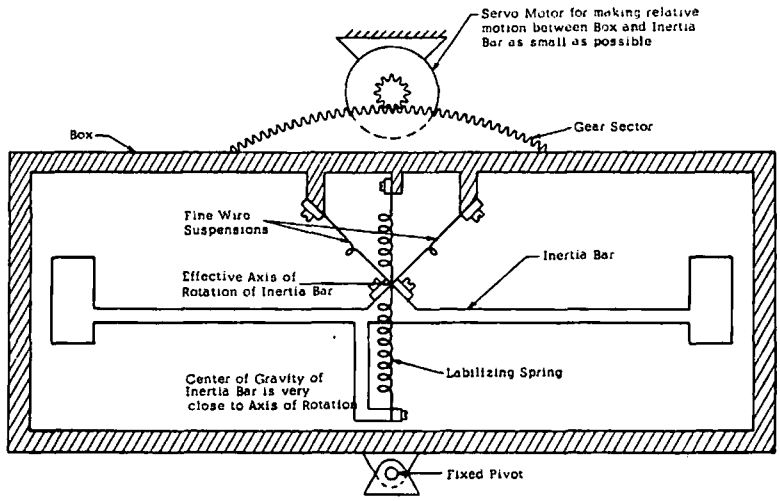

Fig. 5. Long-period inertia bar vertical reference.

that an operator must check them and their servos regularly to keep them in good adjustment. Long-period pendulums are normally operated at periods of 2 min, which appears to be sufficiently long on a ship traveling on a straight line but which is short for airplane work. They also have a slight nonlinearity which causes them to give a slight indication proportional to changes in wave amplitude, but this effect has been made almost negligible up to accelerations of 0.05 g in late models. Their performances can certainly be improved further, but this refinement is not worth while since gyro life is now adequate.

An important element in gravity meter accuracy is the accuracy of the stabilized reference. The effect of an error e in the reference can be determined as follows. Equation 14 gives the Browne correction that must be subtracted from the gravity meter reading as $g\theta^2/2$. If an angle $(\theta - e)$ is substituted into this formula in place of θ, the error in gravity will be

$$\begin{aligned} e_g &= g_a - g(\theta - e)^2/2 - g_a + g\theta^2/2 \\ &= g\theta e - ge^2/2 \end{aligned} \tag{25}$$

Equation 25 can be simplified by making use of the differential equation of the gimbal suspended gravity meter:

$$l_0\theta'' + g\theta = -x_G'' \tag{26}$$

where $l_0 = g/w_G^2$ is the length of a simple pendulum having the same period as the gimbal suspension and x''_G is the horizontal acceleration at the gimbal joint. Equation 26 can be written as

$$-g\theta = x_G'' + l_0\theta'' \tag{27}$$

The right side of (27), however, is the horizontal acceleration x'' at the gravity meter, which is always placed a distance l_0 below the gimbal joint. Therefore (25) becomes

$$e_g = -x''e - ge^2/2 \tag{28}$$

It will later be shown that (28) is also the error equation for a stabilized platform.

The last term of (28) refers to steady-state errors or to random errors. For a 1-mgal accuracy in gravity measurement this term requires an accuracy in the stabilized reference of 5′. The first term, however, depends not only on the stabilized reference error but also on the magnitude of the horizontal acceleration and on the correlation between the two. For example we will consider a sinusoidal horizontal acceleration x'' of amplitude 0.05 g. For a 1-mgal accuracy this limits the permissible sinusoidal error in e to an amplitude of 8″ in phase with x''. This is not an easy requirement to meet. Laboratory and sea tests indicate, however, that long-period pendulums very nearly satisfy it and the other requirement for accelerations up to about 0.05 g.

Stabilized platform. The second method of handling horizontal accelerations is to mount the gravity meter on a stabilized platform as shown in Figure 6. To determine what accuracy is required in the stabilized platform, it is neces-

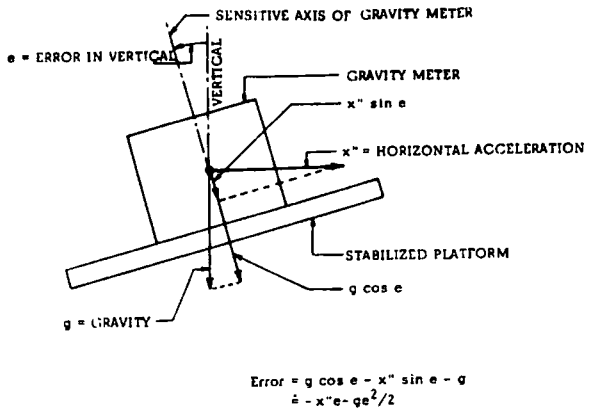

Fig. 6. Gravity meter on stabilized platform.

sary to find out how the gravity reading is affected by errors in verticality [*LaCoste*, 1959]. In Figure 6 the sensitive axis of the gravity meter is shown to be off level by an angle e. The error in measuring gravity is then

$$e_g = g \cos e - x'' \sin e - g \tag{29}$$

or

$$e_g \doteq -x''e - ge^2/2 \tag{30}$$

Equation 30 is exactly the same as equation 28, which gives the error for a gimbal suspended gravity meter after the Browne correction has been made. It is therefore apparent that the two systems are mathematically equivalent up to fourth-order terms.

The stabilized platform accuracy requirements given by (30) for a 1-mgal accuracy can easily be satisfied for horizontal accelerations of 0.1 g if good gyros are used and if proper precautions are taken in the design of the stabilized platform. The major precautions will be discussed later. Steady-state and long-period verticality errors have been checked at sea by comparison with oil filled levels when the ship was traveling in a straight line, and these errors were found to be less than 1′, which is considerably less than the 5′ requirement for 1-mgal accuracy. It is difficult to check directly the component of stabilized platform error in phase with the horizontal acceleration, because this check would require an extremely accurate additional vertical reference. The accuracy that has been achieved in laboratory and sea tests shows, however, that the requirements have been satisfied.

The operation of the stabilized platform is indicated in the block diagram of Figure 7. This figure shows only one of the two required vertical erecting units. Each of the two units can operate from a single-axis gyro, or the two units can both operate from a two-axis gyro. In the unit shown the gyro controls a servo amplifier and motor that makes the platform follow the gyro. This feedback loop is not sufficient, however, to ensure verticality of a reference line on the platform because: (1) the reference line might not have been vertical to begin with, (2) gyros have some drift, and (3) the earth rotates and gyros tend to remain fixed in space. To attain verticality it is necessary to mount accelerom-

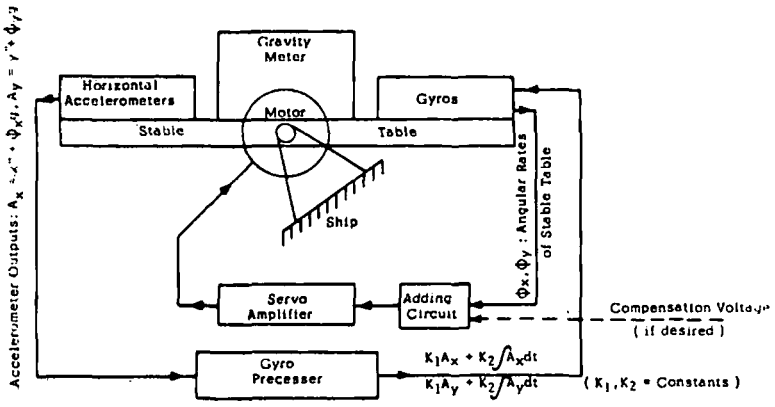

Fig. 7. Block diagram of stabilized platform.

eters (or levels) on the platform as shown and to use them in the second feedback loop. If the accelerometers do not indicate level, they put out error signals. A function of each error signal is fed to the corresponding gyro to precess it gradually to bring the reference line on the platform to vertical.

The simplest function of the accelerometer error signal to feed to the gyro is a constant times the error. This gives the gyro precession rate in space as

$$\phi' = -k_a(\phi + x''/g) \tag{31}$$

where $(\phi + x''/g)$ is the accelerometer error signal and k_a is a constant. Since ϕ represents the angular position of the stabilized platform, (31) is the differential equation for the assumed accelerometer feedback for the stabilized platform. An inspection of (31) will show that it does not represent very good stabilized platform behavior. For one thing ϕ will have to match the corresponding component of the earth's rotation in order for the platform to remain fixed relative to the earth. This will mean that the error signal $(\phi + x''/g)$ must differ from zero and there will be an error in platform verticality. Although this error can be adjusted out, the adjustment has to be changed whenever the platform is rotated about the vertical. A similar error is produced by gyro drift. Furthermore, it can be shown that long-period wave motions cause greater errors with this simple type of accelerometer feedback than with some other types of feedback.

A better type of signal to feed to the gyro is a constant times the accelerometer output plus a constant times its integral. This expression gives for the equation of motion of the platform

$$\phi' + 2fw_0\left(\phi + \frac{x''}{g}\right) + w_0^2 \int \left(\phi + \frac{x'''}{g}\right) dt = 0 \tag{32}$$

or

$$\phi'' + 2fw_0(\phi' + x'''/g) + w_0^2(\phi + x''/g) = 0 \tag{33}$$

It should be noted that the integral term in (32) eliminates errors in ϕ due to

rotation of the earth. Also, an inspection of (33) will show that it is the differential equation for a pendulum. The period is determined by the amount of integral feedback, and the damping is determined by the amount of ordinary feedback. It is interesting that there is mathematical equivalence between this type of stabilized platform and the long-period pendulums used with gimbal suspended gravity meters.

We will now determine permissible accelerometer feedback constants for the stabilized platform by means of the stabilized platform equation (33) and the error equation (30). We will consider a sinusoidal x'' of circular frequency w and will examine the steady-state solution of (33). We can then take $\phi = \phi_0 e^{iwt}$. Substituting this expression into (33) gives

$$\phi = -\frac{w_0^2 + i2fw_0w}{w_0^2 - w^2 + i2fw_0w}\left(\frac{x''}{g}\right) \tag{34}$$

For perfect operation ϕ should be identically equal to zero; therefore, the value of ϕ given in (34) represents the error e in (30), or $\phi = e$. The average value of the second term in (30) then becomes

$$\begin{aligned}\frac{-g\langle e^2\rangle}{2} &= -\left|\frac{w_0^2 + i2fw_0w}{w_0^2 - w^2 + i2fw_0w}\right|^2\left(\frac{\langle x''^2\rangle}{2g}\right) \\ &= -\frac{w_0^4 + 4f^2w_0^2w^2}{w_0^4 + 2w_0^2w^2(2f^2 - 1) + w^4}\left(\frac{\langle x''^2\rangle}{2g}\right)\end{aligned} \tag{35}$$

In the first term of (30) only the component of e (or ϕ) that is in phase with x'' is of significance. This component is the real part of the coefficient of x'' in (34). The average value of the first term therefore becomes

$$-\langle x''e\rangle = \frac{w_0^4 + w_0^2w^2(4f - 1)}{w_0^4 + 2w_0^2w^2(2f^2 - 1) + w^4}\left(\frac{\langle x''^2\rangle}{g}\right) \tag{36}$$

Adding (35) and (36) gives

$$\langle e_o\rangle = \frac{(w_0/w)^4 + 2(2f^2 - 1)(w_0/w)^2}{(w_0/w)^4 + 2(2f^2 - 1)(w_0/w)^2 + 1}\langle x''^2/2g\rangle \tag{37}$$

Equation 37 shows that the error is small only when w_0/w is small, or when the wave frequency is considerably greater than the natural frequency of the stabilized platform. The equation also shows that in such cases the error can be decreased by making $2f^2 - 1 = 0$, which corresponds to making the damping $1/\sqrt{2}$ times critical. This has been done for several years on all gimbal supported gravity meters and on LaCoste and Romberg stabilized platform gravity meters. Equation 37 then becomes

$$\langle e_o\rangle = \frac{(w_0/w)^4}{(w_0/w)^4 + 1}\langle x''^2/2g\rangle \tag{38}$$

To show how (38) limits the stabilized platform parameter w_0, (38) is plotted in Figure 8 for three different values of w_o (= 2π/ natural period of the stabilized platform) and for a horizontal acceleration $x'' = 0.1\ g \sin wt$. The curves show

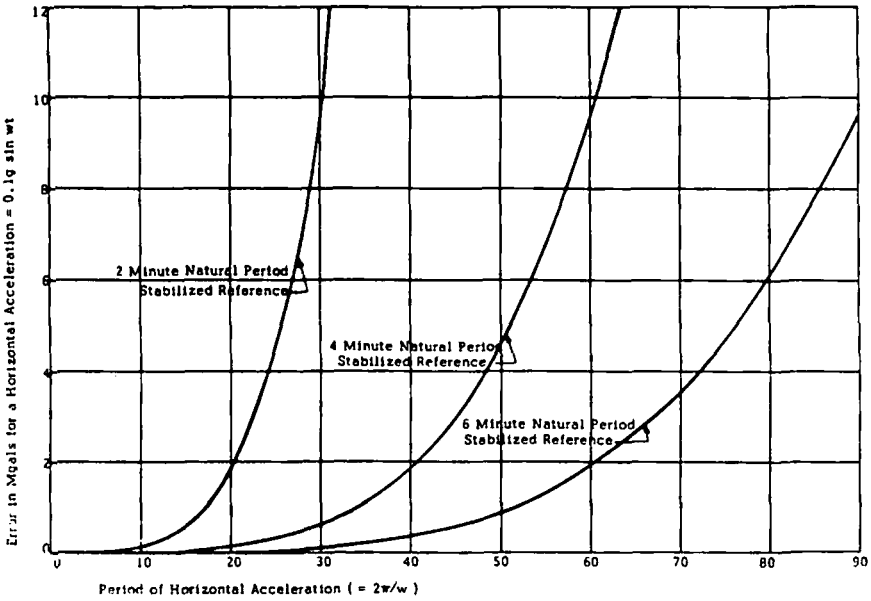

Fig. 8. Variation of gravity meter error with period of horizontal accelerations and period of stabilized reference for $1/\sqrt{2}$ times critical damping of stabilized reference.

that for a stabilized platform with a 2-min period the error is less than 1 mgal for period shorter than 17 sec. Ocean waves have appreciable amplitudes at periods longer than 17 sec, but they do not often have amplitudes as high as 0.1 g at such periods; therefore, a 2-min period stabilized reference can be used. For a horizontal acceleration of 0.05-g amplitude, a 2-min platform would operate up to a wave period of 24 sec with only a 1-mgal error, since the error varies with the square of the acceleration. Another indication that a 2-min period stabilized reference can be used is that gimbal supported gravity meters gave good results with stabilized references of that period.

In order to have some factor of safety the stabilized platforms used with LaCoste and Romberg gravity meters were designed with 4- and 6-min periods and with a selector switch for setting the period. The selector switch makes it possible to change from one period to the other during a run to determine whether the period has an effect on the gravity reading. In actual tests at sea no difference was found; therefore, either period appears to be adequate. The curves in Figure 8 show that for a 4-min stabilized reference the error is within 1 mgal for horizontal accelerations of periods less than 35 sec and amplitudes of 0.1 g. It is very unlikely that ocean waves have amplitudes as high as this at periods as long as 35 sec.

The preceding discussion has dealt with the effects of horizontal accelerations produced by ocean waves. However, horizontal accelerations are also produced when the ship (or plane) does not travel in a straight line at constant speed. To make such accelerations negligible, it is general practice to use an automatic pilot and in all cases the ship (or plane) is run in as straight a

line as is practical and as close to constant speed as is feasible. There are, of course, deviations in both course and speed, and such deviations can have periods longer than the periods of ocean waves. To estimate the magnitude of the errors produced by deviations of the ship's track from a straight line (fishtailing), we will assume that the ship travels along a sinusoidal path whose deviation from a straight line is

$$y = D \sin 2\pi t/T \tag{39}$$

where T = the period. The resulting horizontal acceleration is

$$y'' = -(4\pi^2 D/T^2) \sin 2\pi t/T \tag{40}$$

Substituting (40) into (38) gives

$$D^2 = g\langle e_s \rangle (T^4 + T_0^4)/4\pi^4 \tag{41}$$

Equation 41 is plotted in Figure 9 for a 1-mgal error and for stabilized platform periods of 2, 4, and 6 min. The 2-min curve at short periods shows a permissible lateral ship motion of ±24 feet. For a 4-mgal error the permissible lateral amplitude is twice as great. Since accuracies of 1–4 mgal have been obtained with gimbal supported gravity meters using 2-min stabilized references, it appears that lateral ship motion resulting from imperfect steering can be kept under ±48 feet and probably under ±24 feet. The 4-min curve in Figure 9 shows a permissible lateral amplitude of ship motion of ±95 feet, which can easily be achieved, and the 6-min curve shows a permissible amplitude of over ±200 feet.

Good accuracy has been obtained in airplane gravity work with 1- and 2-min stabilized references [*Thompson and LaCoste*, 1960; *Nettleton, LaCoste, and Harrison*, 1960; *Nettleton, La Coste, and Glicken*, 1962] provided that the

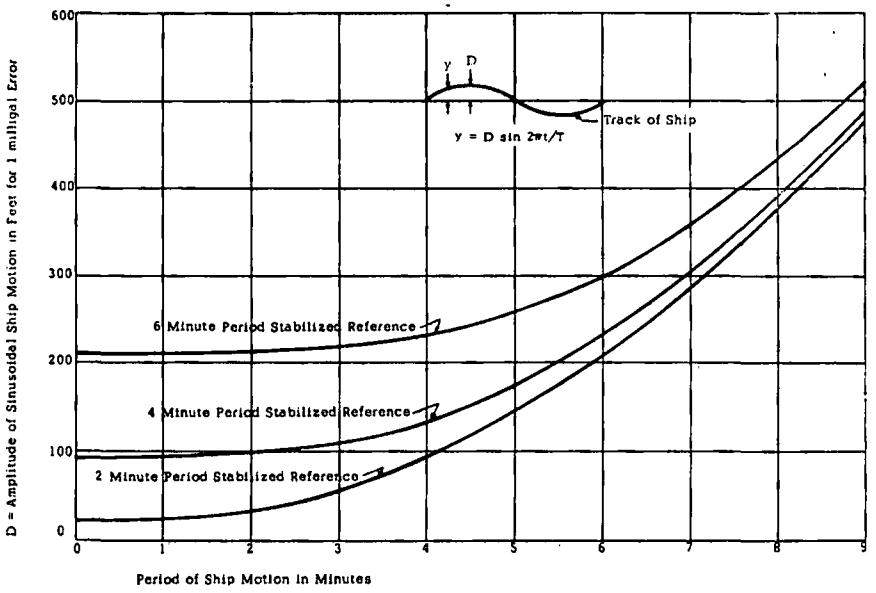

Fig. 9. Gravity meter errors for various sinusoidal ship tracks.

automatic pilot was carefully adjusted, provided that the air was relatively smooth, and provided that course changes were not made. In the tests described in the first two of the above references the automatic pilot had a hunting frequency of about 1 min when the plane flew north, which resulted in large errors. The problem with the automatic pilot was overcome before making the tests described in the third reference, but errors then occurred when the air became somewhat turbulent and when course changes of approximately one degree were made. Such errors could of course have been made negligible by using 4- or 6-min period stabilized references, but it was also found possible to correct for them by the following method.

The correction is based on (38), which gives the error for any frequency. To use this equation it is necessary to have approximate (or accurate) data on the horizontal accelerations. Such data are normally obtained and recorded. Their accuracy, of course, is limited by the accuracy of the stabilized references and therefore is somewhat in error at the long periods being considered, but they are accurate enough to make a good first-order correction. In the case being considered the computations required by (38) were performed by an analog computer. The analog computer consisted of the actual vertical references used in the airplane tests. The horizontal accelerations were applied to the vertical references as tilts rather than as accelerations. It was possible to estimate the accuracy of the corrections by comparing corrected gravity values obtained during course changes with gravity values obtained just before and just after such times. In all cases the gravity data were smooth, and the corrected gravity data were found to be nearly as accurate as those obtained in smooth air when no course changes were made.

There are also other ways in which (38) can be used to make corrections for too short a period in the vertical reference. For instance, data on horizontal accelerations might be obtained from inertial navigation, Doppler radar, or photography if such data are sufficiently accurate. Of course, it is preferable to use adequate periods in the vertical references, but even in this case (38) can be used to check on the adequacy of the periods.

Errors due to inadequate leveling of the gravity meter can also be caused by such things as dead space, hysteresis or too slow a response in the accelerometers, gyros, or servo motors controlling the stabilized platform. Errors can also occur if the sensitive axis of the gravity meter is affected by horizontal or vertical accelerations rather than being in a fixed direction on the gravity meter, as was assumed in the derivation of (30). Evidence that horizontal accelerations or forces can affect the sensitive axis of a gravity meter was given by Alan Goodacre in a private communication. Goodacre's experiments showed slight discrepancies between tilt-table calibrations of gravity meters and other types of calibration. It will also be shown later that the so-called inherent type of cross-coupling effect can be considered as a special case of off- leveling error resulting from shifting of the sensitive axis of the gravity meter when it is subjected to vertical accelerations.

To compensate for errors of the type mentioned in the preceding paragraph, it is possible to add a slight tilt to the gravity meter relative to the stabilized

platform. One method of doing this is indicated in Figure 7. A correction voltage is added to the gyro output, and the sum is fed to the corresponding servo motor. In L&R (LaCoste and Romberg) gravity meters the magnitude of the compensating voltage and its possible dependence on period are determined from tests made on a testing machine that subjects the complete gravity meter system to horizontal accelerations of various amplitudes and periods.

In the previous discussion it has been intimated that it is adequate to use platforms that are stabilized in roll and pitch but not stabilized about the vertical axis. Actual tests indicate that such two-axis stabilization is sufficient for approximately straight line motion of the ship or airplane at constant speed. There are, however, some advantages to be gained by stabilization also about the vertical, as can be seen from the following considerations. In a two-axis system, it is necessary for the sensitive axes of the two gyros to be accurately horizontal; otherwise, rotation about a vertical axis (ship yaw) will affect them in the same way that roll or pitch does. This effect will produce errors in the verticality of the platform. Furthermore, such verticality errors will be in phase with yaw and therefore probably well correlated with horizontal accelerations. Such correlation can produce substantial errors, as shown in (30); therefore, accuracy depends to a considerable extent on the accuracy with which the sensitive axes of the gyros are set.

Since it is impossible to set the sensitive axes of the gyros perfectly, it might be advantageous to stabilize the platform also about the vertical. Furthermore, to initially set the sensitive axes of the gyros accurately, it is necessary to make tests by rotating the entire stabilized platform about the vertical to determine the effect of the rotation. Since a turntable for making this test is not normally available at sea, there is a serious problem in changing gyros at sea unless their sensitive axes are accurately adjusted for uniform orientation in the gyro cases. In view of these considerations a stabilized vertical axis is being provided for LaCoste and Romberg stabilized platform gravity meters. This design has not yet been used at sea and might prove to be more trouble than it is worth, but a test should be made. Long-term vertical stabilization to a definite compass direction is not required; therefore, the LaCoste and Romberg device will be slowly precessed to a fixed direction on the ship.

Until now there has been no need to make gravity observations when traveling in any way other than a straight line at constant velocity. Therefore, there has been no need to use a stabilized platform any more sophisticated than the ones previously described. If, however, the need should ever arise, it is possible to measure gravity when moving in a curved path at nonconstant speed by using what is known as a Schuler tuned stabilized platform. Such a platform is used in inertial guidance; it has the property of remaining vertical regardless of the motion of the ship or airplane. Since there might be reason to use such a platform at some time, a brief description of its principles might be worth while.

In Figure 10 we will assume that the Schuler platform is at A and that it moves to B over the surface of the earth. We will let the angle ϕ denote the direction in space of a reference line on the platform. If the platform is stabilized as the previously described stabilized platforms were, its differential equation

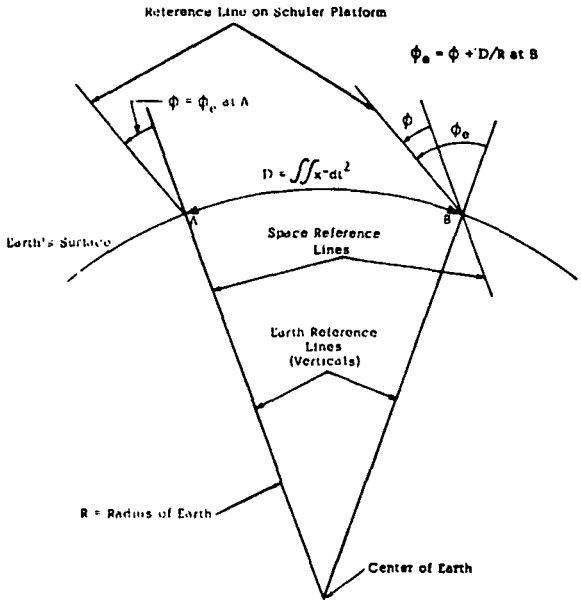

Fig. 10. Diagram for derivation of Schuler stabilized platform equations.

will be given by (33) for an earth of infinite radius. To take into account the finite radius of the earth, (33) must be changed to

$$\phi'' + 2fw_0\left(\phi' + \frac{1}{R}\int x''\,dt + \frac{x'''}{g}\right) + w_0^2\left(\phi + \frac{1}{R}\iint x''\,dt^2 + \frac{x''}{g}\right) = 0 \qquad (42)$$

where R is the radius of the earth.

We wish to use a direction normal to the surface of the earth (vertical) as a reference rather than a direction fixed in space. If we designate angles referred to such a vertical reference by ϕ_e, then ϕ_e will be given by

$$\phi_e = \phi + \frac{1}{R}\iint x''\,dt^2 \qquad (43)$$

Substituting (43) into (42) gives

$$\phi_e'' - x''/R + 2fw_0(\phi_e' + x'''/g) + w_0^2(\phi_e + x''/g) = 0 \qquad (44)$$

It is desired to make (44) independent of x'', which can be done by taking $f = 0$ and

$$w_0 = \sqrt{g/R} \qquad (45)$$

Equation 44 then becomes

$$\phi_e'' + (g/R)\phi_e = 0 \qquad (46)$$

A stabilized platform satisfying these conditions is known as a Schuler tuned stabilized platform.

The characteristics of the Schuler platform follow from the preceding equations. Equation 46 shows the behavior of ϕ_e, which is the angle between the

stabilised platform and the earth's vertical at the point at which the platform happens to be. We note that, if ϕ_e and ϕ_e' are initially zero, ϕ_e will remain identically zero regardless of any horizontal accelerations. Therefore, a Schuler platform will operate satisfactorily for any ship or airplane motion.

There are difficulties in making and operating a Schuler stabilized platform, and therefore it should not be used unless it is needed. Some of the difficulties are as follows: The period of the Schuler platform is given by (45); it is $2\pi/w_0 = 2\pi\ (R/g)^{\frac{1}{2}}$, which is about 84 min. To attain this very long period, it is necessary to use very accurate gyros and accelerometers and to adjust the system very accurately. Furthermore, (46) shows that the system is undamped, and therefore its initial conditions must be carefully controlled to prevent oscillation. Oscillations are also caused by gyro drift and accelerometer imperfections. A Schuler platform requires accurate stabilization about the vertical axis as well as about the two horizontal axes. For these reasons a Schuler tuned stabilized platform has both a high initial cost and a high maintenance cost.

It has been mentioned that in the L&R stabilized platform the damping is adjusted to $1/\sqrt{2}$ times critical. The importance of this adjustment can be demonstrated by comparing the performance of such a stabilized platform with one in which the precessing signal to the gyro is equal to a constant times a filtered signal from the accelerometer. For a single-stage filter the precession rate is given by

$$s\phi = -k_a(\phi + x''/g)w_1/(s + w_1) \tag{47}$$

where s is the Laplace operator. To evaluate the platform (47) can be treated similarly to the way in which (32) was treated. This will determine the resulting error in gravity reading as a function of the period of the horizontal accelerations.

Differentiating (47) gives

$$s^2\phi + sw_1\phi + k_aw_1(\phi + x''/g) = 0 \tag{48}$$

Equation 48 is a second-order equation that is fairly similar in form to the equation for the L&R stabilized platform (and to the equation for the long-period pendulum references). It differs in having no term in x'''. Writing (48) in the standard form of (33) gives

$$\phi'' + 2fw_0\phi' + w_0^2(\phi + x''/g) = 0 \tag{49}$$

If the same analysis is applied to (49) that was applied to (33), the resulting average error becomes

$$\langle e_v' \rangle = \frac{(w_0/w)^4 - 2(w_0/w)^2}{(w_0/w)^4 + 2(w_0/w)^2(2f^2 - 1) + 1} \langle x''^2/2g \rangle \tag{50}$$

For frequencies considerably higher than the natural frequency, (50) becomes approximately

$$\langle e_v' \rangle \doteq -2(w_0/w)^2\langle x''^2/2g \rangle \tag{51}$$

which is the approximate expression for (37) for the L&R stabilized platform for the case of no damping. If, however, the damping constant f in (37) is taken equal to the optimum value $1/\sqrt{2}$, $\langle e_g \rangle$ is given by (38), which reduces approximately to

$$\langle e_g \rangle = (w_0/w)^4 \langle x''^2/2g \rangle \qquad (\text{for} \quad w \gg w_0) \tag{52}$$

which is much smaller than $\langle e_g' \rangle$. For example, for $w_0/w = 1/10$, $\langle e_g \rangle$ for the L&R platform is 200 times smaller than $\langle e_g' \rangle$ for the other platform.

Another requirement of stabilized platforms is that they must not produce or transmit any vibrations that can cause resonance in the gravity meter itself. Most, if not all, gravity meters have certain resonant frequencies that must be avoided if they are to give accurate results. The resonant frequencies are generally higher than 10 per sec and therefore it is possible to avoid them or to shock-mount to eliminate them. A possible source of objectionable vibration is the hunting of the erection servo motors controlling the stabilized platform. Good servo design will of course eliminate such vibration.

Ship or airplane vibrations can easily be made negligible by shock-mounting a gimbal supported gravity meter, but shock-mounting a stabilized platform introduces some difficulties because an ordinary shock-mounted frame does not provide a firm base against which the servomotors can react. This makes it difficult to avoid hunting unless the servo gain is kept low or unless carefully designed lead networks are used. It is possible to provide a firm base against which the servos can react by making the shock-mounted supporting frame heavy compared with a gravity meter or by using parallel linkages between the supporting frame and the fixed base so as to permit translation but not rotation. The first L&R stabilized platforms [*LaCoste, et al.*, 1967] used parallel linkages, but the linkages were discarded when the servos were improved enough to make them unnecessary. This was a welcome simplification because the parallel linkages had to be well made and carefully adjusted to avoid transmitting high-frequency angular oscillations of the ship. The angular oscillations are transmitted unless the centers of gravity of the supporting frame and of the gimbal ring are on the apropriate gimbal axis.

There is another reason for preventing vibrations from reaching the stabilized platform, which was pointed out by J. J. Jarosh of Hughes Research Laboratories in a proposal to the Naval Oceanographic Office. Jarosh called attention to the well-known fact that torques on a stabilized platform are produced by horizontal and vertical accelerations when the platform is not perfectly balanced, and these torques must be counterbalanced by the servos. He also noted that the servo gain falls off at high frequencies(limited servo bandwidth), and therefore appreciable verticality errors can be produced by horizontal accelerations at these frequencies. Since these verticality errors are in phase with the horizontal accelerations, significant errors in gravity can occur. Jarosh made some computations with reasonable values of servo gain and bandwidth and with reasonable amounts of platform unbalance and found errors of the order of a milligal. He also showed that suitable shockmounting reduced them greatly.

Cross-Coupling Effects

General. Another source of error in shipboard gravity meters is cross coupling between horizontal and vertical accelerations. There is an inherent type of cross-coupling effect in certain kinds of gravity meters. It can be avoided by making the gravity meter symmetrical about a vertical axis or by accurately nulling the meter continuously, or the effect can be corrected for. There is also an imperfection type of cross coupling that is due to imperfections in the gravity meter. It can be made negligible by careful design and construction, or it can also be corrected for. The so-called 'inherent' type was described by *LaCoste and Harrison* [1961]. The equations for it can be obtained as follows.

Inherent cross coupling. The differential equation for a spring type of gravity meter is given in (3) for the case in which horizontal accelerations are absent or neglected. This equation will be modified to take care of horizontal accelerations for a gravity meter with a beam hinged about a horizontal axis as shown in Figure 2. If all terms in (3) are multiplied by $MD \cos \beta$, they will represent torques. The torque $-MDx'' \sin \beta$ due to horizontal acceleration can then be added. The resulting equation is

$$g + z'' - x'' \tan \beta + bB'' + fB' + kB - cS = 0 \tag{53}$$

This equation gives the correct value of g. If the horizontal acceleration term is omitted, an incorrect value g_e is given for gravity; the equation is

$$g_e + z'' + bB'' + fB' + kB - cS = 0 \tag{54}$$

The error in g_e is then

$$\begin{aligned} e = g - g_e &= x'' \tan \beta \\ &\doteq x''\beta \end{aligned} \tag{55}$$

If we take

$$\beta = \beta_0 + \beta_1 \sin (w_3 t + \psi) \tag{56}$$

and

$$x'' = x_1'' \sin w_1 t \tag{57}$$

where $\beta_0, \beta_1, x''_1, \psi, w_1$, and w_3 are constants, then (55) becomes

$$e = x_1''\beta_0 \sin w_1 t + x_1''\beta_1 \sin w_1 t \sin (w_3 t + \psi) \tag{58}$$

The average value of e is zero except when $w_1 = w_3$, in which case it becomes

$$\langle e \rangle = \tfrac{1}{2} x_1''\beta_1 \cos \psi \tag{59}$$

Equation 59 is the expression for the 'inherent' type of cross coupling. Since the beam is driven by vertical accelerations, β will have the same period as the vertical accelerations. Therefore, inherent cross coupling can exist if components of horizontal and vertical acceleration have the same period. This condition generally exists to some extent at sea. One reason is that water particles undergo approximately circular motion in waves. This results in a phase difference of $\pi/2$.

Also, if the gravity meter is mounted off the ship's roll axis in both the horizontal and the vertical directions, the gravity meter will be subjected to a ramp motion when the ship rolls. This motion will give zero phase difference between horizontal and vertical accelerations.

For a highly overdamped gravity meter the damping coefficient f in (3) is very large, and therefore B' (and β') are approximately proportional to z''. There will therefore be a phase difference of about $\pi/2$ between β and z''. If x'' and z'' also have a phase difference of $\pi/2$, then $\cos\psi = \pm 1$ in (59), and $\langle e \rangle$ can be large. This condition exists if the ship follows the water particle motion in the waves. This is roughly what takes place.

It is of interest to estimate the magnitude of the inherent cross-coupling effect for a recent LaCoste and Romberg gravity meter. In such a gravity meter the damping allows an angular beam motion of ± 0.001 radian for a vertical acceleration of $\pm 0.1\ g$ at a period of 3.5 sec. Therefore, for a horizontal acceleration of $\pm 0.1\ g$ and $\psi = 0$, (59) gives a cross-coupling effect of

$$e = 49 \text{ mgal} \tag{60}$$

Sea data have given cross-coupling effects as high as 20 mgal for LaCoste and Romberg gravity meters. Cross coupling has also been reported by *Bower* [1966], *Talwani* [1966], *Talwani et al.* [1966], *Wall et al.* [1966].

As mentioned in the stabilized platform section, inherent cross-coupling errors can be considered as a special case of off-leveling errors caused by shifting of the sensitive axis of the gravity meter when subjected to vertical accelerations. It will be recalled that in the derivation of the off-leveling equations (29 and 30) the sensitive axis of the gravity meter was assumed fixed on the gravity meter. However, as previously mentioned, the direction of the sensitive axis can sometimes be affected by accelerations. A study of Figure 2 will show how this effect can occur in a beam-type gravity meter. The sensitive axis is the axis along which there is a maximum effect of gravity or acceleration and perpendicular to which there is no effect. The sensitive axis is therefore in the direction OC perpendicular to the beam OP. It is apparent that this axis shifts as the beam moves in response to vertical accelerations.

If the gravity meter is tilted relative to the stabilized platform through the required angle to keep its sensitive axis vertical, horizontal accelerations will have no effect on the gravity meter and there will be no inherent cross-coupling errors. One method of accomplishing this tilting is to add a suitable compensating voltage to the gyro output that controls the corresponding servo motor as shown in Figure 7. In this case the compensating voltage should be proportional to the displacement of the gravity meter beam from horizontal.

The preceding method of handling cross coupling by tilting the gravity meter relative to the stabilized platform is simple, but in the case of L&R gravity meters it introduces a small second-order error because of tilting of the gravity meter relative to vertical. An analysis will show that the tilting results in changes of gravity meter sensitivity to the pull of gravity which introduce an error of $g\,\phi^2/2$ where ϕ is the angle of tilt. This error is entirely negligible for the tilting pre-

viously described in the stabilized platform section but might be an appreciable fraction of a milligal if cross coupling were compensated by tilting. For this reason tilting has not been used in operation at sea to compensate L&R gravity meters for inherent cross coupling, although it has been used to compensate them for other errors. Corrections for cross-coupling errors in L&R meters have been made by using a simple analog computer to evaluate (55), which is an accurate equation. Means for compensating for cross-coupling effects are also described by *Talwani* [1966] and *Jacoby and Schulze* [1967].

Cross-coupling effects can be eliminated in gimbal supported gravity meters by correctly placing the gravity meter relative to the gimbal as was explained in the discussion of (24). Equation 24 applies when $l \cos \alpha$ in Figure 3 is taken equal to g/w_0^2; this relation determines the distance the gravity meter weight is below the gimbal. If the angle α and the gimbal damping F are also taken equal to zero, (24) gives the acceleration a_n normal to the sensitive axis of the gravity meter as zero. Since a_n corresponds to the acceleration x'' in Figure 2 and equation 55, it can be seen that the cross-coupling effect e will be zero in this case. *LaCoste and Harrison* [1961] have considered the cross-coupling effect for the case in which $F = 0$ but $a \neq 0$ and have found that cross coupling is negligible even in this case.

Imperfection cross coupling. The imperfection type of cross-coupling effect was described by *LaCoste et al.* [1967]. This effect is due to imperfections in the design or construction of the gravity meter, and there are many ways in which it can occur so that determining its major cause is often difficult. It can be comparable to or larger than the inherent type of cross coupling.

Imperfection type cross coupling can occur if the damping coefficient in (3) is affected by horizontal accelerations or if horizontal accelerations cause vertical forces to vary. Two examples will be given to illustrate. Figure 11 shows a gravity meter with a hinged beam moving up and down a ramp. There will always be some elasticity in the beam and in the wires providing a hinge for it. This elasticity will allow the center of gravity of the beam to move horizontally in response to the horizontal accelerations, thereby changing the moment arm of the beam. The moment arm on the right of the figure will be denoted by $L + \Delta L$ and that on the left by $L - \Delta L$. Also, because of vertical acceleration the vertical force per unit mass on the right will be $g + z''$, where z'' is the vertical acceleration necessary to reverse the motion. Similarly, on the left the force per unit mass will be $g - z''$. The average of the two moments will be $Lg + z''\Delta L$, as shown. However, the average would have been Lg if there had been no motion. Therefore, the term $z''\Delta L$ is a cross-coupling effect.

The previous considerations show how important it is to restrict the gravity meter beam to only one degree of freedom. Even if this is done, however, the center of gravity of the spring can still shift in response to horizontal accelerations, and such a shift can have the same effect as a shift in the center of gravity of the beam.

Another example of imperfection type of cross coupling is shown in Figure 12, which is a top view of the gravity meter. The spring supporting the beam is shown at the right, and wires providing a hinge are shown at the left. The hinge axis is labeled. To restrict horizontal translation along the axis of rotation, the two wires

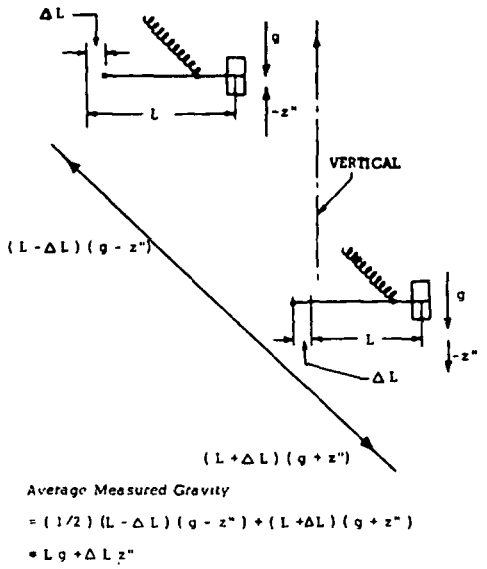

Fig. 11. Example of imperfection cross coupling. (Reprinted from *Geophysics, 32,* p. 107, 1967.)

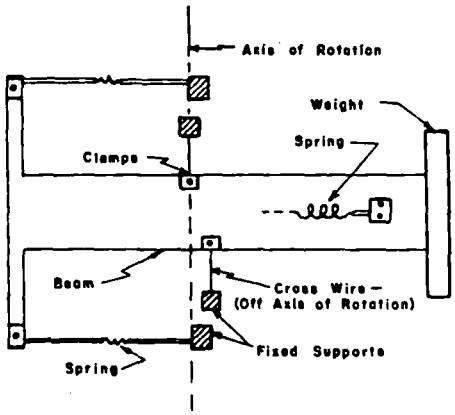

Fig. 12. Example of imperfection cross coupling. (Reprinted from *Geophysics, 32,* p. 108, 1967.)

shown are used. The wire at the top of the figure is shown in the axis of rotation and gives no trouble with cross coupling. The wire at the bottom, however, is shown to the right of the axis of rotation and will give a cross-coupling effect, as can be seen from the following considerations.

The effect of vertical accelerations will be considered first. It will be assumed that the beam will yield to some extent in response to such accelerations. The point of attachment of the lower (off axis) wire to the beam will then move up and down in space (in and out of the plane of the figure). When it moves down, the wire will tend to raise the right end of the beam and vice versa. Since the upward and downward accelerations will average out to zero, there will be no net effect.

If horizontal accelerations are present as well as vertical, however, there can be a cross-coupling effect. The horizontal accelerations will have the effect of tightening or loosening the wire, and, if the wire is always tight when it is pulling up and always loose when it is pulling down, there will be a net upward pull on the weight, which is a cross-coupling effect.

To make imperfection types of cross coupling negligible, it is necessary to make tests with various types of motion in addition to designing and adjusting carefully. Imperfection cross coupling can of course be corrected for with an analog or digital computer if its effects have been calibrated in tests.

The imperfection types of cross coupling just described can not be considered as special cases of off-leveling errors, because they do not involve a shift in the direction of the sensitive axis of the gravity meter. The mathematical expression for them ($x''z''$ times a constant) is, however, very similar to the more important first term $-x''e$ in the off-leveling equation (30). It therefore is possible to very nearly correct for imperfection types of cross coupling by intentionally in-

troducing an equal and opposite off-leveling error. For example, in Figure 7 the compensating voltage can be made proportional to z''. This will give an off-leveling error proportional to $-x''z'' - gz''^2/2$. With a proper choice of the proportionality factor the first term will balance out the imperfection cross coupling and the second term will generally be negligible because it is of the second order in z''.

The LaCoste and Romberg Shipboard Gravity Meter

Figure 13 is a photograph of an L&R gravity meter on a stabilized platform. A diagram showing the operation of the gravity meter is shown in Figure 2 [*LaCoste,* 1961]. The beam is pivoted about the horizontal rotational axis O and is supported at its center of gravity P by a spring, whose unstretched length is zero (a 'zero length spring'). Actual mechanical details are shown in Figures 14 and 15. In these figures the horizontal rotational axis is shown to be provided by the fine wires h. The beam B is very highly damped by the air dampers D and D1. The two movable dampers on the beam and the two fixed dampers on the frame consist of several concentric cylinders. The cylinders of the fixed and movable dampers interweave each other so as to provide high resistance to the flow of air

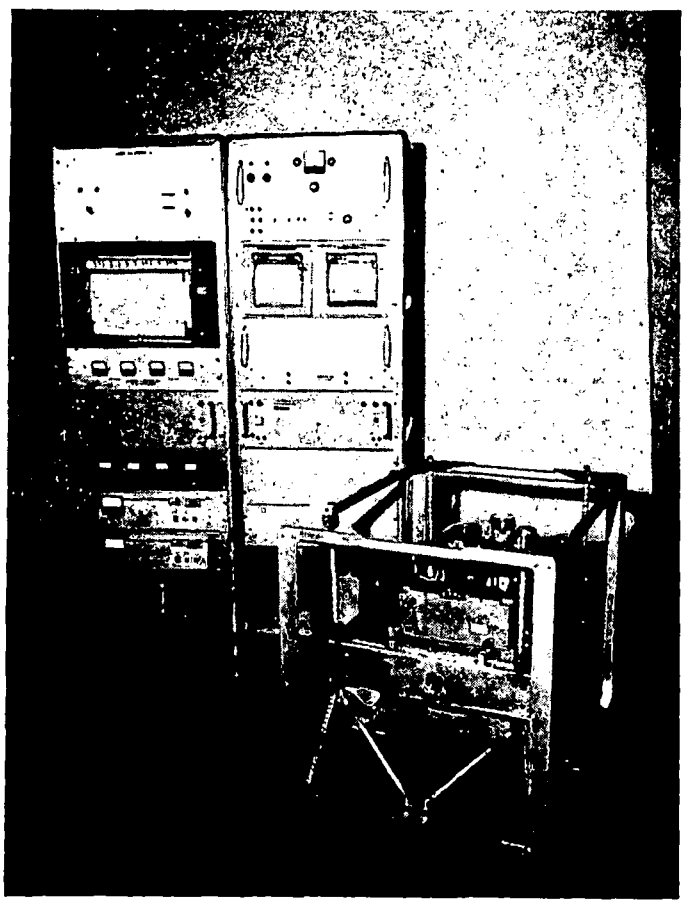

Fig. 13. Photograph of LaCoste and Romberg stabilized platform air-sea gravity meter.

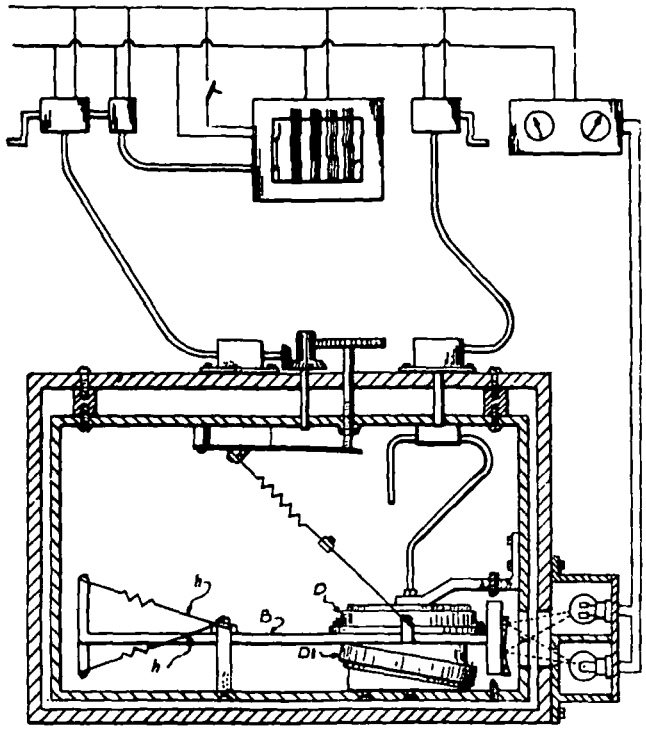

Fig. 14. LaCoste and Romberg air-sea gravity meter.

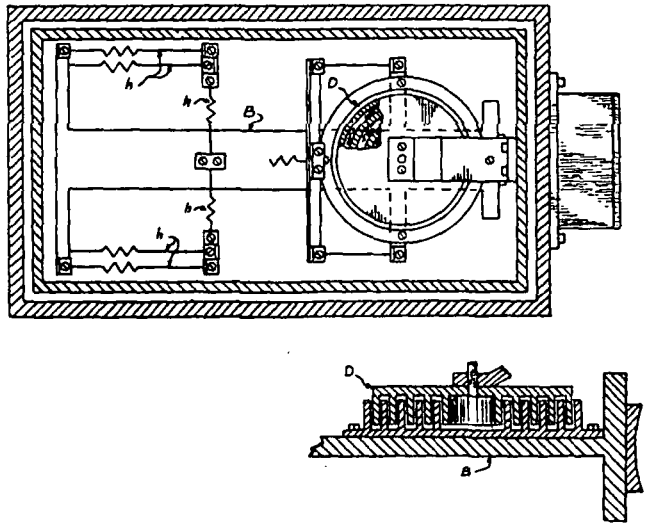

Fig. 15. LaCoste and Romberg air-sea gravity meter.

into and out of the dampers. The upper end of the spring, as is shown in Figure 14, can be adjusted to take care of variations in gravity. A more sophisticated means of adjusting the spring is actually used [*LaCoste and Romberg*, 1945].

The differential equation can be derived from Figure 2 as follows. The spring PA is a zero length spring; i.e., its unstretched length is zero. If K denotes the spring constant, the force exerted by the spring at P is K times the distance PA, according to Hooke's law. The force can therefore be represented by the vector PA. The force exerted by the beam at P is in the direction OP, and its horizontal component equals the horizontal component of the force exerted by the spring if no horizontal accelerations are present. The force exerted by the beam can therefore be represented by the vector OP. The vector sum of the forces exerted by the spring and beam at the point P can therefore be represented by the vector sum OA. If the distance OA is taken as S, then the vector OA represents a force KS where K is the spring constant.

The total static vertical force acting at P will then be $KS - mg$. The gravity meter is operated with the beam approximately horizontal and therefore its center of gravity P has very little horizontal motion. If this horizontal motion is neglected, the differential equation becomes

$$B'' + FB' = KS - m(g + z'') \tag{61}$$

This equation is the same as (3) with $K = 0$. The time constant is equal to the time required for B to reach 0.6 of its steady-state velocity when an input step function is applied to it. From the equation it can be seen to be $1/F$, which shows that the time constant is reduced by increasing the damping.

A typical value of the time constant is 4×10^{-4} sec. Since this time constant is so much smaller than any time over which gravity readings are averaged, there is no need to consider the transient response of (61) and the equation can be replaced by

$$g + z'' = (K/m)S - (F/m)B' \tag{62}$$

or, if it is desired to include cross coupling, by

$$g + z'' = (K/m)S - (F/m)B' + \beta x'' \tag{63}$$

(See equation 53.)

Equation 63 shows one of the features of the L&R gravity meter. Since the gravity reading does not depend on B, it is not adversely affected by drift in the device used to measure B as long as the drift is not fast enough to give an appreciable contribution to the B' term. This feature helps to give long-term stability to the gravity meter.

Even though the gravity meter accuracy is relatively unaffected by drift in the photoelectric device used to measure beam position, a chopper is used in it. Its operation is as follows [*Clarkson and LaCoste*, 1957]. A beam of light is reflected by a mirror on the gravity meter beam. When the beam is nulled, the light falls equally on two slits; when the beam moves up, more light goes through the upper slit and vice versa. A chopping disk lets light through the two slits alternately. The light going through the two slits falls on a single photoelectric cell.

From this description it can be seen that, when the beam is nulled, the photocell output is ideally dc; there is no ac component. As the beam moves from null, an ac output appears and is proportional to the displacement of the beam from null. The direction of the displacement determines the phase of the ac. The ac is rectified by a phase sensitive detector. The advantage of using a single photocell is that drift of the photocell does not affect the reading when the beam is nulled. Actually the light from the two slits is even focused on the same part of the photocell.

Another feature of the L&R spring suspension was pointed out by *Harrison* [1960]. He considered the effects of spring vibrations on the average pull exerted between the ends of a zero length spring. He first pointed out that longitudinal vibrations had no effect because they increased and decreased the force equally. He then analyzed the effects of transverse vibrations and showed that their effects also were negligible for a zero length spring. The following considerations will show why transverse vibrations have no effect.

Referring to Figure 16, consider the spring to be made up of weightless zero length springs with identical masses between spring segments and attached to the fixed points A and B, which are in line vertically. For simplicity the effect of gravity on the masses will be ignored. Since the spring segments are zero length springs, the forces each spring exerts on the adjacent masses are proportional to the spring length. Also, the vertical components of the forces are proportional to the vertical component of the spring length. Therefore, if the masses are equally spaced vertically, the vertical component of force exerted on each mass will be zero regardless of its horizontal position or horizontal motion. Also, the vertical force on A and B will be independent of any horizontal motions.

Until 1965 LaCoste and Romberg shipboard gravity meters were operated suspended from gimbals and were placed at the proper distance below the gimbal joint to make negligible all acceleration forces normal to the sensitive axis of the gravity meter. The method of doing this has already been described in the gimbal suspension section. In these gravity meters it was not necessary to make the beam and the springs in the fine wires providing a hinge for the beam very stiff. Therefore, they were not made stiff, although there actually was an advantage in making them stiff that was not realized at the time. Stiffness makes it easier to achieve

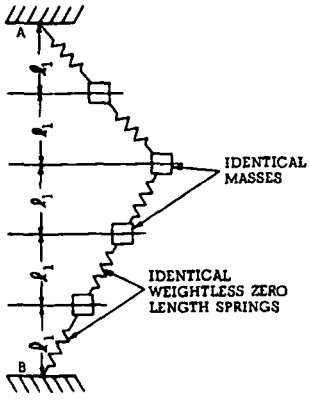

Fig. 16. Lateral vibrations in a zero length spring.

high gravity meter linearity, which in turn determines the magnitude of vertical acceleration errors. At the time, the linearity was considered adequate for operation at vertical accelerations of ±50 gals, which was the limit of operation for horizontal accelerations. Later it was realized that operation at greater vertical accelerations would have been a distinct advantage because vertical accelerations are often several times larger than horizontal accelerations.

When it was decided to mount L&R gravity meters on stabilized platforms, it was realized that the previously made gravity meters might not be satisfactory, but even so it was considered worth while to make tests with them. The tests showed the need for modification, and the gravity meter was accordingly redesigned to more nearly restrict the beam motion to one degree of freedom. Stiffness with respect to unwanted modes of motion was increased by a factor of 40 without noticeably affecting stiffness in the desired mode.

These modifications not only made the imperfection type of cross coupling negligible but also made it easy to attain sufficient gravity meter linearity to limit vertical acceleration errors to less than 1 mgal at vertical accelerations of ±100 gals. Another modification was to approximately double the damping so as to reduce the inherent type of cross-coupling effect. The increased damping permits operation at $\pm 1g$ at a period of 3.5 sec without having interference between the beam and the case of the gravity meter.

Both the inertia bar vertical references used with gimbal supported L&R gravity meters and the stabilized platforms used after 1965 are described in the section on horizontal accelerations. The stabilized platforms use inertial guidance quality gyros controlled by accelerometers to give 4- or 6-min periods (or longer if desired) and damping of 0.7 times critical. The platform has a range of ±30° and is powered by fast acting torque motors. It has never failed to operate because of roughness of the sea. To compensate for small platform errors of undetermined origin, a compensating voltage is added to the gyro output as shown in Figure 7 and as explained in the stabilized platform section.

The cross-coupling computer is a simple analog computer that multiplies beam position by horizontal acceleration along the beam. A servo follows the beam position, and the servo drives a potentiometer that forms two adjacent arms of a Wheatstone bridge. The voltage across the bridge is made proportional to the horizontal acceleration, and therefore the bridge output is proportional to the cross coupling.

The block diagram of Figure 17 shows the operation of the gravity meter as well as the operation of the stabilized platform. A simple analog computer referred to as a beam nuller uses the beam position as a signal to a slow servo to approximately null the beam. The servo is made slow so that it will not have to follow the wave accelerations, which normally amount to thousands of milligals. It performs the approximate nulling by controlling the 'spring tension,' S in (63).

A second analog computer referred to as the automatic reader computes an average value of gravity from (63). The computation is accomplished by filtering S, filtering and differentiating B, filtering the cross coupling, and adding them. The filtering is the same for each variable. Obviously this second function can be performed by a digital computer.

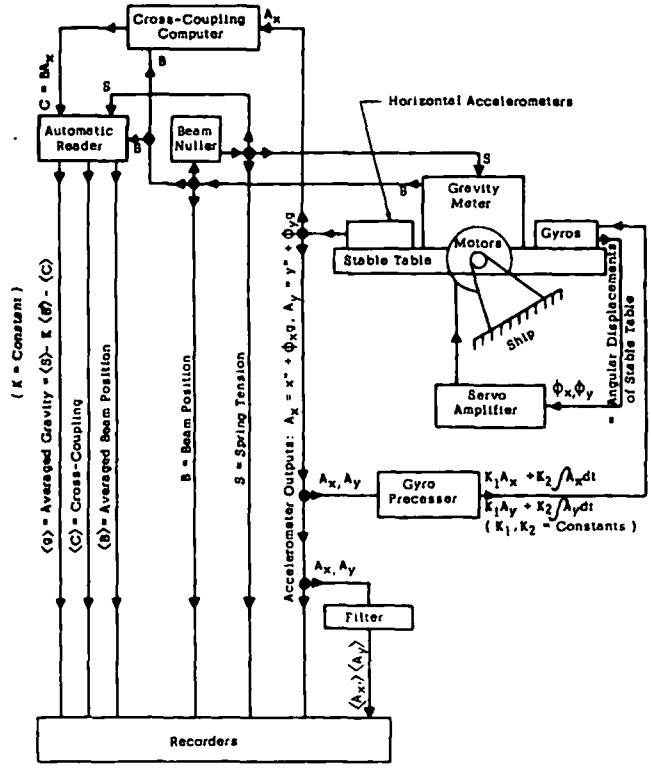

Fig. 17. Block diagram for LaCoste and Romberg air-sea gravity meter.

The value of gravity computed by the reader is recorded on a strip chart recorder and on magnetic or punched tape. Spring tension and averaged beam position are also recorded so that gravity can be computed even though there is a malfunction in the reader. Instantaneous beam position and filtered and unfiltered horizontal accelerations are also recorded for monitoring purposes. The filtered horizontal accelerations are useful in checking gyro performance. In late models a voltage proportional to vertical acceleration is provided by a tachometer mounted on a servo that follows beam position.

The Graf Askania Sea Gravity Meter

The Graf Askania sea gravity meter is also a highly damped type of gravity meter, but it uses magnetic damping and torsion springs. Because the author has not had experience with it, details of its construction and operation will not be given here. However, many of the fundamental principles previously discussed also apply to it. It has been well described in the literature [*Graf and Schulze*, 1961; *Schulze*, 1962; *Schulze et al.*, 1964; *Hayes et al.*, 1962].

Accuracy at Sea

Worzel [1959] made the first extensive gravity measurements on a surface ship in 1957, using a Graf Askania sea gravity meter on a stabilized platform on

the U.S.S. *Compass Island*. Since that time parallel developments of the Graf Askania and the LaCoste and Romberg sea gravity meters have taken place. Since the author was not involved in the development of the former gravity meter but actively participated in the development of the latter, this article will trace through only the development of the L&R instrument. For information on the development of the Graf Askania sea gravity meter the reader is referred to the original articles in the literature [*Worzel*, 1959; *Graf and Schulze*, 1961; *Allan et al.*, 1962; *Fleischer*, 1963; *Wall et al.*, 1964; *Loncarevic*, 1964; *Bower and Loncarevic*, 1967; *Graham and Hales*, 1965; *Bower*, 1966; *Wall et al.*, 1966; *Loncarevic*, 1966].

The accuracy of gravity meters at sea depends greatly on the accelerations to which they are subjected. The previously discussed gravity meter theory indicates that most errors can be expected to be proportional to the squares of the three components of acceleration and to cross-coupling effects, which are products of velocity and acceleration components or products of two different components of acceleration. The first L&R gravity meter that was operated on a surface ship [*LaCoste*, 1959] could tolerate vertical accelerations slightly greater than ±50 gals but required a linearity correction for vertical accelerations even below ±50 gals [*Harrison*, 1959]; Harrison made these corrections. (After the tests the gravity meter linearity was adjusted in the laboratory to give errors within 2 mgal at a vertical acceleration of ±50 gals, which was the standard at that time.) Harrison estimated an accuracy of ±5 mgal in his tests.

In 1960 the damping in the L&R gravity meter was increased, but the meter was designed and adjusted for operation at horizontal and vertical accelerations of only ±50 gals. The horizontal acceleration limitation of ±50 gals was made in order to retain adequate accuracy in the analog computer for the Browne correction, which is required on a gimbal supported gravity meter. The use of a gyro stabilized platform instead of a gimbal was rejected at that time because of the short advertised lives of gyros. The design limitation for vertical accelerations was set at ±50 gals because of the erroneous impression that the vertical accelerations would not greatly exceed the horizontal accelerations. This conclusion was based on the assumption that a ship undergoes approximately the same accelerations as the water particles in waves; it neglects the effects of the response of the ship. The fact that vertical accelerations of a ship can be several times larger than horizontal accelerations when going into the waves was not unknown at the time; therefore, a more thorough investigation would have avoided a serious mistake.

The 1960 L&R gravity meters were capable of withstanding vertical accelerations several times greater than the design limit of ±50 gals, but their linearity was not sufficiently well adjusted to make the errors small at accelerations greater than this limit. In a way it was a disadvantage that the meters were capable of being operated above their design limit because operators often did so. On the other hand, it was also an advantage because, when the error was finally located, it was possible to compute corrections for previous data.

Another cause of trouble in the 1960 L&R gravity meters, which was not known at the time, was that the linearity adjustments in some of them changed during use. It is still not known whether the change was due to rough handling in shipment or to a gradual aging effect. It is known, however, that the change

was due to balancing large nonlinearities against each other rather than reducing each nonlinearity to a small amount before balancing them. Balancing the large nonlinearities required extremely critical adjustments and therefore made it likely that the adjustments would be adversely affected by time or rough handling. As soon as it was determined that linearity adjustments changed, design modifications were introduced to make linearity very insensitive to the parameters affecting it. In the meantime, of course, the linearity changes that occurred resulted in increased errors, but fortunately these errors can be corrected even in old data, as has been mentioned.

Because of the acceleration design limitations of ±50 gals on the 1960 L&R gravity meters, they were not capable of operating under very adverse conditions. This situation continued until 1965, when a redesigned L&R gravity meter was introduced that operated on a stabilized platform. Some of the main tests made on L&R gravity meters in the period from 1960 to 1965 will now be discussed.

The largest errors observed with L&R gravity meters during that time were reported by *Allan et al.* [1962] and *Dehlinger and Yungul* [1962]. Allan's test was made on the 3000-ton ship *Aragonese* in the Mediterranean Sea with L&R meter S9. It gave errors of only about ±2 mgal in calm seas, but the errors increased to 10 to 25 mgal when the ship was headed into a moderate sea. Dehlinger's tests were also made with S9 on the 250-ton ship *Hidalgo* in the Gulf of Mexico. He too found large errors when going into the sea, even as high as 49 mgal. It now appears to be almost certain that the large errors were due to operating the gravity meter at vertical accelerations greater than the design limits of the meter, but this was not realized at the time, nor were any measurements of the vertical accelerations made either by the users or by the manufacturers of the gravity meters.

One reason for not having measured vertical accelerations was that they were not expected to exceed horizontal accelerations, as was previously mentioned. Another reason was that the long-period pendulum horizontal references of the gravity meter were almost universally thought to be the weakest link in the system and to be the main source of error. This belief was strengthened when *Dehlinger and Yungul* [1962] noted correlation between error and horizontal accelerations. The correlation very likely existed because there is also some correlation between horizontal and vertical accelerations. Nevertheless, Dehlinger was able to work out an empirical correction based on horizontal acceleration that reduced the errors to about ±10 mgal.

In later tests with S9 *Dehlinger* [1964] was able to establish a criterion, other than excessive vertical accelerations, for rejecting poor data. He noted that the gravity meter beam record (which indicates the integral of gravity when the spring tension is constant) was smooth on good readings but irregular on bad readings. These irregularities can probably be explained as variations of the error when the vertical acceleration varies. The acceleration varies because waves generally come in packets and because the amplitude of the ship motion changes slowly as the ship resonates with the waves (beat notes). Dehlinger also stated that errors were often present when there were large variations in the amplitudes of the accelerations. This statement is reasonable because large variations occur

in resonance and resonance in heave is generally responsible for the large vertical accelerations that occur when going into the waves.

Although these criteria were not as relevant as excessive vertical accelerations, Dehlinger was able to use them to improve greatly the accuracy of the results obtained with S9. In his article [*Dehlinger*, 1964] he gives errors of 3 mgal at Browne corrections up to 300 mgal, 5 mgal at corrections of 300 to 400 mgal, and 8 mgal at corrections of 400 to 500 mgal.

The next significant tests made with S9 were made in 1963 by Harrison [*Harrison and LaCoste*, 1968]. In the three years preceding these tests the performance of the long-period pendulums had been greatly improved at periods shorter than 2 sec and at periods longer than 12 sec. In view of this improvement, better performance was expected from the gravity meter, since it was still not realized that vertical accelerations were the main source of error. No criteria were used to reject bad data except that the horizontal accelerations should not exceed ±50 gals. The errors were still large, particularly when going into the sea. The improvements in the long-period pendulums appeared to have made no significant improvement in accuracy.

It was not until tests were made on an experimental L&R stabilized platform gravity meter in 1964 [*Harrison and LaCoste*, 1968] that large vertical accelerations were recognized as the major source of error in L&R gravity meters. The tests were made in very rough weather, which probably helped to show the source of the error. Vertical accelerations were measured in this test and were found to have far exceeded the design limits during much of the test. Vertical acceleration corrections were made from data previously obtained in the laboratory and were found to account for the larger part of the errors. The remainder of the errors appeared to be due to cross-coupling effects.

After it was determined that large vertical accelerations accounted for most of the errors in L&R gravity meters, Harrison [*Harrison and LaCoste*, 1968] applied the corrections to the 1963 data he had obtained with S9. Before making the correction the mean error was 8.4 mgal and the rms errors had ranged from 5 to 20 mgal on lines made with horizontal accelerations ranging from ±20 to ±45 gals. After making the corrections the mean error was reduced to 1.1 mgal and rms error to 3.6 mgal. LaCoste made a similar correction to data obtained with S11 over a test range and obtained a similar improvement. LaCoste's corrections were sent to various users of L&R gravity meters with data for making similar corrections for the individual meters, but these corrections were never published.

To make vertical acceleration corrections, *Dehlinger et al.* [1966] worked with several years of data obtained with S9. In making the corrections, however, the vertical accelerations were inadvertently taken proportional to B/T^2 rather than proportional to B/T, where B is the amplitude of the beam motion and T is the period. The former expression applies to a long-period gravity meter with normal damping, in which case the acceleration is proportional to the second derivative of the beam displacement. The latter expression applies to a highly damped gravity meter, in which case the acceleration is proportional to the first derivative of the beam displacement as previously explained. The error in Dehlinger's computations made it impossible to use the numerical constant determined

in the L&R laboratory for vertical acceleration corrections, and therefore Dehlinger et al. determined a constant for a best fit of the data. The best fit constant turned out to give the same corrections as the L&R formula for a 7-sec period, and therefore it gave too small a correction at periods longer than 7 sec and too large a correction at periods shorter than 7 sec. Even so, Dehlinger's corrections did improve the accuracy considerably. He estimated his gravity meter errors to vary from 1.5 mgal at low Browne corrections to ±4 mgal at Browne corrections of 500 mgal.

It has been mentioned that the linearity adjustments of some L&R gravity meters has changed with time, before certain design modifications were made. Gravity meter S9 has been particularly bad in that respect. According to the L&R records its error at vertical accelerations of ±50 gals was within 1 mgal in 1960, when it was completed. In 1961, when it was tested again, the error was found to be 6 mgal at the null position. In view of what is now known, it should certainly have been readjusted then, but it was not. It was not tested again until 1964, when the error was found to be 16 mgal. It has of course been readjusted.

In the period from 1960 to 1964 a considerable amount of good data has been obtained with other L&R gimbal type gravity meters. One comprehensive and well controlled test was made by *Bower and Loncarevic* [1967] [*Loncarevic*, 1964, 1966] on the C.S.S. *Baffin* in October 1963 over the Halifax gravity range. L&R gravity meter S8 and a Graf meter were both aboard the ship. Two precisely located tracks were traversed a total of 108 times. Decca was used for navigation and was considered to have more than the required accuracy. Gravity values on the range had previously been obtained with an underwater gravity meter [*Goodacre*, 1964]. A wide variety of weather conditions was experienced. Vertical accelerations ranged from 2 to 78 gals rms or about ±3 to ±110 gals.

About the same number of usable records were obtained from the two instruments, although the Graf operated in rougher weather. Loncarevic reported useful readings with the L&R meter with vertical accelerations up to about ±42 gals and with the Graf up to ±71 gals. The mean error was +0.6 mgal for the L&R meter and −0.4 mgal for the Graf. The standard deviation was 3.9 mgal for the L&R and 2.7 mgal for the Graf. Drift for the entire test was negligible for the L&R and irregular over a 7.0 mgal range for the Graf. D. R. Bower (personal communication) noted a correlation between vertical acceleration and error in the L&R gravity meter but did not make corrections for it.

In 1959 *Harrison and Spiess* [1963] made tests in the Gulf of California on the research vessel *Horizon*. Sea conditions were better than average. Shipboard gravity readings were compared with readings taken with an underwater gravity meter at 27 stations. The mean difference at the 27 stations was 2.7 mgal, and the rms departure was 1.5 mgal. Gravity meter drift was 1.6 mgal in 7 weeks. Discrepancies at intersections were not given.

Caputo et al. [1963] describe gravity measurements made in the continental borderland off southern California. They obtained 231 track intersections made on different ships. Most of the data was obtained with L&R gravity meter S3 in various stages of development, but some data were obtained with S5. The

average discrepancy at all 231 crossings was 6.8 mgal, and two-thirds of the discrepancies were within 7 mgal. These values included navigational errors, and at 40 track intersections there were depth discrepancies of more than 90 meters. If these 40 intersections are disregarded, the mean discrepancy is only 5 mgal and two-thirds of the intersections are within this value. The 5-mgal discrepancy at intersections implies a mean observational error of 3.5 mgal. Data from the later cruises were more self-consistent than data from the earlier cruises, which indicates that the gravity meter had been improved somewhat. All the data considered by Caputo et al. were obtained before it was realized that the greatest source of error in L&R gravity meters was due to large vertical accelerations; no corrections have yet been made for these vertical accelerations.

L&R gravity meter S8 has been used in oil explorations. The first tests for this purpose, made in 1961, were used to make a gravity contour map of an area where gravity data were known only to the oil company sponsoring the test. When the oil company data were later made available, the map was found to be accurate to about 2 mgal and showed several salt domes that were present. The following year S8 was used in actual oil exploration by a major oil company. Track intersections and occasional data obtained where gravity had been previously measured with underwater gravity meters indicated that anomalies of 2 mgal could be detected.

Although cross-coupling effects were described in the literature in 1960 [*LaCoste and Harrison*, 1960] and were known several years earlier, they have not been considered as a serious source of error until fairly recently. Early estimates of their magnitude were given as small [*Wall et al.*, 1964]. Later measurements [*Wall et al.*, 1966; *Bower*, 1966] showed however, that they were often of the magnitude of 10 mgal or even 30 mgal in very rough weather. It is a simple matter to compute these errors with an analog computer; thus, corrections will certainly be made where they are not already being made.

As previously mentioned LaCoste and Romberg substantially redesigned their gravity meter in 1965 for use on a stabilized platform [*LaCoste et al.*, 1967]. The first of the new models, S20, was tested against the last of the old gimbal models, S19, in the Gulf of Mexico over an area where gravity had previously been accurately surveyed with an underwater gravity meter. The results of the test are given by *LaFehr and Nettleton* [1967].

The test was made over the San Luis Pass salt dome about twenty miles southeast of Freeport, Texas. A 100-foot boat was used in sea conditions considered average for shallow offshore areas, running about 2 to 6 feet. Navigation was done by means of Raydist, which gave adequate accuracy. The comparison underwater gravity data had a probable error of about 0.1 mgal. Shipboard gravity data were taken on ten lines run in six different directions across the salt dome, giving twenty-five line intersections. The sea was rough enough to prevent the gimbal meter from operating 15–20% of the time, but the stabilized platform meter gave good data at all times. In six months of subsequent operation the stabilized platform gravity meter has never failed to operate because of roughness of the sea.

For the stabilized platform gravity meter the average observed difference

between lines for all twenty-five intersections is 0.90 mgal. Of these differences 64% are within 1.0 mgal. The maximum observed difference, 2.5 mgal, occurred on line A-1 on whose run there was a short power failure on the ship. These statistics compare with an average difference for the gimbal gravity meter of 4.6 mgal and a maximum difference of 19.5 mgal. Actually, the 19.5-mgal discrepancy should have been rejected because the horizontal acceleration exceeded the ±50-gal design limit on one of the lines concerned (personal communication).

If line A-1 on which a power failure occurred is discarded, the remaining eighteen line intersections give the following results for the stabilized platform meter: the average observed difference is 0.68, and 78% of the differences are 1.0 mgal or less; the maximum observed difference is 1.5 mgal.

LaFehr and Nettleton point out that the preceding statistics do not represent the true capability of the instrument for measuring gravity anomalies either in the relative or the absolute sense. They note that shipboard gravity data usually have systematic errors that are fairly constant along each line and these systematic errors can be adjusted out. They have written a computer program to make this adjustment and to automatically make contour maps.

In this computer program the systematic error of each line is determined from its discrepancies at line intersections. (See Tables 1 and 2.) Table 1 shows the observed intersection differences. It can be seen that line C is running about 0.8 mgal higher than the lines intersecting it; this average line difference is listed in column 4 of Table 2. The average adjustment for each line is given in column 5 of Table 2 and indicates a systematic error considerably less than 1 mgal.

To compare the shipboard gravity data with the reference data obtained with the underwater gravity meter, it is necessary to refer them to the same datum. An absolute datum was available for the shipboard data but not for the underwater data; therefore, a best fit datum shift was determined for 158 samples. This datum shift was applied to the original data to give column 8 and to the computer adjusted data to give column 9, which shows smaller errors than column 8.

Errors determined at 158 points of the known gravity field were determined for the computer adjusted shipboard data, after making the single datum change

TABLE 1. Observed Differences at Intersections in Milligals
Sign is Plus if the Row Line is High

	A−1	*B*	*C*	*F*	*A*−2	*C*−1	*D*−1	*D*	*E*
A − 1		+2.1	+1.2	−0.5	+1.6	+0.7	−2.5	+1.5	
B	−2.1		−1.5	−0.8	−0.9	−1.0	+0.9	−0.3	
C	−1.2	+1.5			+0.6	+0.2	+1.5	+1.2	
F	+0.5	+0.8			−0.1				+0.4
A − 2	−1.6	+0.9	−0.6	+0.1		−0.3	−0.3	0.0	−0.6
C − 1	−0.7	+1.0	−0.2		+0.3		+0.3	+1.4	
D − 1	+2.5	−0.9	−1.5		+0.3	−0.3			
D	−1.5	+0.3	−1.2		0.0	−1.4			
E				−0.4	+0.6				

TABLE 2. Computer and 'Best Fit' Adjustments and Known Field Comparisons

		Based on Intersections Alone			Based on Known Field Comparisons			
Line	Heading	Number of Intersections	Statistical Line Mean Difference,[a] mgal	Average Computer Adjustment,[b] mgal	Absolute Datum Difference,[c] mgal	Relative Datum Difference,[d] mgal	Known Field Minus 'Best Fit,'[e] mgal	Known Field Minus Adjustment,[f] mgal
A − 1	NE	7	+0.5	0.9	−6.7	+0.5	1.1	0.4
B	W	7	−0.7	0.8	−8.7	−1.5	0.5	0.4
C	SE	6	+0.8	0.5	−5.5	+1.7	0.5	0.3
F	S	4	+0.2	0.3	Insufficient known gravity			
A − 2	NE	8	−0.1	0.3	−6.7	+0.5	0.4	0.4
C − 1	NW	6	+0.4	0.2	−6.8	+0.4	0.4	0.5
D − 1	N	5	−0.5	0.8	−8.3	−1.1	0.3	1.1
D	S	5	−0.4	0.7	−7.4	−0.2	0.9	0.0
E	W	2	+0.2	0.2	Insufficient known gravity			

[a]Computer determined mean difference for line intersections based on entire network; negative of first computer adjustment.
[b]Average difference between observed data and adjusted data.
[c]Datum for each line arbitrarily determined by 'best fit' technique.
[d]Difference between mean datum shift and line datum shift: a measure of systematic error; should agree qualitatively with column 4.
[e]Average difference between known field and line data after constant shift of column 6 using 'best fit' technique on 158 samples.
[f]Average difference between known field and computer-adjusted intersections using 25 intersections.

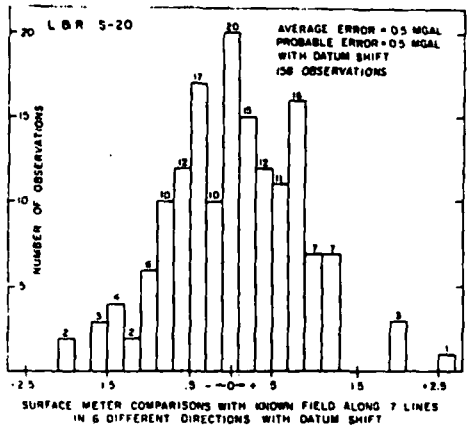

Fig. 18. Histogram of LaFehr and Nettleton's errors with L&R stabilized platform gravity meter. (Reprinted from *Geophysics*, *32*, p. 117, 1967.)

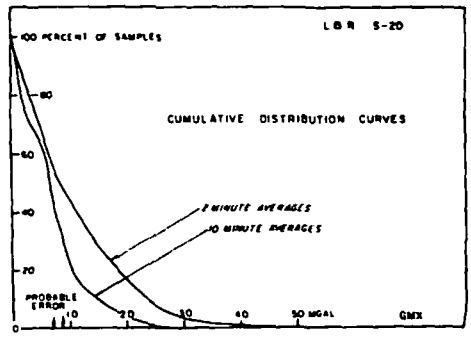

Fig. 19. Cumulative errors in LaFehr and Nettleton's test of L&R stabilized platform gravity meter. (Reprinted from *Geophysics*, *32*, p. 117, 1967.)

previously mentioned. The results are shown in the histogram of Figure 18; the probable error is 0.5 mgal. Since data were recorded only to ±0.5 mgal, it appears that results might be improved by recording data more accurately. These more accurate recordings are now being made.

A comparison was also made of the relative accuracy of 2- and 10-min averaging of unadjusted data. The results are shown in the cumulative error curve of Figure 19. Here it is seen that the probable error is smaller for the 10-min average. Even for 2-minute unadjusted data, however, the probable error is less than 1 mgal.

It has been mentioned that LaFehr and Nettleton's article is based on only 25 intersections and about 53 miles of continuous data. Since writing the article, however, they (personal communication) have obtained data at thousands of intersections and have found that their results have been borne out by the new data. They also have evidence that navigational errors are appreciably greater than the gravity meter errors even when the best means of navigation are used. They have found that they can improve their accuracy by better control of the ship motion, so that it more nearly travels in a straight line at consant speed, thereby reducing changes in the Eotvos correction.

The existence of some systematic error in LaFehr and Nettleton's results is not surprising, because errors can always be found if they are searched for diligently enough. Although LaFehr and Nettleton's computer program substantially reduces these errors, work is under way to locate their causes and then to correct for them.

The great improvement in the new model L&R stabilized platform gravity meter over the old model has made it practicable to use it in detailed exploration for oil, which is now being done on a considerable scale. There is no reason to believe that the accuracy cannot be improved further, because the L&R shipboard gravity meter is essentially the same as the land gravity meter except for

high damping and therefore the same instrumental accuracy can be approached by tracking down the various errors still present. Stationary readings are accurate to ±0.01 mgal, as can be seen in the earth-tide record shown in Figure 20 which was obtained with shipboard meter S22. Data for this record were obtained overnight when the earth tide happened to be particularly small. The record shows that the integral of gravity and, therefore, its slope represent gravity. Reference slopes corresponding to ±0.01 mgal are shown.

An interesting way of looking at systematic errors is as follows. Since these errors are approximately constant along any line, they depend on quantities whose average values are also approximately constant along each line. The quantities are certainly functions of the accelerations and velocities; therefore, it appears that a good expression for the systematic error e_s will be given by a power series of the accelerations and velocities. Furthermore, there will be no first-order terms in this power series because the average value of all first-order acceleration terms will be zero on a ship, and first-order velocity terms will have no effect other than the Eotvos effect. The power series will then be

$$e_s = a_1\langle x''^2\rangle + a_2\langle y''^2\rangle + a_3\langle z''^2\rangle + a_4\langle x'^2\rangle + a_5\langle y'^2\rangle + a_6\langle z'^2\rangle + a_7\langle x''z'\rangle + a_8\langle y''z'\rangle + a_9\langle x''z''\rangle + a_{10}\langle y''z''\rangle + \cdots \quad (64)$$

where the a's are constants.

In (64) the first two terms have been discussed in connection with stabilized platform performance and the third term has been discussed in connection with gravity meter nonlinearity. The fourth and fifth terms produce no effect on the gravity meter and can be disregarded. The sixth term can occur because of nonlinearity in some types of gravity meters, as has been explained previously. The seventh and eighth terms give the inherent type of cross coupling in overdamped meters, and the ninth and tenth terms give imperfection types of cross coupling. Higher-order terms can probably be disregarded but can be included if necessary.

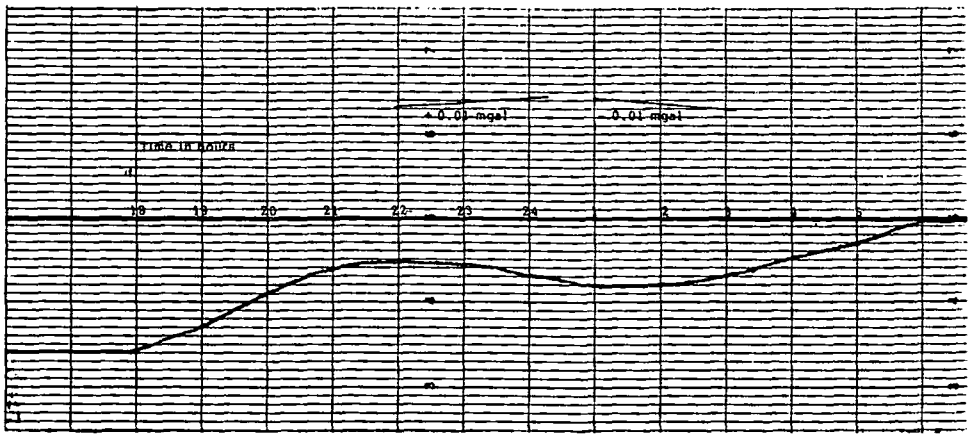

Fig. 20. Earth-tide record obtained with L&R air-sea gravity meter S22. Record shows integral of gravity; therefore, gravity is represented by slope of curve.

LaCoste and Romberg has recently provided means for recording the terms in (64) that might be expected to be significant. A study of the correlation between each term and the error will determine a correction that can either be applied to the data or can be made to the gravity meter. A simple method of making the correction directly to the gravity meter is being used. The final error calibration can then be made at sea rather than in the laboratory, although laboratory calibration is still done as carefully as possible.

Accuracy in the Air

Airborne gravity measurements were first made in 1958 [*Thompson and LaCoste* 1960]. Flights were made in a U. S. Air Force KC-135 jet tanker over Edwards Air Force Base, California. LaCoste and Romberg gimbal supported gravity meter S5 was used. Accurate navigational data were provided by phototheodolites on a tracking range on the ground. It was believed that the phototheodolites gave the airplane altitude to an accuracy of about ±2 feet. The airplane was operated on an automatic pilot, which was adjusted as carefully as possible to give smooth flight. Doppler radar was available for measuring velocity but was not used because data from the tracking range were considered to be more accurate. Altitude variations were measured by a very sensitive pressure transducer or hypsometer. A hypsometer measures pressure by measuring the temperature of the boiling point of a liquid. Flights were made in the morning so as to have smooth air.

The gravity meter performed well in most cases. On a northbound flight the automatic pilot caused the plane to hunt with a 42-sec period, and this caused a 78-mgal error because the periods of the long-period pendulum vertical references were only 1 min. The presence of the 42-sec period was evident from the horizontal acceleration records; therefore, there was no question that the data for that run should be discarded. Vertical accelerations were only of the order of 10 gals. The navigational accuracy was adequate to permit gravity readings to be averaged over times as short as five minutes without a great loss in accuracy. (Velocities and accelerations can be measured more accurately over long times or distances because a given uncertainty in position has a smaller percentage effect if the distance involved is large.) Corrections were made for vertical accelerations determined by the pressure sensitive altimeter. The need for these corrections was shown by the fact that they greatly smoothed the final gravity data.

The accuracy of the results of the airborne measurements was estimated from a comparison with the available ground gravity data after they were corrected for the elevation difference. It appeared that an accuracy of 10 mgal or better was obtained. This accuracy was also borne out by gravity readings at flight crossings. It was not surprising that the gravity meter performed well because the accelerations present in the flights were much smaller than those normally encountered on ships. With these accelerations the gravity meter errors should be considerably smaller than the 10-mgal errors observed. The navigational accuracy is therefore the limiting factor in airborne gravity measurement.

Shortly after the first airplane test a second test was made in a B 17 airplane operated by Fairchild Aerial Surveys [*Nettleton et al.*, 1960]. The gravity meter used was L&R S3, which was loaned by the Institute of Geophysics and Planetary Sciences at the University of California, Los Angeles. The airplane was equipped with a mapping camera to determine its position and an APR precision radar altimeter and a hypsometer for determining the altitude. Again flights were made in the morning in order to have calm air, and the airplane was flown on an automatic pilot which was carefully adjusted to minimize hunting, particularly long period-hunting. Flights were made over the Imperial Valley in California.

Again it was found that good gravity data were obtained on all flights except on one going north when the automatic pilot again caused the airplane to hunt at a period of 1 to 2 min. The problem in the automatic pilot has since been solved; it occurred because of the dip of the magnetic field. The airborne gravity results were evaluated in several ways: (1) by a comparison with a ground gravity contour map, (2) by repeat observations over almost the same course, (3) by comparisons at flight intersections, and (4) by comparisons with values calculated from known ground gravity stations. In correcting ground values for altitude differences, it was necessary to correct for attenuation or smoothing of details at flight altitudes. Again the estimated errors were found to be within 10 mgal. Also, it was found that gravity values could be averaged over times as short as three minutes without losing much accuracy, this corresponds to a distance of about ten miles for the aircraft used.

Thompson and LaCoste [1960] noted that airplane velocity errors have less effect on gravity meter accuracy when the airplane is flying west, because the airplane speed is subtracted from the surface speed of the earth due to its rotation. The resulting reduction in speed not only reduces the centripetal acceleration (which varies with the square of the speed) but also reduces its derivative with respect to speed (which is its sensitivity to errors in speed). *Glicken* [1962] has extended this analysis of the effects of various errors on the accuracy of gravity observations. He gives useful curves.

The first well controlled airborne gravity meter test was made by Fairchild LaCoste Gravity Surveys, Inc., for the U. S. Army Map Service [*Nettleton et al.*, 1962]. The test was made over the triangle formed by Houston, Texas, Shreveport and Baton Rouge, Louisiana. The triangle was flown twice in opposite directions. The reasons for picking this triangle were (1) gravity values on the ground were well known over that region, (2) the topography was relatively flat so that there would be little uncertainty in computing gravity at flight altitudes from the ground data, and (3) good aerial photographs of the region were available so that flight positions could be accurately determined.

The flights were made in a B 17 aircraft with a Bendix autopilot which had been adjusted for small amplitude and short-period hunting. As in the previous test, photography was used for navigation and an APR radar altimeter and hypsometer were used for determining altitude. Doppler radar was carried on the flights in orders to evaluate it. The gravity meter used was L&R S8. It was a gimbal supported gravity meter, but the long-period vertical references had been adjusted to 2-min periods, and the damping had been made 0.7 times critical.

Flights were made at 12000 feet. The airplane altitude was determined with the radar altimeter at the corners of the flight triangle where the elevations of the ground were known. Along the flights the altitude of the airplane was determined by means of the hypsometer by using *Henry's* [1948] formula for the isobaric surface. Henry's formula is $dh/ds = 0.035A \sin \phi \sin \delta$, where dh/ds is the slope of the isobaric surface in feet per mile, A is the true air speed in statute miles per hour, ϕ is the latitude, and δ is the angle of drift of the aircraft. The airplane was flown in a straight line except for occasional course changes of *about* 1°.

Most of the flights were made early in the morning to obtain smooth air, but some turbulent air was encountered before flying each complete triangle. The turbulence caused the automatic pilot to hunt at a long enough period to cause small errors even though the periods of the long-period pendulum vertical references had been increased to 2 min. Similar errors were produced when the airplane made 1° course changes. A first-order correction for these errors was made, as explained in the discussion of equation 38. Essentially the correction consisted of applying the recorded horizontal accelerations to the vertical references as tilts, in the laboratory. The difference between the inputs and outputs in the laboratory permitted an extrapolation to the original input that occurred during flight. The application of this first-order correction made the gravity records smooth at the places where course changes were made and reduced turbulent air errors to about the same value as smooth air errors.

The airplane gravity results are compared with the ground gravity data corrected for altitude in Figure 21 for the Houston–Baton Rouge flights. For these two flights the mean error was 2.2 mgal and the rms error was 6.5 mgal. The values for all the flights was +1.55 mgal for the mean error and 6.6 mgal for the rms error. All readings were calculated over 3-min intervals. The small values of the mean error indicate an accurate gravity meter calibration because

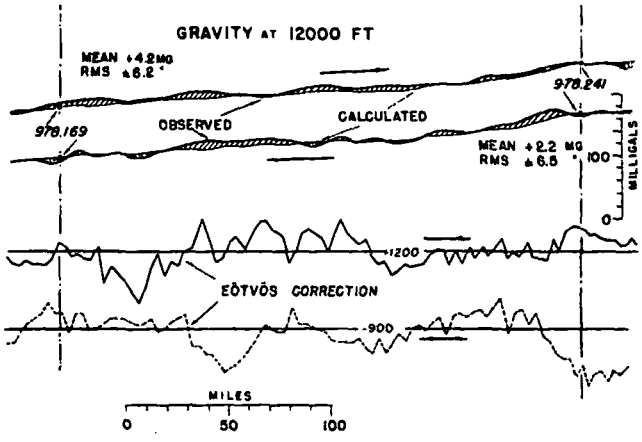

Fig. 21. Results of airplane flight tests of L&R gravity meter between Houston and Baton Rouge on Army Map Service test. (Reprinted from *Journal of Geophysical Research, 67,* p. 4405, 1962.)

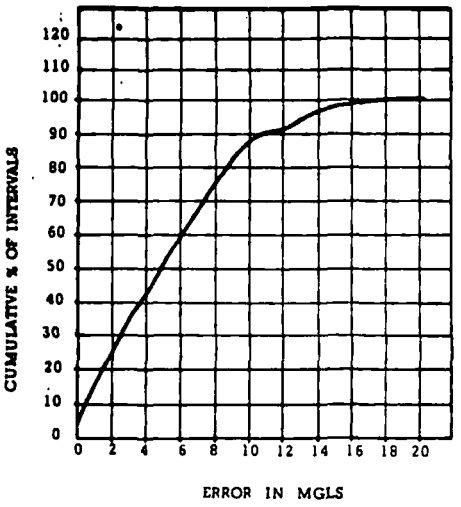

Fig. 22. Cumulative error curve between measured and calculated gravity at 12,000 feet for L&R gravity meter on Army Map Service test. (Reprinted from *Journal of Geophysical Research, 67*, p. 4409, 1962.)

there are large altitude and Eotvos corrections in all flights. A cumulative error curve is shown in Figure 22.

The preceding test and the entire data reduction procedure were independently evaluated by the University of Wisconsin [*Coons et al.*, 1962]. To the extent that it was feasible, the various inputs were digitized and the data reduction was carried out on an electronic computer: Although the digital filtering was somewhat different, the errors were almost the same. The digital analysis gave a mean error of 1.75 mgal instead of 1.55 mgal and an rms error of 6.0 mgal instead of 6.6 mgal.

In 1962 *Thompson* [1965] made over 100 test flights over a calibration range to evaluate (1) a Graf-Askania Gss 2 gravity meter on a stabilized platform, (2) LaCoste and Romberg gimbal supported gravity meter S6, and (3) L&R gravity meter S6 on a stabilized platform. The stabilized platform was an Aeroflex ART-25 camera mount whose accuracy was given as ±5 min of arc by the manufacturer. Gravity meter S6 was not modified for operation on a stabilized platform. The tests were made over the Edwards Air Force Base test range. Navigational data were provided by phototheodolites on the ground as in the first airplane gravity test. Tracking was thought to be accurate to ±2 feet in altitude, ±½ knot in ground speed and, ±½ min of arc in true course.

Unfortunately, phototheodolite tracking was available for only 30 to 40 miles of each flight, which corresponded to only 5 to 6 min of flying time for the C 130 aircraft used. The short length of the flights where navigational control was available could result in errors caused by initial conditions (acceleration) preceding the usable 6-min parts of the flights. Also, since the various 6-mir parts of flights are independent of each other, their average is not as meaningfu as it would be if they were all consecutive parts of a single flight. In the latte case a periodic acceleration error giving a high gravity value over one par would probably give a low gravity value over the next.

Thompson considered about half of the flights usable and found an rms erro of 7.2 mgal for the Graf, an rms error of 8.5 mgal for S6 suspended from gimbal

and an rms error of 7.3 mgal for S6 on the stabilized platform. He found it necessary to make a 5-mgal correction for the long-period pendulum reference for the gimbal supported S6, but after making this correction he found that the mean for each of the three systems tested agreed within 1 mgal with the gravity values computed from ground data. The accuracy with which the mean values checked the ground data might have been somewhat fortuitous because some of the gravity values from individual flights differed over 20 mgal from the ground data.

In view of the results of *Harrison and LaCoste* [1968] at sea it is somewhat surprising that L&R gravity meter S6 performed as well as it did on a stabilized platform in the airplane, because it had not been modified for such use. The answer probably lies in the fact that the accelerations in the airplane were small, generally below 10 gals. Thompson did report errors when the air became turbulent.

It is obvious that gravity values obtained in a fast moving airplane cannot show detail because of the speed of the airplane and the need for an averaging time of a few minutes. Also, detail is lost if the airplane is flying high. Gravity measurements can, however, be obtained rapidly in an airplane and are sufficiently accurate to be useful in geodetic work. Navigational accuracy will have to be improved before over-all accuracy can be improved.

Other Uses of Air-Sea Gravity Meters

The difficulty of obtaining gravity details in airplane measurement can be overcome in some cases by operating in a helicopter rather than in an airplane. A helicopter can be hovered very accurately at 200 feet or less from the ground. This will greatly reduce errors in the Eotvos correction and acceleration corrections for altitude variations. Also, surveying techniques for accurately locating helicopters have been worked out by the U. S. Geological Survey using Telurometers and transits. Tests of air-sea gravity meters have already been made in helicopters by the U. S. Naval Oceanographic Office and the U. S. Army Map Service, and the results have been very good.

A somewhat similar method is to operate air-sea gravity meters in hovercraft, which ride on a cushion of air a few feet above the ground or water. Hovercraft can not operate over rough terrain or over a rough sea, but they have an advantage over helicopters in that they do not sink in case they fall into water. Hovercraft can travel at speeds of 60 miles per hour.

REFERENCES

Allan, T. D., P. Dehlinger, C. Gantar, C. Morelli, M. Pisano, and J. C. Harrison, Comparison of Graf-Askania and LaCoste-Romberg surface ship gravity meters, *J. Geophys. Res., 67,* 5157–5162, 1962.

Beyer, L. A., R. E. von Huene, T. H. McCulloh, and J. R. Lovett, Measuring gravity on the sea floor in deep water, *J. Geophys. Res., 71,* 2091–2100, 1966.

Bower, Donald R., The determination of cross-coupling errors in the measurement of gravity at sea, *J. Geophys. Res., 71,* 487–493, 1966.

Bower, D. R., and B. Loncarevic, Sea-gravimeter trials on the Halifax test range aboard C.S.S. Baffin, 1963, *Publ. Dominion Astrophys. Obs., 36*(1), Ottawa, Canada, 1967.

Browne, B. C., The measurement of gravity at sea, *Monthly Notices Roy. Astron. Soc., Geophys. Suppl., 4*, 271–279, 1937.

Browne, B. C., and R. I. B. Cooper, The British submarine gravity surveys of 1938 and 1946, *Trans. Roy. Soc. London, A, 242*, 243–310, 1950.

Browne, B. C., and R. I. B. Cooper, Gravity measurements in the English Channel, *Proc. Roy. Soc. London, B, 139*, 426–447, 1952.

Caputo, M., J. C. Harrison, R. von Huene, and M. D. Helfer, Accuracy of gravity measurements off the coast of southern California, *J. Geophys. Res., 68*, 3273–3282, 1963.

Clarkson, H. N., and L. J. B. LaCoste, An improved instrument for measurement of tidal variations in gravity, *Trans. Am. Geophys. Union, 38*, 8–16, 1957.

Coons, R., W. Strange, and G. P. Woollard, Evaluation and study of airborne gravimeter operational test, Reference 62-2, Geophysics and Polar Research Center, Department of Geology, University of Wisconsin, Madison, Wisconsin, 1962.

Dehlinger, P., Reliability at sea of gimbal-suspended gravity meters with 0.7 critically damped accelerometers, *J. Geophys. Res., 69*, 5383–5394, 1964.

Dehlinger, P., R. W. Couch, and M. Gemperle, Surface-ship gravity meter measurements corrected for vertical accelerations, *J. Geophys. Res., 71*, 6017–6023, 1966.

Dehlinger, P., and S. H. Yungul, Experimental determinations of the reliability of the LaCoste and Romberg surface ship gravity meter S-9, *J. Geophys. Res., 67*, 4389–4394, 1962.

Fleischer, U., Surface ship gravity measurements in the North Sea, *Geophys. Prospecting, 11*, 535–549, 1963.

Gilbert, R. L. G., A dynamic gravimeter of novel design, *Proc. Phys. Soc. London, B, 62*, 445–454, 1949.

Glicken, Milton, Eotvos corrections for a moving gravity meter, *Geophysics, 27*, 531–533, 1962.

Goodacre, A. K., A shipborne gravimeter testing range near Halifax, Nova Scotia, *J. Geophys. Res., 69*, 5373–5381, 1964.

Graf, A., and R. Schulze, Improvements on the sea gravimeter Gss 2, *J. Geophys. Res., 66*, 1813–1821, 1961.

Graham, K. W. T., and A. L. Hales, Surface-ship gravity measurements in the Agulhas Banks Area, south of South Africa, *J Geophys. Res., 70*, 4005–4011, 1965.

Harrison, J. C., Tests of the LaCoste-Romberg surface ship gravity meter, 1, *J. Geophys. Res., 64*, 1875–1881, 1959.

Harrison, J. C., The measurement of gravity at sea, in *Methods and Techniques of Modern Geophysics*, edited by S. C. Runcorn, Interscience Publishers, New York, 1960.

Harrison, J. C., and Lucien LaCoste, The performance of LaCoste-Romberg shipboard gravity meters in 1963 and 1964, *J. Geophys. Res., 73*, 1968.

Harrison, J. C., and F. N. Spiess, Tests of the LaCoste and Romberg surface-ship gravity meter, 2, *J. Geophys. Res., 68*, 1431–1438, 1963.

Hayes, D. E., J. L. Worzel, and H. Karnick, Tests on the 1962 model of the Anschütz gyrotable, *J. Geophys. Res., 69*, 749–757, 1964.

Henry, T. J. G., Determination of topographic profiles by use of radar and pressure altimeters (unpublished), Meteorological Division, Department of Transport, Ottawa, Ontario, Canada, 1948.

Jacoby, H.-D., and R. Schulze, New method to eliminate the cross-coupling effect in gravity measurements at sea, *J. Geophys. Res., 72*, 2199–2207, 1967.

LaCoste, L. J. B., *U. S. Patent 2 589 709*, 1952*a*.

LaCoste, L. J. B., *U. S. Patent 2 589 710*, 1952*b*.

LaCoste, Lucien, Surface ship gravity measurements on the Texas A and M college ship, the *Hidalgo, Geophysics, 24*, 309–322, 1959.

LaCoste, L. J. B., *U. S. Patent 2 964 948*, 1960.

LaCoste, L. J. B., *U. S. Patent 2 977 799*, 1961.

LaCoste, L., N. Clarkson, and G. Hamilton, LaCoste and Romberg stabilized platform shipboard gravity meter, *Geophysics, 32*, 99–109, 1967.

LaCoste, L. J. B., and J. C. Harrison, Some theoretical considerations in the measurement of gravity at sea, *Geophys. J. Roy. Astron. Soc., 5*, 89–103, 1961.

LaCoste, L. J. B., and A. Romberg, *U. S. Patent 2 577 889*, 1945.

LaFehr, T. R., and L. L. Nettleton, Quantitative evaluation of a stabilized platform shipboard gravity meter, *Geophysics, 32*, 110–118, 1967.

Loncarevic, B. D., Sea gravimeter reliability tests (abstract), *Trans. Am. Geophys. Union, 45*, 34, 1964.

Loncarevic, B. D., *Bulletin d'Information No. 12 of the Bureau Gravimétrique International*, Paris, France, 1966.

Nettleton, L. L., L. J. B. LaCoste, and Milton Glicken, Quantitative evaluation of precision of airborne gravity meter, *J. Geophys. Res., 67*, 4395–4410, 1962.

Nettleton, L. L., L. J. B., LaCoste, and J. C. Harrison, Tests of an airborne gravity meter, *Geophysics, 25*, 181–202, 1960.

Schulze, Reinhard, Automation of the sea gravimeter Gss 2, *J. Geophys. Res., 67*, 3397–3401, 1962.

Schulze, R., E. Brede, and E. Thebis, *German Patent 1 165 290*, 1964.

Talwani, Manik, Some recent developments in gravity measurements aboard surface ships, *Gravity Anomalies: Unsurveyed Areas, Geophys. Monograph 9*, edited by H. Orlin, pp. 31–47, American Geophysical Union, Washington, D. C., 1966.

Talwani, M., W. P. Early, and D. E. Hayes, Continuous analog computation and recording of cross-coupling and off-leveling errors, *J. Geophys. Res., 71*, 2079–2090, 1966.

Thompson, L. G. D., and L. J. B. LaCoste, Aerial gravity measurements, *J. Geophys. Res., 65*, 305–322, 1960.

Thompson, L. G. D., Comparison of LaCoste-Romberg and Askania-Graf gravity meters in gimbal and stabilized mounts, *J. Geophys. Res., 70*, 5599–5613, 1965.

Tsuboi, C., Y. Tomoda, and H. Kanamori, Continuous measurements of gravity on board a moving surface ship, *Geophys. Notes, Tokyo, 14*(2), 1961.

Vening Meinesz, F. A., *Theory and Practice of Pendulum Observations at Sea*, Waltman, Delft, The Netherlands, 1929.

Vening Meinesz, F. A., Gravity measurements at sea, 1, 2, and 3, *Publ. Neth. Geodesy Comm., Delft*, 1932, 1934, and 1948.

Vening Meinesz, F. A., *Theory and Practice of Pendulum Observation at Sea*, vol. 2, Waltman Delft, The Netherlands, 1941.

Wall, R. E., M. Talwani, and J. L. Worzel, Measurement of the cross-coupling effect for gravity measurements at sea using a stable platform (abstract), *Trans. Am. Geophys. Union, 45*, 33, 1964.

Wall, R. E., M. Talwani, and J. L. Worzel, Cross-coupling and off-leveling errors in gravity measurements at sea, *J. Geophys. Res., 71*, 465–485, 1966.

Worzel, J. L., Continuous gravity measurements on a surface ship with the Graf sea gravimeter, *J. Geophys. Res., 64*, 1299–1315, 1959.

Worzel, J. L., and M. Ewing, Gravity measurements at sea, 1947, *Trans. Am. Geophys. Union, 31*, 917–923, 1950.

Worzel, J. L., and M. Ewing, Gravity measurements at sea, 1948 and 1949, *Trans. Am. Geophys. Union, 33*, 453–460, 1952.

Worzel, J. L., G. L. Shubert, and M. Ewing, Gravity measurements at sea, 1950, 1951, 1952, and 1953, *Trans. Am. Geophys. Union, 36*, 326–338, 1955.

(Manuscript received March 28, 1967.)

Geothermal Resources Council, TRANSACTIONS Vol. 7, October 1983

GRAVITY STUDIES IN THE CASCADE RANGE

Carol Finn and David Williams

U.S. Geological Survey
P.O. Box 25046, Denver, Colorado 80225

ABSTRACT

We have compiled a compatible set of gravity data for the entire Cascade Range. From this data set we prepared a series of interpretive color gravity maps including a free air anomaly map, Bouguer anomaly map at a principle (2.67 g/cm^3) and an alternate (2.43 g/cm^3) reduction density, and filtered and derivative versions of the Bouguer anomaly map. The set is accompanied by a color terrain map at the same scale.

The regional anomaly pattern and gradients outline the various geological provinces adjacent to the Cascade Range and deliniate major structural elements in the range. The more local anomalies and gradients may delineate low density basin and caldera fill, faults, and shallow plutons.

Introduction

The U.S. Geological Survey (USGS) has supported gravity studies as part of its Cascades Geothermal Program. Gravity data are particularly useful in areas where there are large lateral density contrasts such as in volcanic regions. These density contrasts cause variations in the earth's gravity field which can often be related to subsurface geologic features such as faults, intrusions, ore bodies, etc.

We have compiled digital gravity data for the entire Cascade Range. Our sources of data were: the U.S. Defense Mapping Agency, the Earth Physics Branch, Department of Energy, Mines and Resources, Ottawa, Canada; Oregon State University (Couch, et al, 1981a, 1981b); University of Puget Sound (Danes and Phillips, 1983); and USGS files. The data have been re-reduced to form a consistent data set from which we have produced a free-air anomaly map, a terrain-corrected Bouguer anomaly map, a horizontal gradient version of the Bouguer anomaly map and filtered versions on the Bouguer anomaly map, one containing wavelengths greater than 100 km and the other with wavelengths less than 100 km. The Bouguer anomaly map with a principle Bouguer reduction density of 2.67 g/cm^3 will be published in color at a scale of 1:500,000 to be comparable to other USGS Cascades geologic maps which are in preparation. The rest of the above-mentioned maps will be published in color at a scale of 1:2,500,000 to agree wih the U.S. tectonic, geologic, and basement map series. This set will also include a color terrain map and two Bouguer anomaly maps one at the principle, 2.67 g/cm^3 reduction density and the other as an alternate Bouguer reduction density of 2.43 g/cm^3. The terrain map, the Bouguer anomaly map with a reduction density of 2.67 g/cm^3, and a horizontal gradient map are shown in Figures 1, 2, and 3, respectively. The purpose of this paper is to introduce the full set of gravity maps and to provide preliminary interpretations of some of the regional and local gravity features apparent in them. Place names referred to in the text are shown in Figure 1.

The Pacific Northwest, the location of the Cascade Range, has a complex tectonic history involving changes in plate tectonic setting from a passive Atlantic-type margin to an active subduction zone (Dickinson, 1976; Hamilton, 1978; and Hammond, 1979), changes in the location of the subduction zone and its asscociated magmatic arc, accretion of various terranes and micro-plate rotations. The Cascade Range is a volcanic arc extending from Lassen Peak, California to Mt. Garibaldi, British Columbia and is related to subduction of the Juan de Fuca and Gorda plates. The Cascades consist of a wide range of rock types and ages ranging in composition from basalt through rhyolite and in age from Miocene to recent (they do, however, overlie Mesozoic and Paleozoic rocks in Washington and Canada). The diversity of rock types results in numerous density contrasts that produce a wide variety of gravity anomaly patterns.

Regional Gravity Anomalies

The major geologic provinces generally have distinctive gravity signatures (Fig. 2). The Oregon Coast Range, an accreted island-arc terrane is a Bouguer gravity high with values averaging about +30 mgals. Another accreted island arc terrain, the Klamath Mountains, has values averaging about -100 mgals, lower than those for the Coast Range. The major gravity

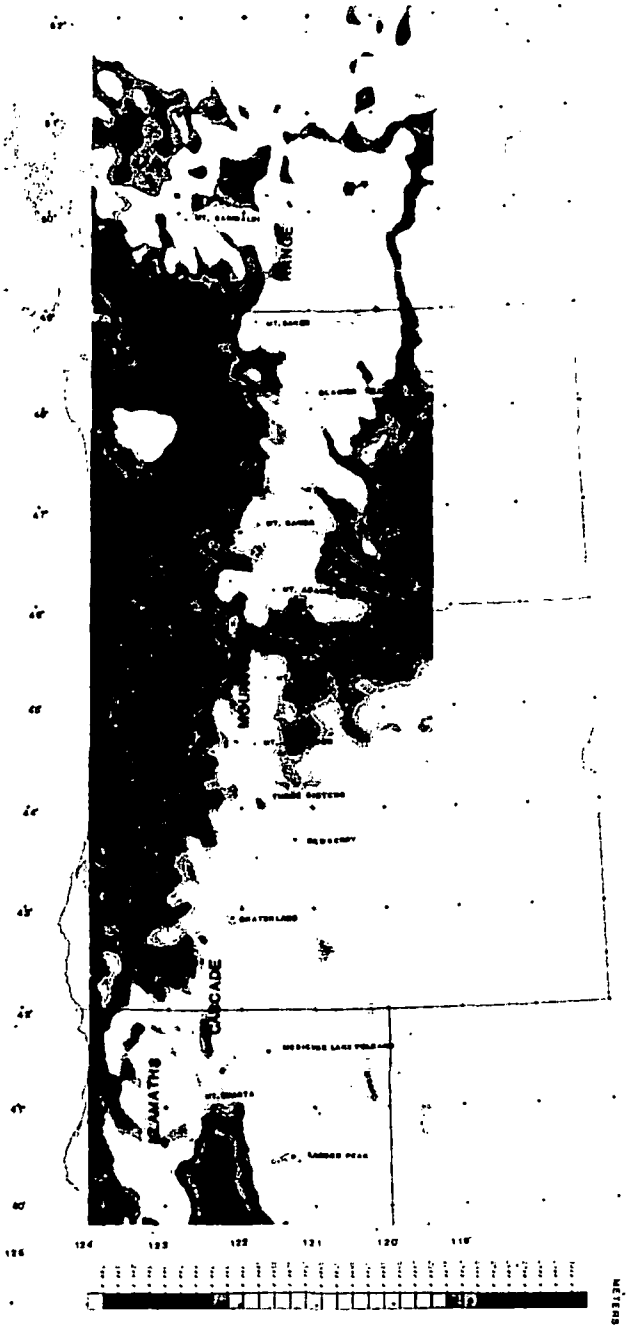

Figure 1. Terrain and location map

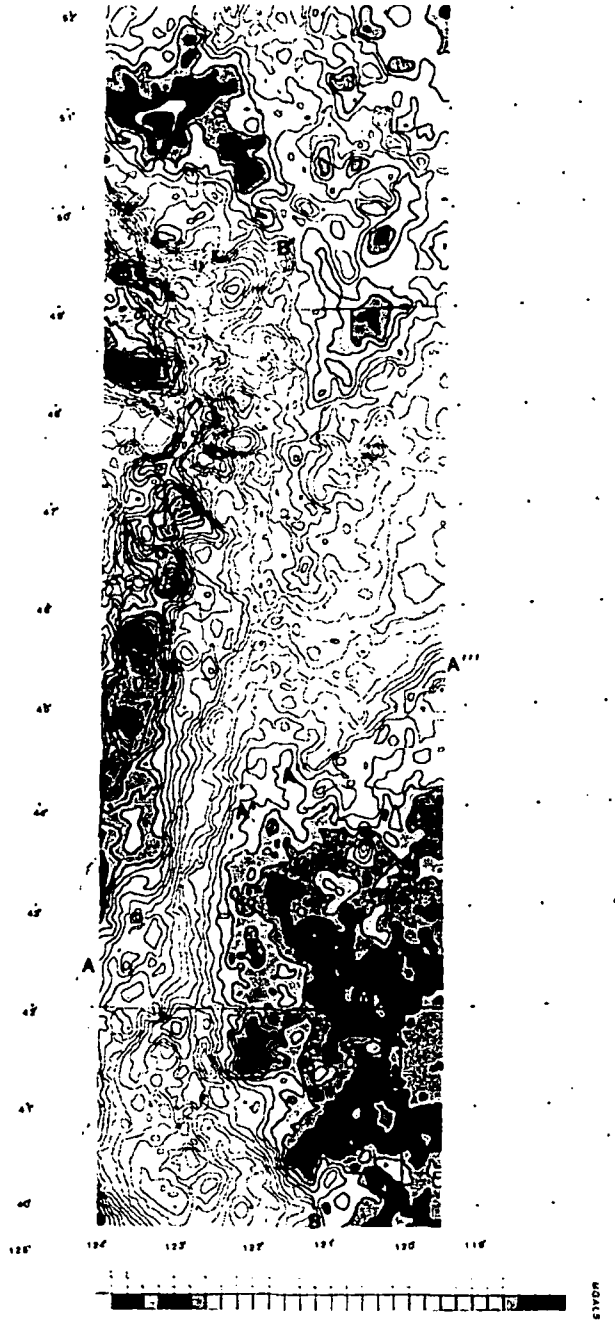

Figure 2. Bouguer Anomaly map

high in the center of Figure 2 averaging about -60 mgals may reflect shallow mantle associated with the Columbia Plateau, a province of extensive flood basalts. The gravity low associated with the Cascade Range is not apparent in Figure 2 because it is partially masked by the Basin and Range gravity low in the southern part of the range and by the low associated with the Columbia and Rocky Mountains in Canada (where values range from -200 mgals to -110 mgals).

North of Mt. Rainier in Washington and Canada a Bouguer reduction density of 2.67 g/cm^3 is probably appropriate because much of the surface rocks are Paleozoic and Mesozoic oceanic and granitic rocks. South of Mt. Rainier and in Oregon and California the surface rocks are generally composed of lower density volcanic rocks. Because the density of 2.67 g/cm^3 is a standard reduction density and roughly half of the Cascades should probably be reduced at this density, we used it for the principle reduction density on the Bouguer anomaly map of the range. A problem arises in using a single reduction density. For example the gravity anomaly associated with the California and Oregon Cascades is erroneously low because the Bouguer reduction of 2.67 g/cm^3 was used; a density of 2.43 g/cm^3 (Couch, et al, 1982) is more appropriate there.

Most mountain ranges produce Bouguer gravity lows. The source of the gravity low is assumed to be a low density root which provides isostatic compensation for the elevated topography of the mountain range. According to gravity and seismic evidence (Hill, et al, 1981; Leaver, et al, 1983; Dehlinger, et al, 1968, 1970), the crust thickens from 25 - 30 km east of the Cascades to 35 - 45 km below and west of them. If we were to assume isostatic compensation is principally accomplished by variations in crustal thickness then the low gravity values of the Basin and Range would imply thick crust. In fact the opposite is true. In the Basin and Range and perhaps the Cascades much of the isostatic compensation is provided by anomalously low density mantle materials.

A strong curvilinear gravity gradient (B-B' in Figs. 2 and 3) bounds the western edge of the Cascades gravity minima. This may be caused by as much as 2 km of vertical structural offset (Couch, et al, 1982, Zucca, et al, 1981) and may represent the western edge of the graben in which the Cascades lie (Couch, et al, 1982). This strong gradient is superimposed on a broader trend of eastward decreasing gravity values due to thickening of the crust and lithosphere from oceanic in the west to continental in the east (Couch, et al, 1982; LaFehr, 1965).

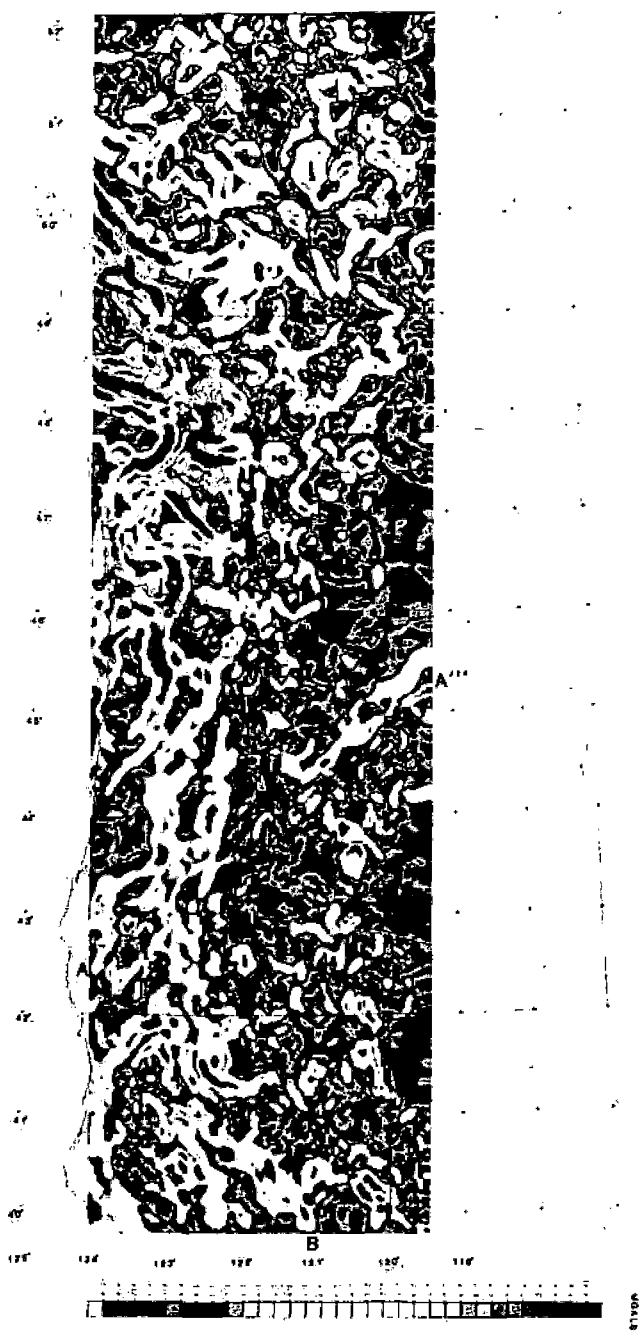

Figure 3. Map of the horizontal gradient of the Bouguer anomaly.

Figure 3 shows the magnitude of the horizontal gradient of the gravity field. The gradient magnitudes are maximum at inflection points of the gravity field which, by inference, delineate major sharp density boundaries (Cordell and Grauch, 1982). The sharp gradients bounding the Coast Range and Vancouver Island are probably related to density differences between oceanic and continental terranes. The gravity gradient on the western edge of the Cascades (B-B') discussed above can be seen in Fig. 3. Lineament A-A', A''-A''' may be related to the density change between oceanic and continental terrane. It follows the northern extent of pre-Tertiary terrane (the Klamath Mountains on the south-west and the Blue Mountains in the north-east). These terranes may have been connected in the early Tertiary (Hamilton, 1978) and then rotated clockwise westward creating a gap that is now occupied by the Cascade Range (Hamilton, 1978, Dickinson, 1976).

Local Gravity Anomalies

Local gravity anomalies in the Cascades are generally caused by sediment filled basins (gravity lows), an incorrect Bouguer reduction density (can cause either gravity highs or lows, but lows are more common when a Bouguer reduction density of 2.67 g/cm^3 is used), intrusions (gravity highs) and caldera fill (gravity lows). Since the Cascades south of Mt. Rainier are mantled by a layer of low density volcanics, gravity anomalies in this region usually deliniate rocks which differ from the density of these volcanic rocks. Although the proper Bouguer reduction density for much of the High Cascades is between 2.67 and 2.43 g/cm^3, most of the young, recently active volcanoes in the range have a bulk density of 2.2 g/cm^3. When this density is used to reduce the gravity data for most individual volcanoes, gravity highs, not lows, are commonly observed (Finn and Williams, 1982; Williams and Finn, in press). These positive anomalies are due to shallow, dense intrusions that probably range in composition from intermediate to mafic. Many other local gravity highs have been identified with old, eroded volcanic centers. Examples are the Goat Rock volcano in the Goat Rocks Wilderness, Washington and the Still Creek and Laurel Hill plutons just southwest of Mt. Hood (Williams and Finn, 1983).

Geothermal Resources

The delineation of structural features like faults and local features such as intrusions is useful for geothermal exploration. Faults can be zones of increased permeability. Intrusions under active volcanoes are often asymmetric to the volcanic cone and could be reached at a shallower depth if drill holes are sited with the benefit of the gravity data.

References

Cordell, L., and Grauch, V. J. S., 1982, Mapping basement magnetization zones from aeromagnetic data in the San Juan Basin, New Mexico (abs.): Soc. of Expl. Geophysicists Fifty-Second Annual International Meeting and Exposition, pp. 246 -247.

Couch, R.W., Pitts, G.S., Braman, D. E., and Gemperle, M., 1981a, Free-air gravity anomaly map and complete Bouguer gravity anomaly map, Cascade Mountain Range, northern Oregon: Oregon Dept. of Geology and Mineral Industries Geological Map Series GMS-15.

Couch, R.W., Pitts, G.S., Veen, C.A., and Gemperle, M., 1981b, Free-air gravity anomaly map and complete Bouguer gravity anomaly map, Cascades Mountain Range, southern Oregon: Oregon Dept. of Geology and Mineral Industries Geological Map Series GMS-16.

Couch, R.W., Pitts, G.S, Gemperle, M., Braman, D.E., and Veen, C.A., 1982, Gravity anomalies in the Cascade Range in Oregon: Structural and thermal implications: State of Oregon, Dept. of Geology and Mineral Industries Open-File Report O-82-9.

Danes, Z.F., and Phillips, W.M., 1983, Principal facts and a discussion of terrain correction. methods for the complete Bouguer gravity anomaly map of the Cascade Mountains, Washington: Washington Div. of Geology and Earth Resource Open-File Report 83-1.

Dehlinger, P., Couch, R.W., and Gemperle, M., 1968, Continental and oceanic structure from the Oregon coast westward across the Juan de Fuca Ridge, in Symposium on Continental margins and island arcs, 3rd, Zurich, 1967: Canadian Journ. of Earth Sciences, v. 5, pp. 1079-1090.

Dehlinger, P., Couch, R.W., McManus, D.A., and Gemperle, M., 1970, Northeast Pacific structure, in Maxwell, A.E., The sea: New York, N.Y., John Wiley, v. 4, pt. 2, pp. 133-189.

Dickinson, W.R., 1976, Sedimentary basins developed during the evolution of Mesozoic and Cenozoic arc-trench systems in western North America: Can. Jour. of Earth Sci., v. 13, pp. 1268-1287.

Finn, Carol, and Williams, D.L., 1982, Gravity evidence for a shallow intrusion under Medicine Lake Volcano, California: Geology, v. 10, pp. 503-507.

Hamilton, Warren, 1978, Mesozoic tectonics of the western United States: in D. G. Howell and K.A. Mc Dougall, eds., Mesozoic paleogeography of the western United States: Pacific section, Society of Econ. Paleontologists and Mineralogists, Pac. Coast Paleogeography Symp. 2, pp. 33-70.

Hammond, P.E., 1979, A tectonic model for evolution of the Cascade Range, in J.M. Armentrout, M.R. Cole and H. TerBest Jr., eds., Cenozoic paleogeography of the western United States: Pac. sect., Soc. of Econ. Paleontologists and Mineralogists, Pacific Coast Paleogeography Symp. 3, pp. 219-237.

Hill, D.P., Mooney, W.D., Fuis, G.S. and Healy, J.H., 1981, Evidence on the structure and tectonic environment of the volcanoes in the Cascade Range, Oregon and Washington, from seismic-refraction/reflection measurements (abs.): Soc. of Expl. Geophysicists 51st Annual International Meeting, Los Angeles, CA.

LaFehr, T.R., 1965, Gravity, isostacy, and crustal structure in the southern Cascade Range: Journ. of Geophy. Res., v. 70, pp. 5581-5597.

Leaver, D.E., Mooney, W.D., and Kohler, W.M., 1983, A refraction study of the Oregon Cascades: in press.

Williams, D.L., and Finn, Carol, 1983, Analysis of gravity data in volcanic terrain and gravity anomalies and subvolcanic intrusions in the Cascade Range and at other selected volcanoes: in press.

Zucca, J.J., Catchings, R.D., Fuis, G.S., and Mooney W.D., 1981, Preliminary report on a seismic refraction study in the Mt. Shasta region of northern California (abs.): EOS (Amer. Geophys. Union Trans.), v. 62, p. 1089.

Gravity and Magnetic Studies of The Geysers–Clear Lake Geothermal Region, California, USA

WILLIAM F. ISHERWOOD
U.S. Geological Survey, Denver, Colorado 80225, USA

ABSTRACT

Gravity and magnetic fields in The Geysers-Clear Lake region are interpreted in relation to the known geology and other available geophysical data. New gravity data provide additional detail within the area of geothermal steam production. Computer techniques were used for removal of the regional gravity field, anomaly enhancement, and modeling subsurface structures. The gravity field was separated into three components: (1) a regional field presumed to be due to deep crustal structure related to the continental margin; (2) a residual gravity low of approximately 30 mgal centered over Mount Hannah and having an approximate diameter of 20 km, which is caused, according to our model, by a magma chamber whose top lies within 10 km of the surface; and (3) a closed residual low over the original steam production field. This low is probably related to effects within 1.5 km of the surface and was modeled as a steam-saturated reservoir structure. Local magnetic highs correlate with surface outcrops of serpentinite and relief on the volcanic rocks. Upward continuation of the aeromagnetic data suggests that the serpentinite body along the Collayomi fault may extend to a depth of more than 3 km near Boggs Mountain, but that other serpentinite bodies are probably more shallow. A long-wavelength magnetic high (centered at ~39°03'N 122°33'W) and a magnetic low (centered at ~38°43'N 122°47'W) give half-width depth estimates of about 10 km. The center of the Mount Hannah gravity low lies in an area between these features and appears devoid of deep magnetic expression.

INTRODUCTION

In order to explore for economic steam reservoirs, it is important to know the complete, three-dimensional geology which governs such a system. The Geysers-Clear Lake region, California (Fig. 1), has the world's largest production of commercial power from a dry-steam geothermal reservoir. This paper describes gravity and magnetic field analysis at The Geysers which defines a possible deep geologic structure and heat source.

A small area from the recently published Santa Rosa gravity map (Fig. 2) illustrates the previous gravity coverage. The major gravity low centered over Mount Hannah, approximately 11 km northeast of The Geysers, drew the attention of several workers. Rodger Chapman (1966) first suggested a magma chamber at depth as a possible source of the anomaly, the volcanic activity, and the geothermal reservoir. Although several other models have been investigated, the present study supports the presence of a magma chamber whose center is deeper than 10 km.

During the summer of 1974, I added 150 gravity stations with special attention to improving control in the region of steam production and the Mount Hannah low. These data were merged with the previous data and reduced to complete Bouguer gravity values with Bouguer reduction densities of 2.67 g/cm^3 and 2.45 g/cm^3 (Isherwood and Chapman, 1975). These two density values minimize terrain

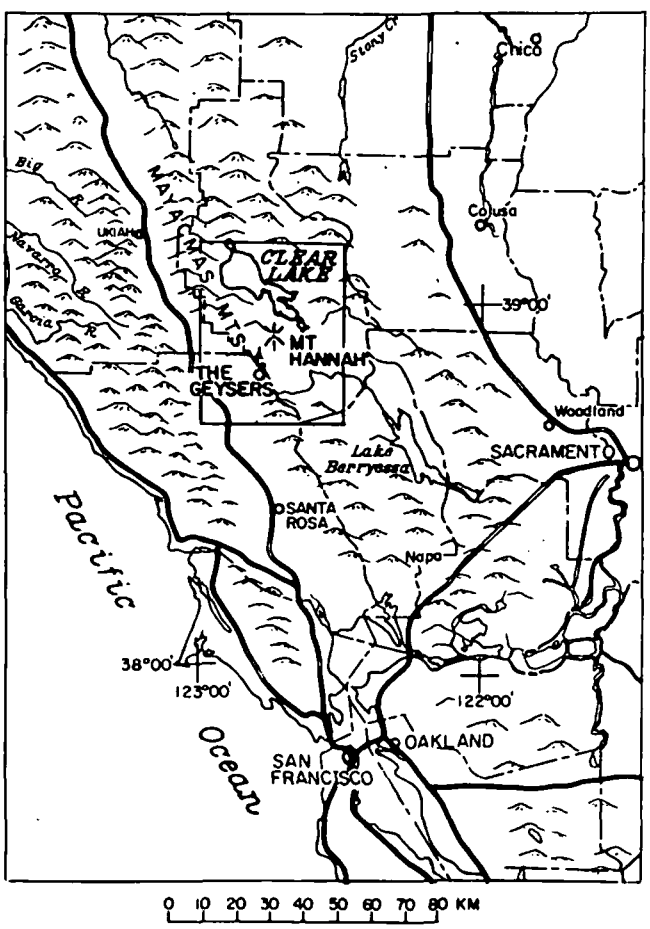

Figure 1. Index map, showing the region of discussion in this paper.

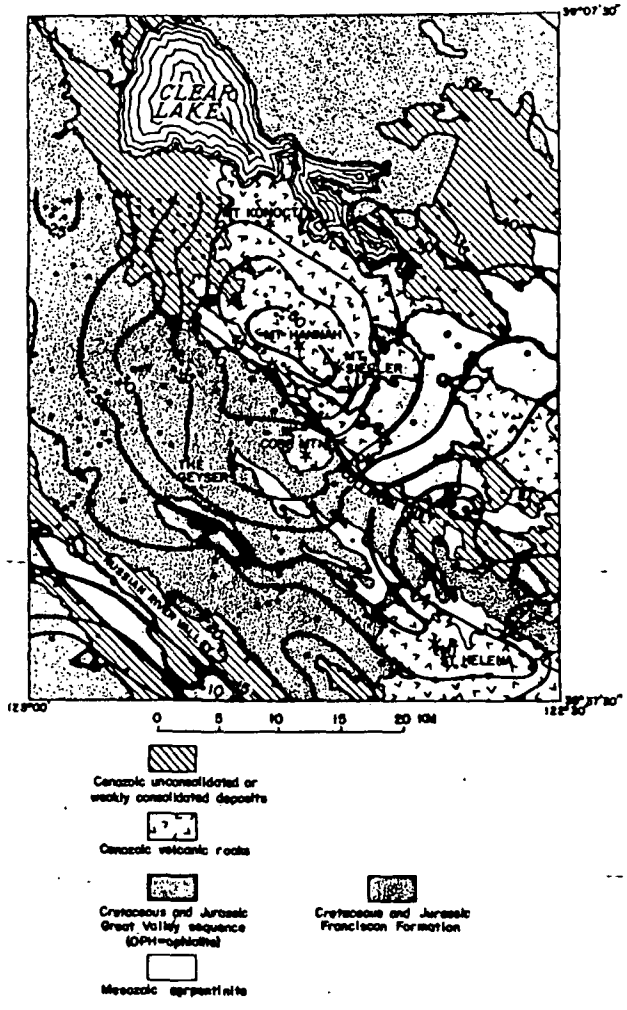

Figure 2. Generalized geology with gravity from Santa Rosa Gravity Map, (Chapman and Bishop, 1974).

effects within the Franciscan and Cenozoic volcanic terranes respectively. Consequently, the gravity field reduced at 2.67 g/cm^3 probably better represents the subsurface structure in the area southwest of the Collayomi fault zone which separates these terranes; and gravity at 2.45 g/cm^3 does similarly to the northeast.

The study of rock samples and well density logs yields a general notion of the physical distinction between rock units in the region (Table 1). Because sampling is usually biased in favor of rock units having conspicuous outcrops, weak (low-density) rocks have possibly been underestimated. In particular, weak shaly rocks in the Franciscan formation—referred to as melange—rarely appear as substantial exposures, but may form a matrix around many of the harder "knockers" which are well exposed. More well-log information is needed to determine the full effect of such units. Figures shown in Table 1 are based on small, not necessarily representative, sample sets of data with considerable scatter and are only intended to represent possible anomaly sources.

The field shown in the Santa Rosa and Ukiah 1:250 000-scale gravity maps (R. H. Chapman, unpub. data) provides the basis for removal of a regional gravity field. These two maps were hand digitized on a 5-km grid. The digital computer fitted polynomial surfaces of order 1 through 7 to the data. The sixth-order surface shown in Figure 3 was chosen as a good representation of the regional field without

Table 1. Rock properties.

Rock type	Density (g/cm^3)	Susceptibility (emu/cm^3)
Franciscan formation		
Greenstone	2.9	1.0×10^{-4}
Graywacke	2.6	2.0×10^{-4}
Melange	2.4	5.0×10^{-5}
Blueschist	3.1	8.0×10^{-5}
Serpentinites	2.5	3.8×10^{-3}
Assumed average	2.67	5.0×10^{-4}
Clear Lake volcanics (upper Tertiary and Quaternary)*		
Olivine basalts	2.8	3.2×10^{-4}
Rhyolites and dacites	2.45	1.5×10^{-4}
Assumed average	2.5	1.7×10^{-4}
Hot silicic magma	2.2†–2.4‡	
Great Valley sequence		
Sediments	2.5	1.0×10^{-4}
Ophiolite	2.9	1.9×10^{-3}

* From Brice (1953).
† From Murase and McBirney (1973).
‡ Average Franciscan material reduced by 10%.

perturbation by local anomalies. Note that this surface is nearly planar over the more restricted region of this study. This component of the total gravity field is attributed to deep crustal and upper mantle structure related to the continental margin. The values of the regional surface were subtracted from the complete Bouguer values at each station and the residuals were machine gridded and contoured.

The maps of residual gravity presented in Figures 4 and 5 show the following:

1. The major gravity feature (referred to as the Mount Hannah low) is a roughly circular depression of about 25

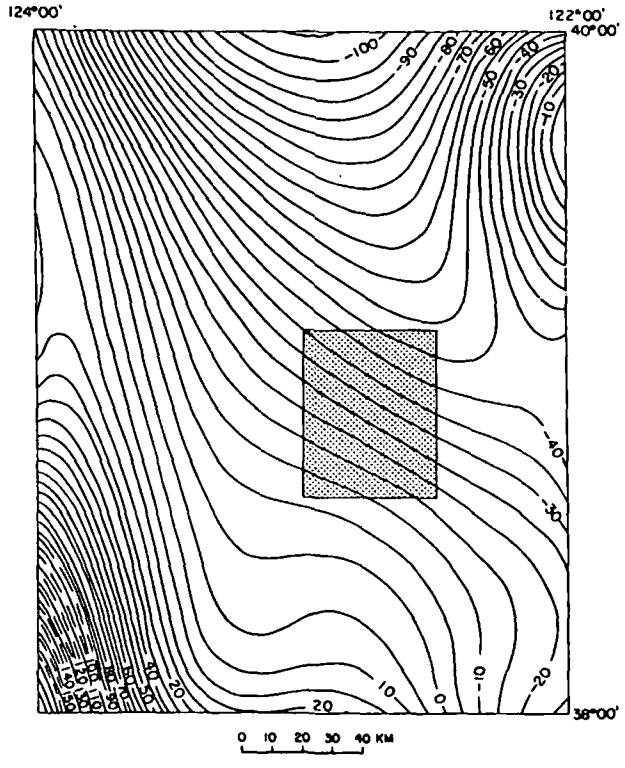

Figure 3. Sixth-order suface fit to regional gravity; 5-mgal contour interval. Shaded rectangle is the portion used to adjust complete Bouguer gravity values in this survey.

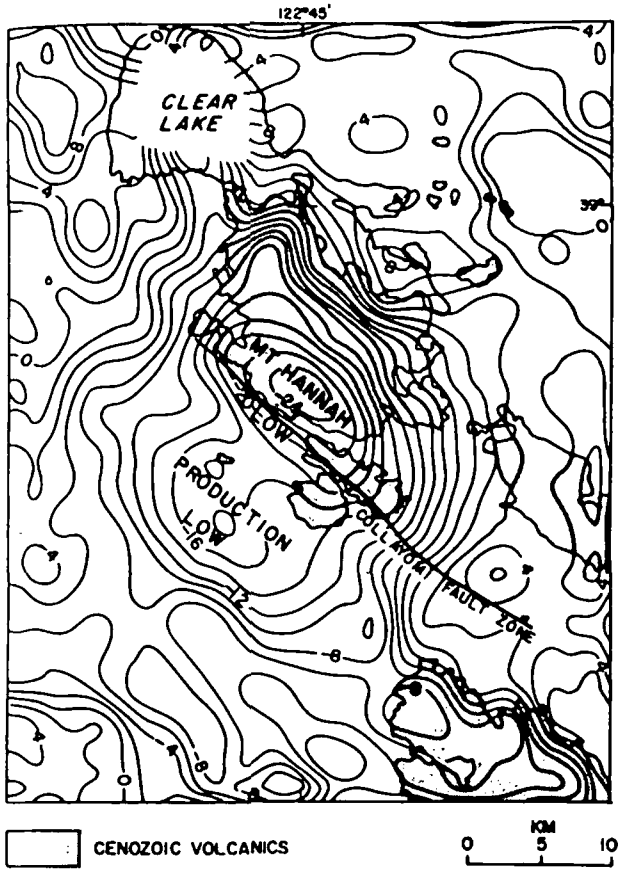

Figure 4. Residual gravity reduced at 2.67 g/cm³; 2-mgal contour interval.

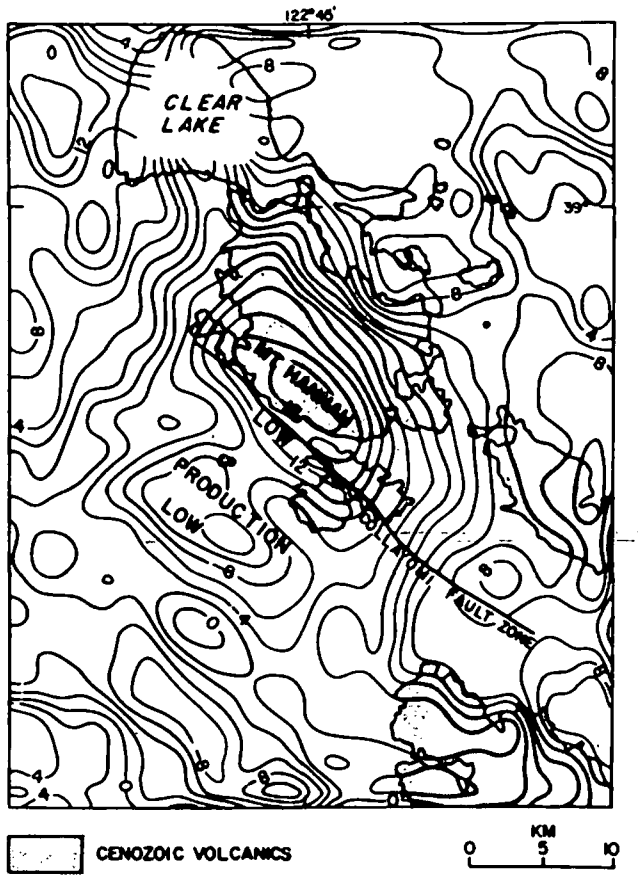

Figure 5. Residual gravity reduced at 2.45 g/cm³; 2-mgal contour interval.

mgal and 30-km diameter. The steep gradients to the northwest and southeast of the center notably cross the structural grain of the region.

2. The Mount Hannah gravity low is centered near the southwest edge of the Quaternary volcanic field, and its gravity gradient extends more than 12 km into the Franciscan terrane.

3. Each of the recognized volcanic vents south of Clear Lake correlates with a residual gravity low. Such correspondence suggests a genetic relation.

4. There is now apparent a secondary closed low in the region of steam production at The Geysers. This closure (referred to as the production low) is separated from the closure near the summit of Mount Hannah by a ridge of higher gravity.

5. A noteworthy gravity high of at least 6 mgal lies northeast of the Mount Hannah low and is centered over the southeast arm of Clear Lake. Correlation with surface geology is not clear.

Table 2. Depth estimates from gravity anomalies.

Anomaly	Half-width estimate to center (km)	Gradient estimate to top (km)
Mt. Hannah low	11.5 (sphere)	7.5
Production low	2.2 (cylinder)	1.9
Southeast Clear Lake high	4.5 (sphere)	2.3

Rough approximations of the source depths are made in Table 2 using the half-width method (Nettleton, 1940) and the ratio of maximum anomaly to maximum gradient (Bott and Smith, 1958).

The depths estimated for the source of the production low have been penetrated by drilling of the producers: at least some of the anomaly, then, may be caused by reservoir structure.

AEROMAGNETICS

The results of an aeromagnetic (total field) survey flown in 1972 were compiled by the U.S. Geological Survey in an open-file report (1973). The flight elevation was 4500 feet (1372 m) barometric, with east-west flight lines at approximately 1.6 km spacing. Superimposing this map on available geologic and topographic reference maps enables the following observations:

1. The overall pattern is complex with high magnetic relief (for example, greater than 700 gamma within 10 km of Mount Hannah).

2. A major magnetic high in the northeast corner of the study area has recognizable expression over greater than 400 km². Although there is no recognized surface exposure in this region which is likely to account for this anomaly, it lies on the trend of major serpentinite bodies (and magnetic highs) which bound the west side of the Great Valley.

3. Several local magnetic highs and lows clearly correspond to volcanic peaks close to the flight line. The signs of the

anomalies would indicate Mount Konocti to be normally magnetized, Cobb Mountain reversed, Mount Siegler normal, and Mount Hannah mixed or weak (see Fig. 2 for location). These findings agree with measured directions determined from rock cores with standard paleomagnetic methods for determining natural remanent magnetizations.

4. Other magnetic highs correlate well with mapped ultrabasic bodies. Such a relation has been noted throughout the California Coast Ranges (Saad, 1969; Byerly, 1966; Chapman, 1975).

A major component in observed aeromagnetic data is the local gradient of the earth's main field. In order to facilitate further processing, the open-file aeromagnetic map was digitized on a 1-km grid, making an array 57 rows by 45 columns. The main field component was then removed on the basis of the eight-order 1965 International Geomagnetic Reference Field (IGRF) updated to 1972, and adjusted by a constant to approximately a zero mean. The resultant residual magnetic field, Figure 6, shows no major differences in the anomaly pattern from the original map (U.S. Geological Survey, 1973).

UPWARD CONTINUATION

The field shown in Figure 6 contains contributions from topographic effects and changes of magnetization of small near-surface bodies primarily in the short-wavelength end of the spectrum. Upward continuation, which acts as a type

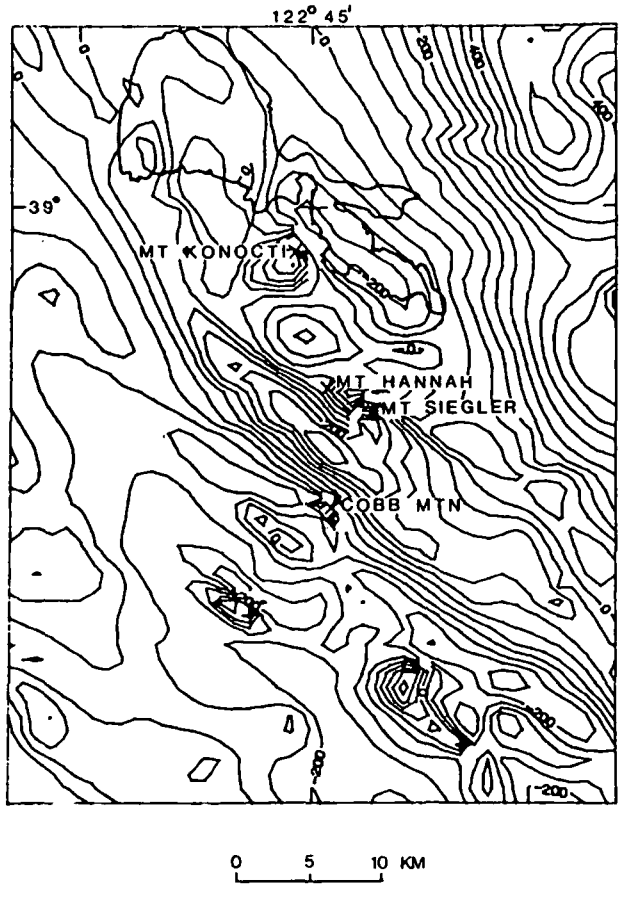

Figure 6. Total field magnetics of The Geysers; 50-gamma contour interval. Digitized on 1-km grid, IGRF removed.

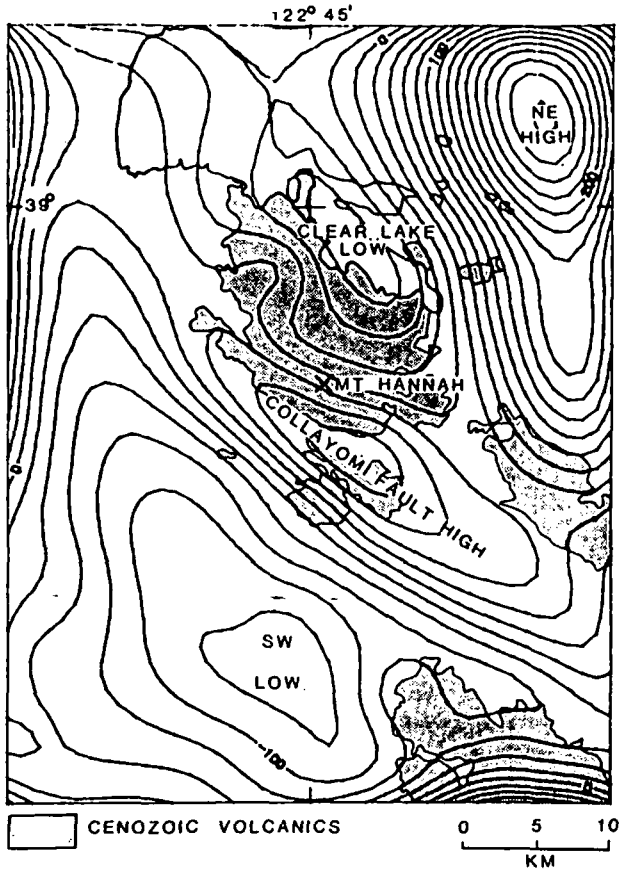

Figure 7. Magnetics continued upward 3 km; 20-gamma contour interval.

of wavelength filter, was used to de-emphasize these features. Figures 7, 8, and 9 show the residual aeromagnetic field continued upward 3 km, 5 km, and 7 km respectively. On the assumption that more superficial effects disappear first with the upward continuation, the following interpretations are made:

1. The most obvious topographic effects are quite subdued by 3-km upward continuation and are no longer recognized at 5 km.
2. With the exception of the serpentinite zone along the Collayomi fault, the magnetic highs associated with surface exposures of ultrabasics disappear by 3-km continuation. This is evidence that serpentinite along the Collayomi fault zone may have considerable depth south of Mount Hannah where the fault zone is buried by volcanics, whereas other ultrabasic bodies may be more shallow.
3. The magnetic low over the southeast arm of Clear Lake and north of the Collayomi fault high has the correct relation for a dipole low, at this magnetic latitude, associated with the high. Alternatively, it may be only a relative low between two magnetic highs. The fact that these two features disappear with the same upward continuation supports the suggestion that they are associated with roughly the same depth.
4. Although the source of these central anomalies may extend several kilometers deep, no sources in the central region are as deep as those apparently causing the magnetic high to the northeast or the magnetic low to the southwest.

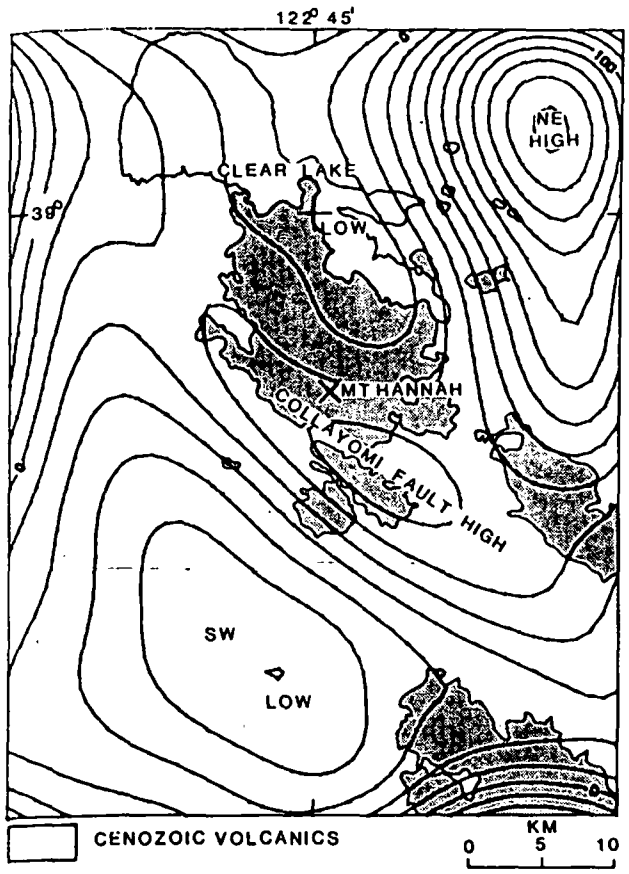

Figure 8. Magnetics continued upward 5 km; 20-gamma contour interval.

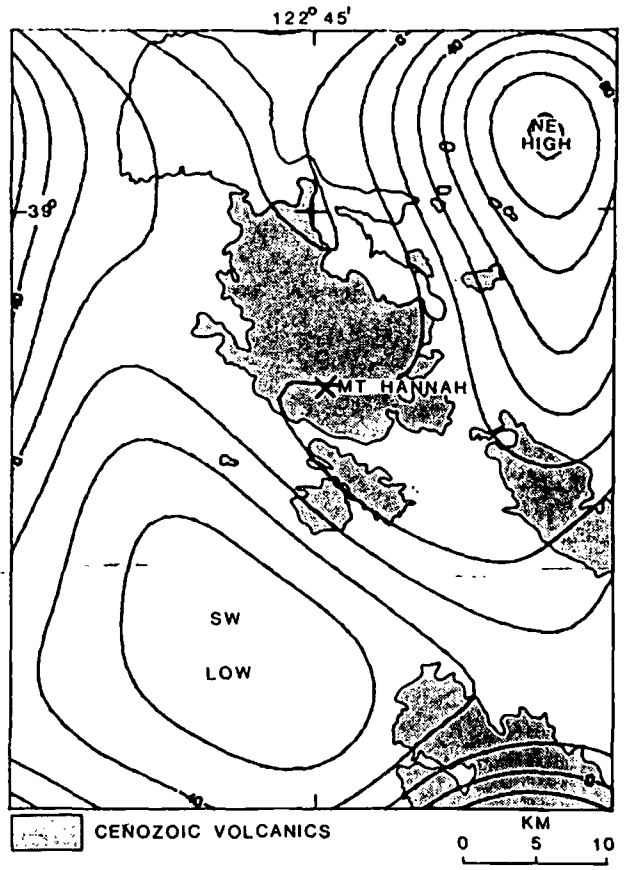

Figure 9. Magnetics continued upward 7 km; 20-gamma contour interval.

Choosing the four major anomalies brought to attention by upward continuation, depth estimates were made similar to those made for the gravity anomalies (Table 3).

Table 3. Depth estimates from magnetic anomalies.

Anomaly	Half-width estimate to center (km) pole	sphere	Gradient estimate to top (km)
Collayomi high	1.9	3.2	1.3
Clear Lake low	1.6	3.1	1.8
Northeast high	6.8	10.8	6.8
Southwest low	6.8	10.8	5.8

PSEUDOGRAVITY

If magnetic and gravity anomalies are caused by the same body of uniform density and magnetization, then Poisson's theorem describes the relation between anomalies (for example, Garland, 1951). These assumptions are tested by computing pseudogravity from the magnetic field and comparing it with the observed gravity. Because of the low Koenigsberger Q ratio (natural remanent magnetism, *NRM*, divided by induced magnetization) found for serpentinites from the area, *NRM* has been discounted as a source of the major anomalies (Saad, 1969). Figure 10 shows the pseudogravity field using test values of apparent susceptibility, k = 0.003 emu and density contrast, $\Delta\rho$, = 0.15 g/cm^3 prepared from a filtered version of the aeromagnetics. Wavelengths shorter than about 6 km were removed to suppress terrain and other superficial effects. Although different choices of k and $\Delta\rho$ will change the magnitude and even the sign of the pseudogravity anomalies, their positions and shapes will remain unchanged. This map shows a pronounced gradient approximately at the Collayomi fault, but the overall pattern differs considerably from the observed gravity. Even allowing for different signs of $k/\Delta\rho$ on opposite sides of the Collayomi fault zone, the anomalies do not match the gravity, apparently because of the difference in wavelength components and an offset in their centers. This is further evidence that the same bodies do not produce both the gravity and magnetic anomalies. One possible explanation, which will be examined more fully in the next section, is that the source body of the Mount Hannah low is above its Curie point, at which temperature remanent magnetization would disappear and suceptibility magnetization would also be exceedingly small. Consequently this body would have no magnetic expression.

SPECTRA

Bhattacharyya and Morley (1965) and Spector and Grant (1970) have popularized the idea of using the spectra of potential fields to estimate the depth to the causative bodies. Spectral methods appear particularly useful in such cases where near-surface sources tend to mask the effects of the deeper bodies of interest. As shown by the above workers and Odegard and Berg (1965), the slope of the gravity spectrum, plotted as the log of the amplitude versus wave

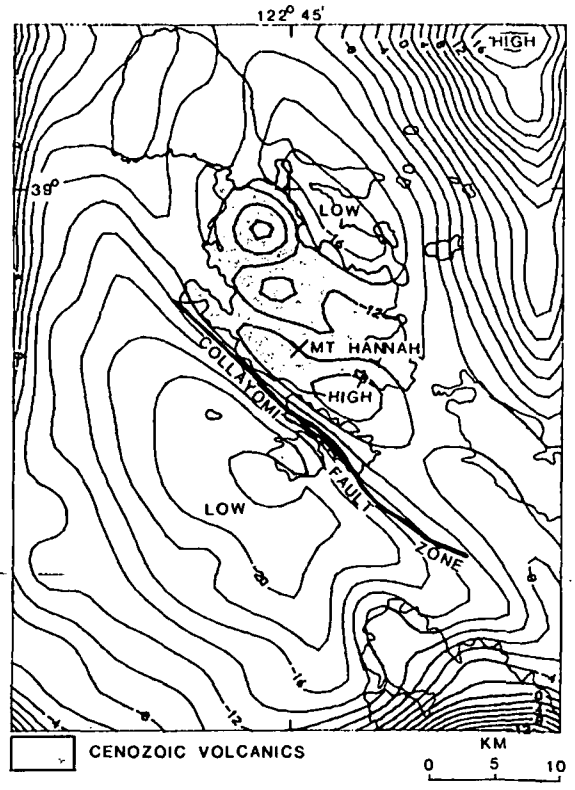

Figure 10. Pseudogravity derived from filtered magnetics (5-km cutoff) $\rho = +0.15$, $k = +0.003$; 2-mgal contour interval.

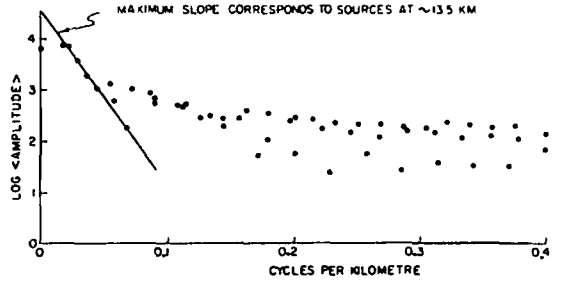

Figure 11. Frequency spectrum of gravity field at The Geysers; from 56-km by 45-km grid (radial averages).

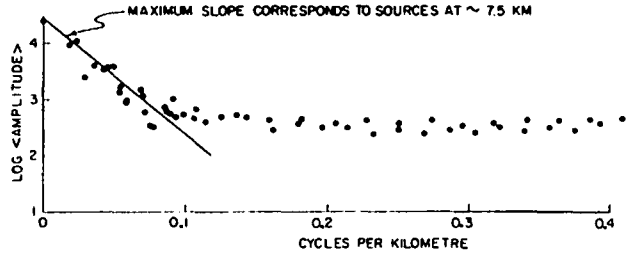

Figure 12. Frequency spectrum of pseudogravity derived from aeromagnetic data, The Geysers; 56-km by 44-km grid.

number, is proportional to the depth of an equivalent point source. Figure 11 shows such a plot obtained from the gridded residual gravity, and Figure 12 shows the same for the pseudogravity grid produced from the magnetics. (Using pseudogravity rather than magnetics assures comparability.) Both graphs show steep slopes at low wave numbers and more gentle slopes at higher wave numbers. Interpretation of these slopes was made after comparisons with spectra derived from synthetic models of spheres at different depths. According to the slopes shown here, the gravity could result in part from a deep source whose depth (center of sphere) is approximately 13.5 km. The deepest component recognized as a magnetic source, reflected in the pseudogravity spectrum, is only about 7.5 km deep; and as we saw from the previous discussions, the deepest sources appear spatially related to the high northeast of Clear Lake and the low 10 km south of The Geysers. It has been reasoned (Bhattacharyya and Morley, 1965; Bhattacharyya and Leu, unpub. data, 1975) that a lack of deep magnetic sources in a region may be due to a rise in the level of the Curie isotherm.

LOW-PASS FILTERING AND DEEP MODEL

On the basis of the spectra, low-pass filters were designed to investigate the long-wavelength anomalies. Figure 13 shows the gravity field (at 2.67 g/cm^3 reduction) filtered to eliminate wavelengths shorter than about 18 km (0.056 cycles/km). From the spectra, we would expect the remaining wavelengths to be dominated by the postulated deep source. This map looks as we might expect from a centrobaric mass centered under the bottom of the low. To test the 13.5-km depth estimation from the previous section, several representative profiles were drawn across the long-wavelength anomaly on the axes indicated in Figure 13. These profiles are compared in Figure 14 with that calculated

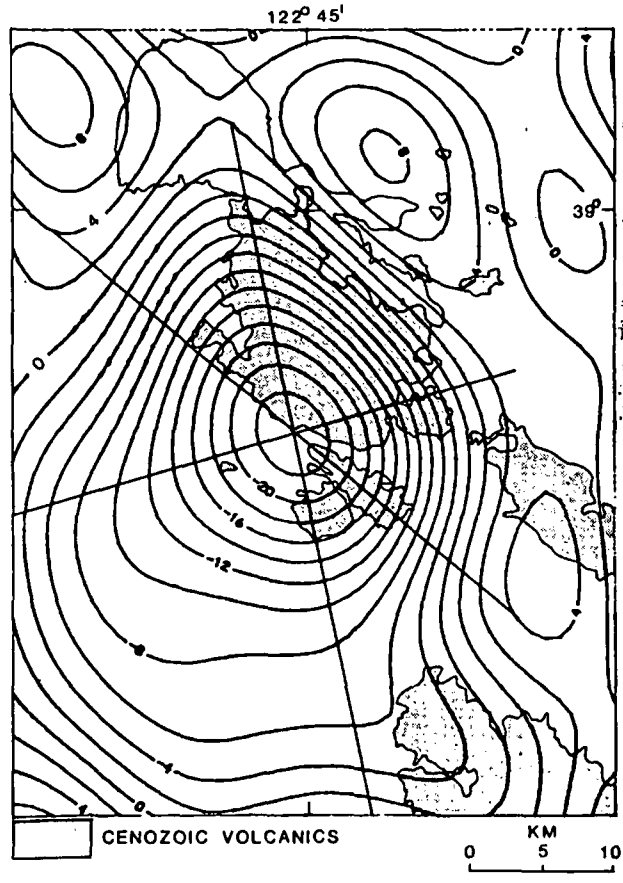

Figure 13. Gravity (at 2.67 g/cm^3) low-pass filtered with approximately 18-km cutoff; 2-mgal contour interval. Lines are representative profiles used in Figure 14.

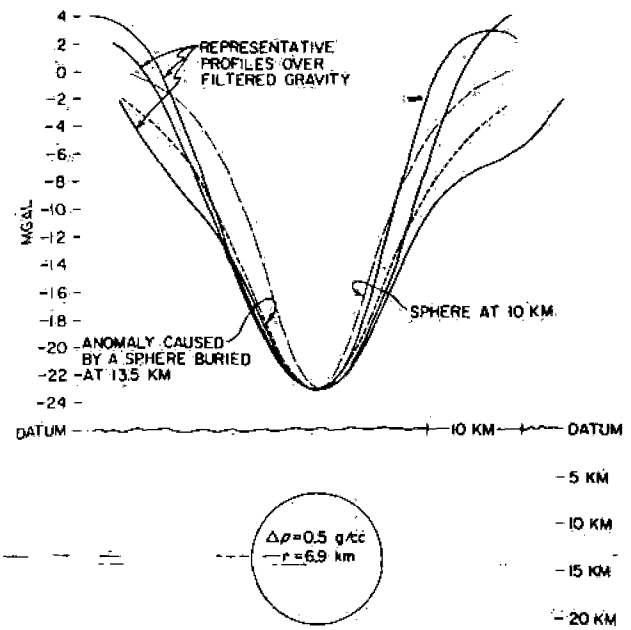

Figure 14. Representative profiles from Figure 13 compared with curves calculated for spheres buried at 13.5 km and 10 km. One possible limiting sphere for the 13.5-km source profile is shown below.

for a sphere with center at 13.5-km depth. Also shown is the calculated curve for a sphere at 10 km to illustrate the sensitivity of the anomaly shape to depth.

Although this anomaly is well-modeled by the field of a sphere at 13.5-km depth, this must be considered a limiting case. A more lenticular body or a body with a graduational density boundary could cause the same anomaly but be less deep.

Calculation can now be made for the mass deficiency, both from the curve for the postulated deep sphere and by Gauss' theorem. Table 4 shows the relation of density contrast, radius, and depth to the top of a sphere at 13.5-km depth (the curve in Fig. 14) and mass deficiency of 6.8 $\times$ 10^{14} kg. In practice, the calculation of mass deficiency by Gauss' theorem requires an assumption about the depth to the source (Grant and West, 1965, p. 270). Provided the regional field yields a reasonable gravity datum, the slightly different values of Table 5 are calculated.

Certain implications are now clear. If the density contrast is small, the source material must extend nearly to the surface. The volcanic rocks at the surface may indeed provide some small density contrast (0.1 to 0.2 g/cm^3) with

Table 4. Limiting sphere with center at 13.5 km depth and 25-mgal anomaly above center (requiring a mass deficiency of 6.8 $\times$ 10^{14} kg).

Δρ (g/cm^3)	Radius (km)	Depth to top (km)
0.1	11.8	1.7
0.2	9.3	4.2
0.3	8.2	5.3
0.4	7.4	6.1
0.5	6.9	6.6
0.6	6.5	7.0
0.7	6.2	7.3
0.8	5.9	7.6

Table 5. Mass from Gauss' theorem.

Δρ (g/cm^3)	Depth of 13.5 km, 5.3 $\times$ 10^{14} kg: Radius (km)	Top (km)	Depth of 12 km, 4.9 $\times$ 10^{14} kg: Radius (km)	Top (km)	Depth of 10 km, 4.2 $\times$ 10^{14} kg: Radius (km)	Top (km)
0.1	10.8	2.7	10.5	1.5	10.0	0
0.2	8.6	4.9	8.4	3.6	7.9	2.1
0.3	7.5	6.0	7.3	4.7	6.9	3.1
0.4	6.8	6.7	6.6	5.4	6.3	3.7
0.5	6.3	7.2	6.2	5.8	5.9	4.1
0.6	6.0	7.5	5.8	6.2	5.5	4.5
0.7	5.7	7.8	5.5	6.5	5.2	4.8
0.8	5.4	8.1	5.3	6.7	5.0	5.0

the Franciscan terrane to the south, west, and possibly north; but to the east this contrast is not apparent in surface rocks. Moreover, it is impossible to match the gravity gradients over the Franciscan terrane with low-density units limited to the northeast side of the Collayomi fault, which might be considered to be a vertical or northeast-dipping local boundary between Franciscan and Great Valley rocks (Garrison, 1972). This does not rule out the possibility of a complex low-density source made up in part by volcanics, Great Valley sediments, serpentinites, and low-density Franciscan melange; however, the required low-density units apparently have not been found in drill holes over 2-km deep south of the Collayomi fault zone.

The Santa Rosa gravity sheet (Chapman and Bishop, 1974) shows several outliers of Great Valley sequence rocks on the Franciscan terrane, none of which produce gravity anomalies comparable to the Mount Hannah low. This anomaly absence suggests that either the Great Valley outliers are generally shallow or that the true bulk-density contrast with Franciscan rocks is small.

On the other hand, if the body primarily responsible for the Mount Hannah gravity low does not come within about 5 km of the surface, it must be less dense than any unit listed in Table 1 except hot silicic magma. The circular appearance of the residual anomaly favors this interpretation as a magma chamber.

At least one hole has been drilled within a few kilometers of the center of the Mount Hannah low (Fig. 15). The well, Sullivan 1, in sec. 18, T. 12 N., R. 8 W., started in the serpentinite associated with the Collayomi fault and has penetrated almost 1900 m without leaving serpentinite (E. B. Towne, written commun.). Another well, about 6.5 km north of Mount Hannah, was drilled through the volcanic surface rocks for about 750 m and continued to about 2380 m depth in a complex sequence containing considerable greenstone and serpentinite. A density log for the hole indicates a range of densities for the volcanics between 2.3 and 2.5 g/cm^3 with an average of about 2.4 g/cm^3 and below the volcanics to the bottom of the available log (1800 m), a range of densities from 2.4 to 2.8 g/cm^3 with an average of about 2.65 g/cm^3. These suggest that the preferred model should include some near-surface contribution from the volcanics, but still requires a deep source to produce gravity expression well into the Franciscan terrane.

Additional subsurface information is available from interpretation of microearthquake surveys (Lange and Westphal, 1969; Hamilton and Muffler, 1972). Hypocenters shown on published maps lie mainly outside the region of the possible

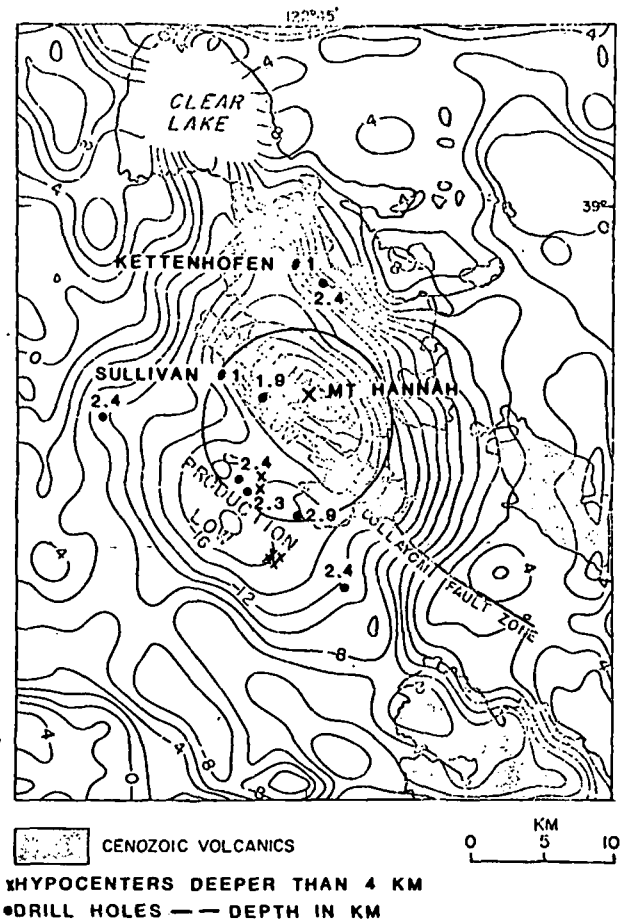

Figure 15. Plan view of a buried sphere of radius 6.9 km superimposed on the gravity shown in Figure 4. Also shown are some representative drill holes with depth in kilometers and epicenters of microearthquakes with focal depth deeper than 4 km (Hamilton and Muffler, 1972).

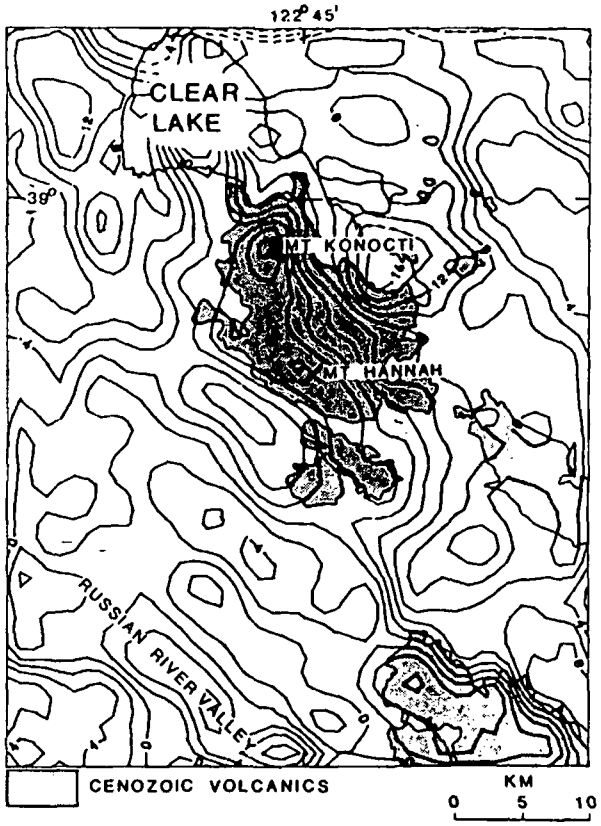

Figure 16. Residual gravity (at 2.67 g/cm^3) after removal of the field from a sphere buried at 13.5 km; contour interval 2-mgal.

anomalous mass (Fig. 15). Two foci, however, were located at 4- and 6-km depths along the ridge of higher gravity separating Mount Hannah summit from the production low. The general shallowness of earthquake foci can be construed as evidence for elevated temperatures (Hamilton and Muffler, 1972). The two deeper earthquakes may then indicate some cooler region—perhaps a sort of roof pendant—separating two cupolas of a magma chamber. An interpretation of similar structure is made by Eaton et al., 1975, at Yellowstone National Park.

REMOVAL OF DEEP STRUCTURE

The nearer surface structures are now investigated by attempting to remove the effect of a simple deep body. Two methods were used to model the field attributable to deep sources: (1) analytic generation of the field produced by the postulated sphere at 13.5 km, and (2) iterative 3-D modeling to match the observed field with a specified top surface based on the field itself. The preliminary results were sufficiently similar that only the sphere is presented here. Figure 16 shows the new residual field at 2.67 g/cm^3. The following interpretations are now made of the remaining anomalies:

1. The residual gravity-high between Mount Hannah and The Geysers may be due to a roof pendant in the magma chamber which was not fully modeled by the sphere. This can alternatively be thought of as a denser caprock (such as northeast-dipping massive greenstone) which directs hydrothermal heat transfer from beneath the volcanic field to the region of surface expression near The Geysers.
2. The residual gravity low near the production region may be related to a cupola of the magma chamber reaching higher in the crust. Probably at least part of this low represents the reservoir itself, made up of a fracture zone or more porous rocks with void space filled with vapor instead of liquid (providing a $\Delta\rho \cong -0.05$ g/cm^3 for a porosity of 5%). The rock unit itself need not be lighter then the graywacke common in the producing zone.
3. A residual low in the region of Mount Konocti and southwest coincides with and is probably related to the apparent thickest portion of near-surface volcanics and the bounding serpentinite. This low also extends over the alluvial valley west of the Clear Lake volcanic field.
4. The high over the southeast arm of Clear Lake remains unexplained in terms of deep sources. It may be related to Franciscan greenstones which are exposed on the north shore, but more data are required to substantiate this.
5. The low in the Russian River valley no doubt arises from a thickness of Quaternary fill.
6. The edge of the Pliocene Sonoma volcanics is outlined by contours indicating another volcanics-related low, study of which is beyond the scope of this paper.

CONCLUSIONS

Evidence supports a model for The Geysers-Clear Lake geothermal system whose essential features are:

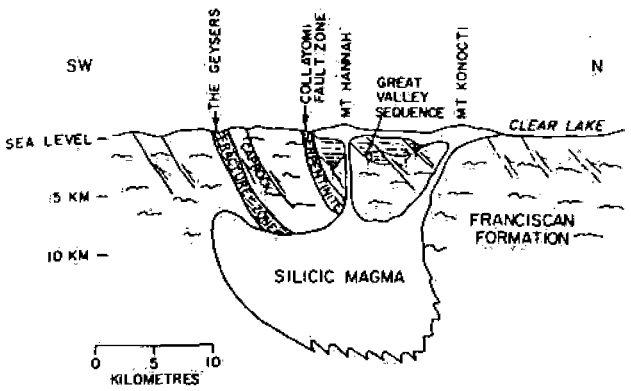

Figure 17. Generalized cross section through The Geysers-Clear Lake geothermal region.

1. A magma chamber which is hot enough to be above its Curie temperature, and is centered more than 10 km below the southwest edge of the volcanic field.
2. An apparent roof pendant and/or caprock which is important in directing hydrothermal activity to the southwest toward the producing steam field.
3. A fracture zone with steam-filled pore space acting as a reservoir capped by less fractured greenstones and, locally, ultrabasics.

Figure 17 combines these features schematically in a southwest-northeast section across the field.

Even simple modeling of the deep source, then, allows easy study of the remaining gravity features in terms of near-surface geology.

ACKNOWLEDGEMENTS

I thank Rodger Chapman, Julie Donnelly, Gordon Eaton, Carter Hearn, Ben Lofgren, Robert McLaughlin, and Dal Stanley for extensive discussions and early information from their own research. I also thank Carlos Bernal for able assistance in the field and all of the lease holders, land owners, and operators at The Geysers area for their cooperation.

REFERENCES CITED

Bhattacharyya, B. K., and Morley, L. W., 1965, The delineation of deep crustal magnetic bodies from total field aeromagnetic anomalies: Jour. Geomagnetism and Geoelectricity, v. 16, p. 237–252.

Bott, M. H. P., and Smith, R. A., 1958, The estimation of the limiting depth of gravitating bodies: Geophys. Prosp. [Netherlands], v. 6, p. 1–10.

Brice, J. C., 1953, Geology of the Lower Lake quadrangle, California: California Div. Mines Bull. 166.

Byerly, P. E., 1966, Interpretation of gravity data from the Central Coast Ranges and San Joaquin Valley, California: Geol. Soc. America Bull., v. 77, p. 83–94.

Chapman, R. H., 1966, Gravity map of Geysers area: California Div. Mines and Geology Mineral Inf. Service, v. 19, p. 148–149.

——, 1975, Geophysical study of the Clear Lake region, California: California Div. Mines and Geology Bull.

Chapman, R. H., and Bishop, C. C., 1974, Bouguer gravity map of California—Santa Rosa sheet: California Division of Mines and Geology, compiled in 1970.

Eaton, G. P., Christiansen, R. L., Iyer, H. M., Pitt, A. M., Mabey, D. R., Blank, H. R., Jr., Zietz, I., and Gettings, M. E., 1975, Magma beneath Yellowstone National Park: Science, v. 188, no. 4190, p. 787.

Garland, G. D., 1951, Combined analysis of gravity and magnetic anomalies: Geophysics, v. 16, p. 51–62.

Garrison, L. E., 1972, Geothermal steam in The Geysers-Clear Lake region, California: Geol. Soc. America Bull., v. 83, p. 1449–1468.

Grant, F. S., and West, G. F., 1965, Interpretation theory in applied geophysics: New York, McGraw-Hill, 583 p.

Hamilton, R. M., and Muffler, L. J. P., 1972, Microearthquakes at The Geysers geothermal area, California: Jour. Geophys. Research, v. 77, p. 2081–2086.

Isherwood, W. F., and Chapman, R. H., 1975, Principal facts for gravity stations in The Geysers-Clear Lake region, California: U.S. Geol. Survey open-file report 75-106, 15 p.

Lange, A. L., and Westphal, W. H., 1969, Microearthquakes near The Geysers, Sonoma County, California: Jour. Geophys. Research, v. 74, p. 4377–4378.

Murase, T., and McBirney, A. R., 1973, Properties of some common igneous rocks and their melts at high temperatures: Geol. Soc. America Bull., v. 83, p. 3563–3592.

Nettleton, L. L., 1940, Geophysical prospecting for oil: New York, McGraw-Hill, 444 p.

Odegard, M. E., and Berg, J. W., Jr., 1965, Gravity interpretation using the Fourier integral: Geophysics, v. 30, p. 424–438.

Saad, A. H., 1969, Magnetic properties of ultramafic rocks from Red Mountain, California: Geophysics, v. 34, p. 974–987.

Spector, A., and Grant, F. S., 1970, Statistical models for interpreting aeromagnetic data: Geophysics, v. 35, p. 293–302.

U.S. Geological Survey, 1973, Aeromagnetic map of the Clear Lake area, Lake, Sonoma, Napa, and Mendocino Counties, California: U.S. Geol. Survey open-file report.

This paper is total bullshit -- lack of geologic reality

Gravity

Gravimetric Survey of Geothermal Areas in Kurikoma and Elsewhere in Japan

KENZO BABA

Geological Survey of Japan, Hisamoto-135, Takatsu-ku, Kawasaki-shi, Japan

ABSTRACT

Some of the results obtained by the gravimetric survey of geothermal areas in Japan are introduced. In these results from northern and southern Kurikoma and Kirishima, many surface geothermal manifestations seem to be connected with the local gravity anomalies, which have been investigated in detail. Geothermal surface activities in northern Shirane apparently exist along the structural line deduced by gravimetric evidence.

Consequently, the results obtained from several geothermal areas show that the gravimetric survey can be considered an effective tool in exploring for geothermal resources.

The writer tentatively assumes the existence of intrusive rock of high density which may be the present heat source, or the existence of a geothermal reservoir which has a higher density than the host rock.

Using the appropriate numerical values and the observed data of heat discharge and the gravity survey in northern Kurikoma, a hypothesis to explain the correlation between the local high anomalies and geothermal manifestations on the surface is examined. Consequently, it is clear that the hypothesis is not unreasonable.

INTRODUCTION

Gravimetric surveys are widely applied in various kinds of fields. In Japan, it is being used as one of the preliminary surveys of some geothermal areas. The writer introduces here the results of a gravimetric survey recently completed at these geothermal areas and shows the apparent correlation between gravity anomalies and surface geothermal manifestations. Therefore, it is thought that gravimetric surveys can be effective exploration tools for geothermal resources in some cases.

Combs and Muffler (1973) wrote that gravimetric surveys were used both to outline major structural features and to delineate local positive anomalies that might be related to a geothermal system. The purpose of applying gravimetric surveys at geothermal areas in Japan is the same.

Many factors, thought to produce local gravity anomalies at the surveyed areas, are explained here, and we can see that some of the local anomalies are apparently associated with surface geothermal manifestations. Such anomalies are thought to have a close relationship with geothermal systems and may be targets for a detailed survey. The writer thinks that the gravimetric survey can be useful in prospecting for geothermal resources, in addition to being useful in surveying the general underground structure.

Because all the areas reported here are covered by recent volcanic rocks, there are many complicated anomalies which do not become significant on the gravity map. The writer applied a filtering process devised by Seya (1959a and b) for the data from some areas. It is a useful method for finding out anomalies which are derived from the appropriate depth by excluding anomalies which are thought to be derived from the density distribution at comparatively shallow and at deep places. A successful result was obtained and will be described in detail in this report.

SURVEYS BY THE GRAVIMETRIC METHOD

Figure 1 shows the recent project map for geothermal exploration by the Geological Survey of Japan. Thirty geothermal areas where the basic survey for geothermal resources will be carried out are shown on it. The gravimetric survey was completed at some of them, and the results from northern and southern Kurikoma (Nos. 10 and 11 in Fig. 1), southern Shirane (No. 18), and Kirishima (No. 28) are introduced in this report to discuss the relationship between gravity anomalies and surface geothermal manifestations. These areas are considered to be the hopeful ones in Japan from the viewpoint of geothermal exploitation.

At northern Kurikoma, there are many geothermal areas—Oyasu, Ohyu, Kawarake, Arayu, Yunotai, and so on (see Fig. 2). Yunotai is exceptional because it has 15 drilled wells from which hot water of about 70°C is being pumped and there is no intense geothermal activity on the surface. Southern Kurikoma also contains several geothermal areas; and, at one of them, a geothermal power station (Onikobe station) has recently begun to produce electricity successfully. In southern Shirane, there are several active geothermal areas. Kirishima on Kyushu island is thought to have the most natural heat discharge of the four areas reported here.

Besides the gravimetric survey, natural heat discharge measurements were carried out at the geothermal area in northern Kurikoma. This is shown in the next section with the result of the gravimetric survey.

NORTHERN KURIKOMA

At geothermal areas, heat is transferred from underground to the surface by convection of geothermal fluid and by

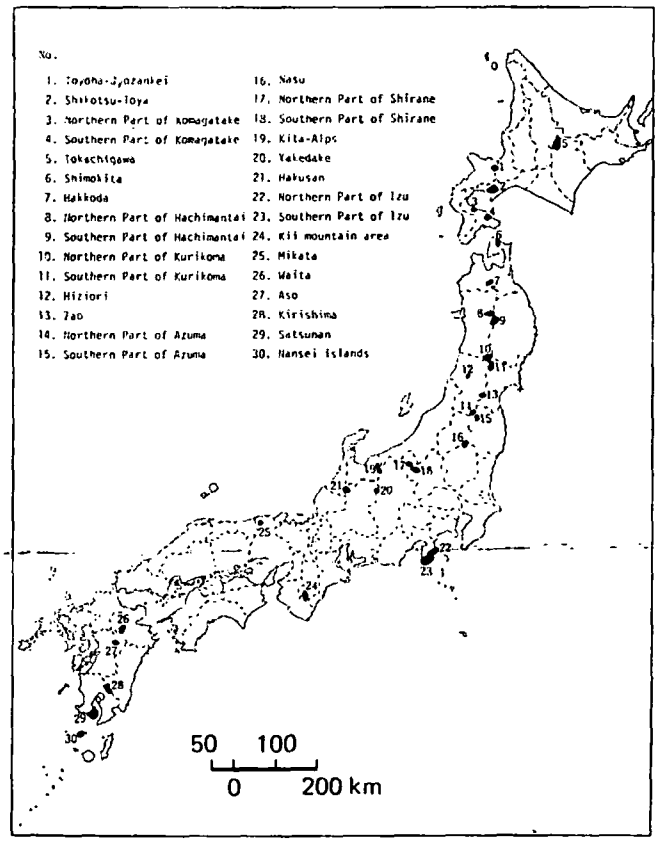

Figure 1. Locations of the 30 geothermal fields to be investigated by the Geological Survey of Japan.

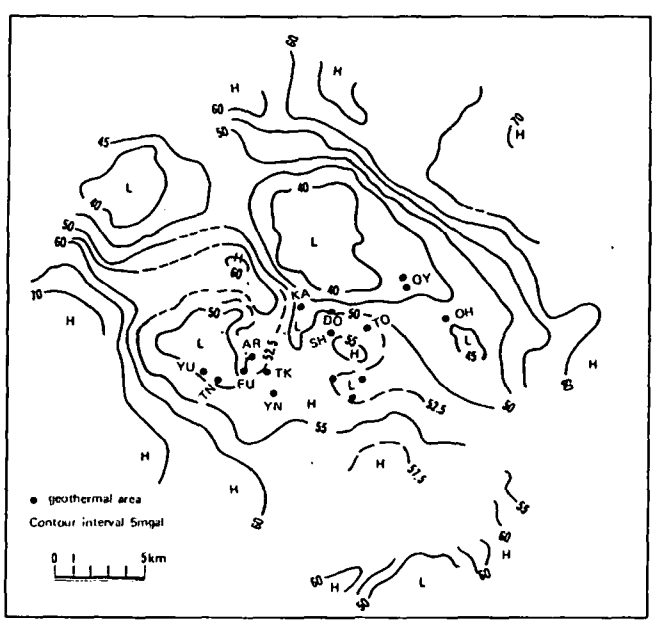

Figure 2. Bouguer anomalies, Kurikoma No. 10 (ρ = 2.3 g/cm^3). Key: YU, Yunotai; TN, Takanoyu; AR, Arayu; FU, Funtokyu; TK, Takakurazawa; KA, Kawarake (two areas); DO, Doroyu; SH, Shinyu; TO, Tochinoyu; OY, Oyasu (two areas); OH, Ohyu; YN, Yunomata.

thermal conduction in the soil. The quantity of total heat discharge from each geothermal area can be considered to indicate, as a first approximation, the magnitude of the geothermal potential.

Table 1. Heat discharge in northern Kurikoma.

Location	Heat Discharge (kcal/sec)				
	Hot spring	Steam well	Steaming ground	Conduction	Total
Yunotai	688				688
Takanoyu	358				358
Arayu	310		303	17	630
Funtokyu	48		32	2.3	82.3
Takakurazawa	9		6	2.7	17.7
Yunomata	66				66
Kawarake			2546		2546
Doroyu	71		11	11	98
Shinyu			215		215
Tochinoyu			5		5
Oyasu	460	760	7838		9058
Ohyu	119		4240	28	4387

In northern Kurikoma, the heat discharge measurement was completed at most of the geothermal areas except for a few. The measured result is shown in Table 1, from which we can compare geothermal activities at each area. As is shown in Table 1, heat discharge is classified into four types—hot spring, steam well, steaming ground, and thermal conduction. The numbers in the "Hot spring" column show total heat discharge from both the hot springs and the drilled holes.

As already mentioned, all of the 688 kcal/sec at Yunotai is transferred by pumping hot water from the drill holes, but there are not so many drill holes at the other areas. At Oyasu, a steam well discharges steam with heat corresponding to 760 kcal/sec. The numbers in the "Steaming ground" column are also considered to be an index of a kind of geothermal potential at each area because natural steam is actually being discharged there. In the fifth column, "Conduction" means heat output by thermal conduction from the anomalous terrestrial temperature areas measured at a 1-m depth. The total is shown in the column at the right in the table. The largest heat discharge was observed at Oyasu in the 12 geothermal areas there. Measurements were not carried out at the few areas south of Shinyu because of bad topographic conditions. According to the local people, the geothermal activity there is not so small as to be considered negligible, but it may not be so large as at Oyasu or Kawarake.

The gravimetric survey was carried out by using a Lacoste gravimeter, and the Bouguer anomaly map shown in Figure 2 was obtained by the usual method. Though the original Bouguer anomaly map used 1-mgal contours, here a simpler map of 5-mgal contours is shown. Several kinds of contour maps were completed by using various assumed densities to calculate Bouguer anomalies. The one shown in Figure 2 is thought to be the most suitable. The geothermal areas are also shown in Figure 2.

The outcrop of basement rock (granodiorite) of this area is only at the western end (Fig. 2). It is characterized by high anomalies, and there is no geothermal activity on the surface. In the basement rock, the geologic sequences from the lower part to the upper part are Neogene (andesites, mudstones, pyroclastic materials, and so on), Pliocene and Pleistocene (volcanic products), and Quaternary (terrace deposits and alluvium). According to the density measurement of rock specimens, the basement rocks have the highest density (2.6 to 2.8 g/cm^3) of all the rock specimens mentioned above.

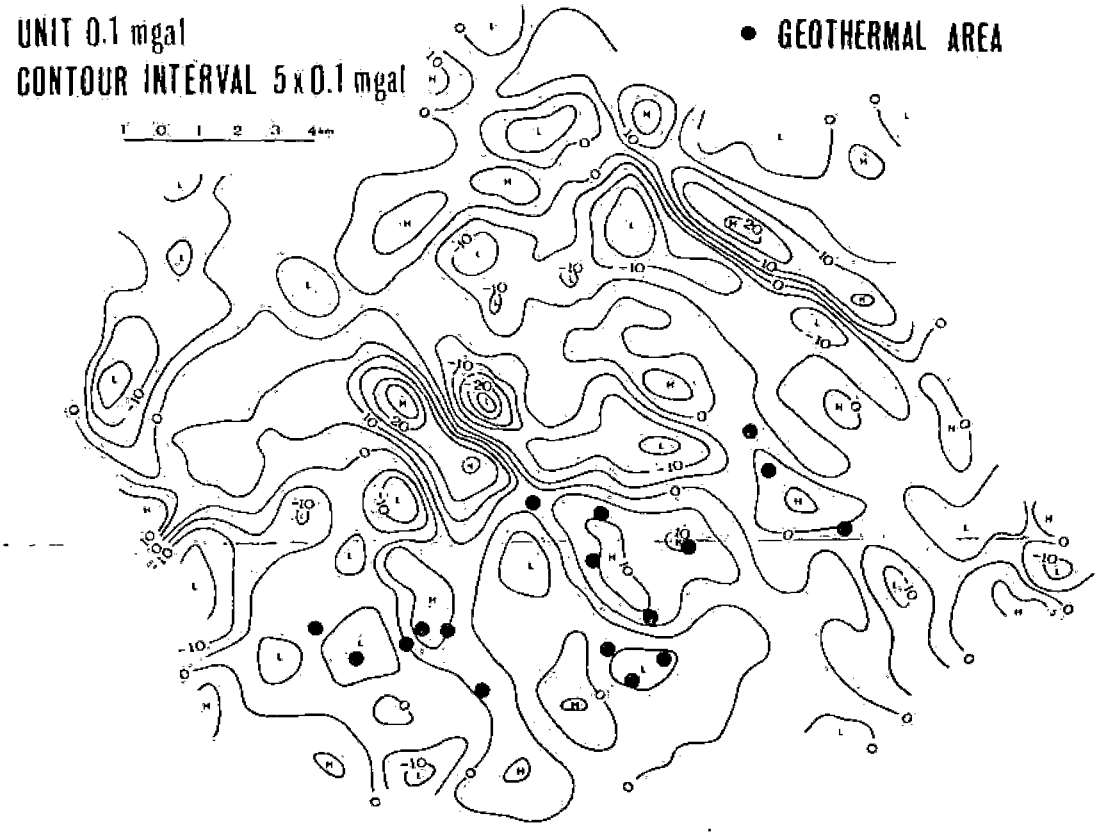

Figure 3. Residual gravity, Kurikoma No. 10.

The large low anomaly, which presumably means the subsidence of basement rocks and the existence of thick younger layers, is in the central part of the area and another low anomaly is in the southwestern side. The geothermal manifestations on the surface are apparently situated around the local gravity low anomalies.

Residual Anomalies in Northern Kurikoma

When we look at Figure 2 carefully, we find that the geothermal areas defined by the existence of surface geothermal manifestations are connected with very local and comparatively small high anomalies. Such anomalies are caused by the existence of high densities at intermediate depths, while large anomalies are from comparatively deep places. In order to locate such anomalies clearly, the writer calculated the residual gravity by using the method devised by Seya (1959a and b). The physical meaning of the obtained residual gravity map shown in Figure 3 is as follows.

When the distribution of anomalies on a plane is expanded by using a Fourier series, the anomalies of low frequency are considered to be those caused by density distribution at deeper places, and those of high frequency, to be caused by density distribution at shallow places. In order to find the anomalies caused by density distribution at the depth which we wish to study, the appropriate filtering process should be applied for the original data. Seya's method is a practical way to apply such filtering. The residual map, which represents mainly anomalies of wavelengths between about 2 km and 5 km according to his theory, is shown in Figure 3. It is easily seen that many geothermal areas exist around or at the place where very local high anomalies are found.

In Figure 3, we can see that two geothermal areas (Oyasu and Ohyu) seem to be connected with one local high anomaly, five areas (Kawarake, Doroyu, and so on) are connected with a second local high anomaly, and three areas (Arayu, Funtokyu, and Takakurazawa) are connected with a third high anomaly.

The exceptional areas which seem to be connected with local low anomalies are Yunotai, Takanoyu, and three geothermal areas which are south of Shinyu. As mentioned previously, though the heat discharge from Yunotai is very large, it is transferred by pumping hot water of about 70°C from the drilled holes, so that Yunotai may not be suitable to be treated as a geothermal area like the other areas. Concerning Takanoyu, it is not remarkable as a geothermal area because it has no steaming ground. As far as another three areas situated in a low anomaly are concerned, they can apparently be considered exceptional cases.

Gravimetric Surveys in the Other Areas

In Figure 4, the Bouguer anomaly map of southern Kurikoma is shown. A caldera exists in the central part of the map, and gravity anomalies reflect its structure, as is clearly seen. In the caldera, there is much geothermal activity, and volcanic and sedimentary rocks of both the Tertiary and the Quaternary are found there. The residual anomaly map, calculated by the same method as for northern Kurikoma, is shown in Figure 5. Many geothermal areas are situated at and around the local high anomalies, except for a group of geothermal areas on the northwestern side. Even the exceptional cases seem to be connected to a local high anomaly on the southeastern side.

In Figure 6, the Bouguer anomaly map of southern Shirane

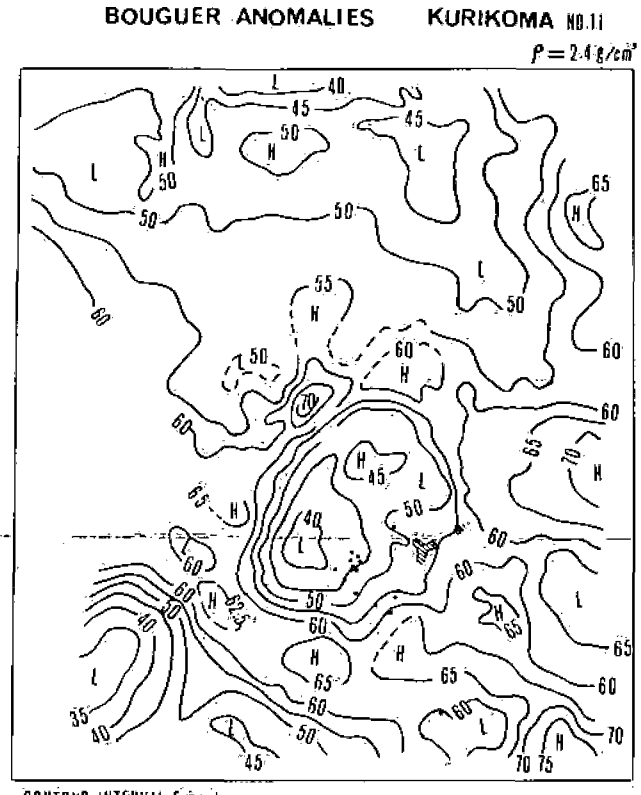

Figure 4. Bouguer anomalies, Kurikoma No. 11 (ρ = 2.4 g/cm^3).

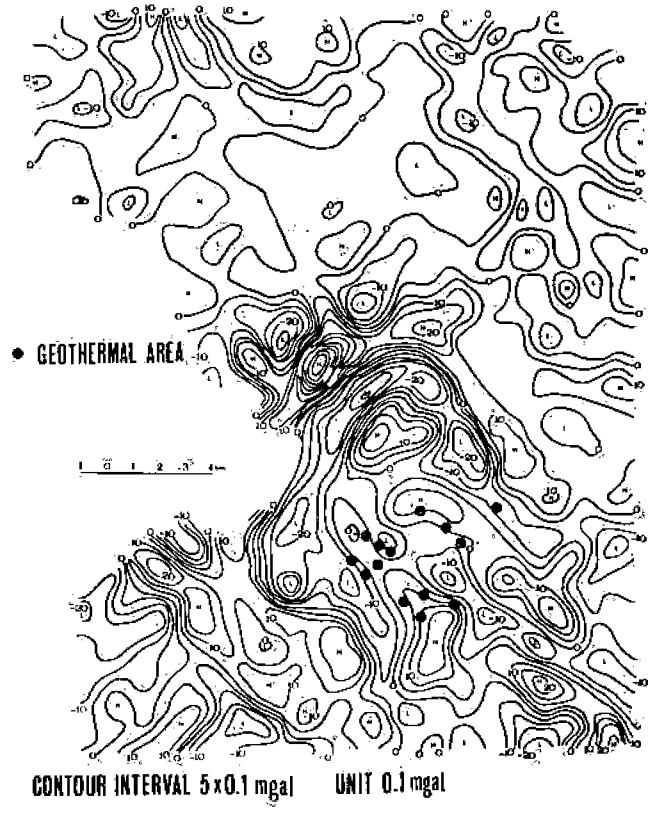

Figure 5. Residual gravity, Kurikoma No. 11.

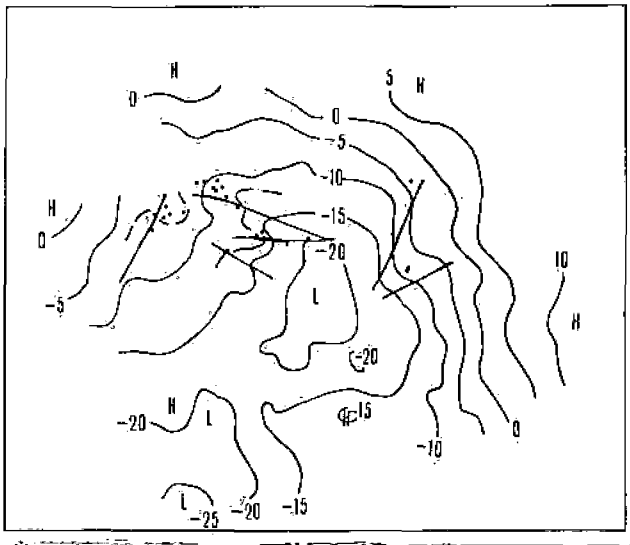

Figure 6. Bouguer anomalies, Shirane No. 18 (ρ = 2.4 g/cm^3).

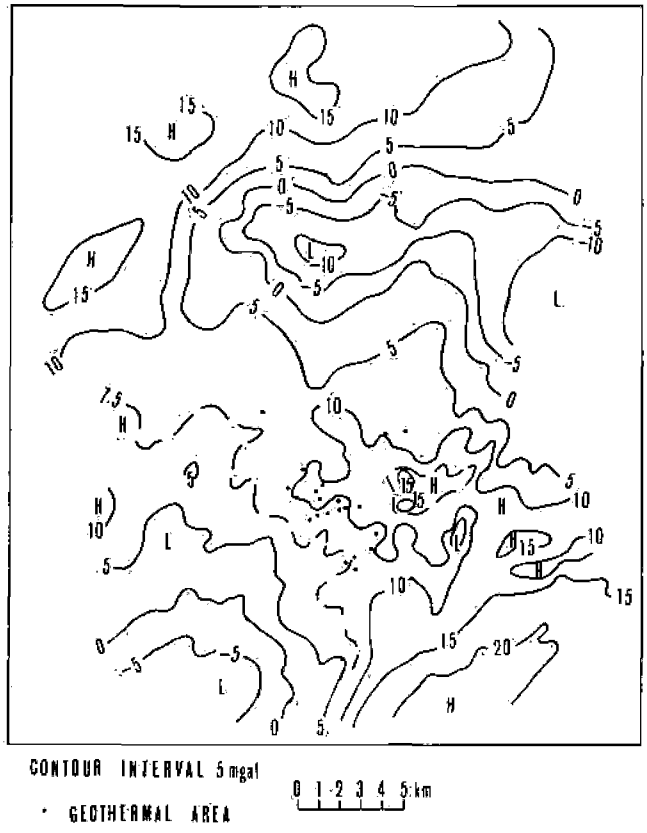

Figure 7. Bouguer anomalies, Kirishima No. 28 (ρ = 2.2 g/cm^3).

is shown. This area is covered mainly by volcanic rocks of the Neogene and the Quaternary. Judging from the shape of the anomaly contours near geothermal areas, the fault structure is presumed to be as shown. The existence of some faults in this area is explained from the geologic

evidence. This is a typical example in which geothermal areas exist along the fault line, and the gravimetric result was successful in delineating the structural lines.

In Figure 7, the Bouguer anomaly map of Kirishima is shown, and this area is also covered by volcanic rocks of both the Neogene and the Quaternary. The geothermal areas exist around high anomalies as is clearly seen without calculating the residual anomalies. The anomaly of 15 mgal on the eastern side of the geothermal areas coincides with the volcanoes.

DISCUSSION

It is thought that from the viewpoint of gravity anomalies, there are four types of distribution of geothermal areas shown in the examples of this report. In the first type, geothermal areas are distributed around very local high anomalies, and in the second type they are around high anomalies. In both cases, they seem to be connected to the local high anomalies. These types were found in northern and southern Kurikoma and Kirishima. In northern Kurikoma, we can point out three interesting local high anomalies which seem to be connected with geothermal activities as shown in Figure 3. In southern Kurikoma, we can also indicate two local high anomalies, shown in Figure 5. Besides these, in Kirishima we can point out an interesting local high anomaly around which many geothermal manifestations are situated, as is seen in the Bouguer anomaly map of Figure 7. In the third type, an example of which is found in northern Kurikoma, the geothermal areas are on a local low anomaly, but this type is thought to be rather exceptional as far as the results introduced here are concerned. In the fourth type, the geothermal areas are along the structural lines deduced from the gravimetric anomalies, examples of which are in southern Shirane. It is interesting that many of the geothermal areas shown in this report are associated with local high anomalies.

One of the possible explanations for this is the existence of intrusive dense rocks which might be the heat source or the existence of a geothermal fluid reservoir which has a higher density than the host rocks. In the second type, the existence of a more fissured structure underneath the geothermal areas, derived from the intrusion of dense rock, is also a possible explanation.

Of course, there is no reason to expect all of the geothermal areas to be connected with a gravimetric anomaly. Generally, the density distribution under a geothermal area is thought to be very complicated because of the complicated geologic structure. As a matter of course, we should investigate gravity anomalies by using geological and geophysical information which will be obtained hereafter. However, the writer tentatively assumes that there is a possibility for a gravity anomaly to be connected with a geothermal reservoir or an intrusive heat source in some cases. He examines this possibility by using a very simple model in the case of northern Kurikoma.

Imagine a buried heat source of spherical shape which has a higher density than the host rock. Assuming a constant temperature, V, of the heat source, the total heat flow through the spherical surface to the infinite region bounded internally by the sphere (radius a) is represented by $4\pi a\bar{V}k$ in a steady-state condition, where k is the thermal conductivity of the region.

Next, we suppose a semi-infinite region in which the spherical body is buried. When the temperature at the surface plane of the semi-infinite medium is kept at zero, the total heat flow on the surface can be estimated to be twice $4\pi a\bar{V}k$ by applying the method of imaging.

Here, we assume that the heat is transferred by conduction from the buried body to a definite plane. We assume that the underground water flow exists on the plane, keeping it at constant temperature and the hydrothermal system appears.

On the other hand, the gravity anomaly which is derived from the density difference between the buried sphere, of which the radius equals a, and the host medium is represented by $\Delta g = (4/3)\pi G a^3 \Delta\rho(1/z^2)$ on the right above the center of the sphere. In this equation, z is the depth from the ground surface to the center of the sphere, and G is the gravitational constant (6.67×10^{-8} cm^3/g sec^2).

Here, we assume that the temperature difference between the heat source and a definite plane is about 200°C; then we can estimate the total heat flow as a few thousand kilocalories per second ($8\pi a\bar{V}k \doteqdot 3000$ kcal/sec) where we assume $a = 1.5$ km and $k = 0.004$ in c.g.s. units. This heat flow is consistent with the observed data in northern Kurikoma.

As previously shown, the heat discharge at Kawarake and the other three areas which are considered to belong to a local high anomaly was 2846 kcal/sec, and at Oyasu and Ohyu it was 13 445 kcal/sec. Some of this heat discharge is thought to be derived from fluid convection directly from the heat source, and the balance is thought to be from heat conduction through the plane. Therefore, the numerical value of the heat flow estimated above should be of the same order as the quantity of heat discharge actually observed on the ground surface, or less.

On the other hand, we assume $z = 5$ km and $\Delta\rho = 0.3$ g/cm^3 for the buried body. Then, we can estimate Δg as about 1 mgal using the same a for estimation of heat flow. As the residual gravity anomaly estimated here is of the same order as the one shown in Figure 3, this estimation is consistent with the observed data.

Therefore, a hypothesis connecting a gravity anomaly with a heat source is not unreasonable from the viewpoint of heat discharge measurement. Because the assumed physical model is too simple, the writer of course intends to investigate this problem in more detail.

CONCLUSION

In this report, the writer studied the results of gravimetric surveys at the four areas where much geothermal activity exists. Consequently, the following conclusions have been obtained:

1. The geothermal areas are distributed so as to be associated with very local high anomalies in some cases; and, on the other hand, some of them are along the structural lines (faults) deduced by gravity anomalies.
2. The correlation between the distribution of geothermal areas and gravity anomalies is expected to exist even in areas other than those introduced here. Therefore, in addition to surveying the general underground structure, a gravimetric survey will be effective in determining the targets for the following detailed survey.
3. Taking the hypothesis that the excess mass which causes a local high anomaly is related to the heat source, the heat

flow and gravity anomalies are estimated tentatively by using a very simple and idealized physical model, and the observed data of the total heat discharge and gravity anomalies were compared with them. Consequently, the hypothesis is not unreasonable from the viewpoint of heat discharge.

REFERENCES CITED

Combs, J., and Muffler, L. J. P., 1973, Exploration for geothermal resources, *in* Kruger, P., and Otte, C., eds., Geothermal energy: Stanford, Stanford Univ.

Seya, K., 1959a, A new method of analysis in gravity prospecting (Running average method), part 1: Butsuri Tanko (Jour. of Soc. of Exploration Geophysicists of Japan) v. 12, no. 2, p. 65–73 (in Japanese with English abstract).

——, 1959b, A new method of analysis in gravity prospecting (Running average method), part 2: Butsuri Tanko (Jour. of Soc. of Exploration Geophysicists of Japan) v. 12, no. 4, p. 166–177 (in Japanese with English abstract).

Geology and Gravimetry of the Quaternary Basaltic Volcanic Field, Southern Cascade Range, Washington

PAUL E. HAMMOND
STEVEN A. PEDERSEN
Department of Earth Sciences, Portland State University, P.O. Box 751, Portland, Oregon 97207, USA
KENNETH D. HOPKINS
Department of Earth Sciences, university of Northern Colorado, Greeley, Colorado 80631, USA
DAN AIKEN
Department of Geology, University of Oregon, Eugene, Oregon 97403, USA
DAVID S. HARLE
Department of Geology, Oregon State University, Corvallis, Oregon 97331, USA
Z. F. DANEŠ
DANIELA L. KONICEK
CLAUDE R. STRICKLIN
Department of Physics, University of Puget Sound, Tacoma, Washington 98416, USA

ABSTRACT

A late Quaternary basaltic field, of about 2200 sq km, lies east of Mount St. Helens and extends eastward and northward of Mount Adams. The flows originated from two north-trending fissure zones: a west fissure, extending 30 km, with 11 distinct centers, which produced at least 14 groups of lava flows; and an east fissure, lying about 25 km to the east, passing beneath Mount Adams, and extending 48 km. The east fissure contains 8 centers, excluding the andesitic Mount Adams volcano, from which at least 10 groups of lava have flowed. Each center consists of a shield volcano surmounted by one or more cinder cones.

Interstratified relations with late Quaternary glacial and tephra deposits of Mount St. Helens indicate that at least 20 different volcanic eruptions have occurred in the field within the last 50 000 years, the last event being the oupouring of the Big Lava Bed between 450 and 4000 years ago.

The fissures strike oblique to regional northeast-trending open folds of early to middle Tertiary volcanic strata. Several north-striking faults extend northward and southward beyond the field. Gravity data reveal a linear local gravity low of −35 mgal, representing possibly less dense strata, hydrothermal alteration, or a magma reservoir, coincident with the west fissure. A Bouguer gravity low of −115 mgal at the northern end of the east fissure may represent part of the buried Mesozoic granitic batholith.

The nearest thermal springs, of low temperature, mixed waters, lie 15 km southwest of the field. Their chemistry indicates aquifer temperatures below 140°C. Continued geophysical investigations of the west fissure are planned.

INTRODUCTION

Hot springs and the High Cascade stratovolcanoes are not the only evidence of geothermal activity in the Cascade Range. Many basaltic shield volcanoes and cinder cones, scattered among the higher cones, give evidence of long and perhaps more frequent volcanic activity. The Quaternary basaltic volcanic field in the southern Cascade Range of Washington is such an example.

Basaltic volcanic fields have been considered unfavorable for geothermal resources. Because these fields are underlain by thin lavas of high permeability and fed by narrow tabular intrusions which produce short-lived eruptions, they are believed to have cooled quickly and not generated sufficient heat to establish a convective geothermal system. However, continued investigation of this field has been encouraged by evidence of frequent eruptions within the last 100 000 or more years; a favorable reservoir zone within the underlying strata; large amounts of ground water; and an unusual gravity anomaly.

The purpose of this report is to summarize the results of the geologic investigations and gravity surveys to date in a continuing program of evaluating the geothermal resources of the southern Cascade Range.

LOCATION

The Quaternary basaltic field, an area of about 2200 sq km, lies east of Mount St. Helens and extends northward and eastward of Mount Adams to merge with the Simcoe Basalt field (Sheppard, 1960, 1962, 1967) in the western

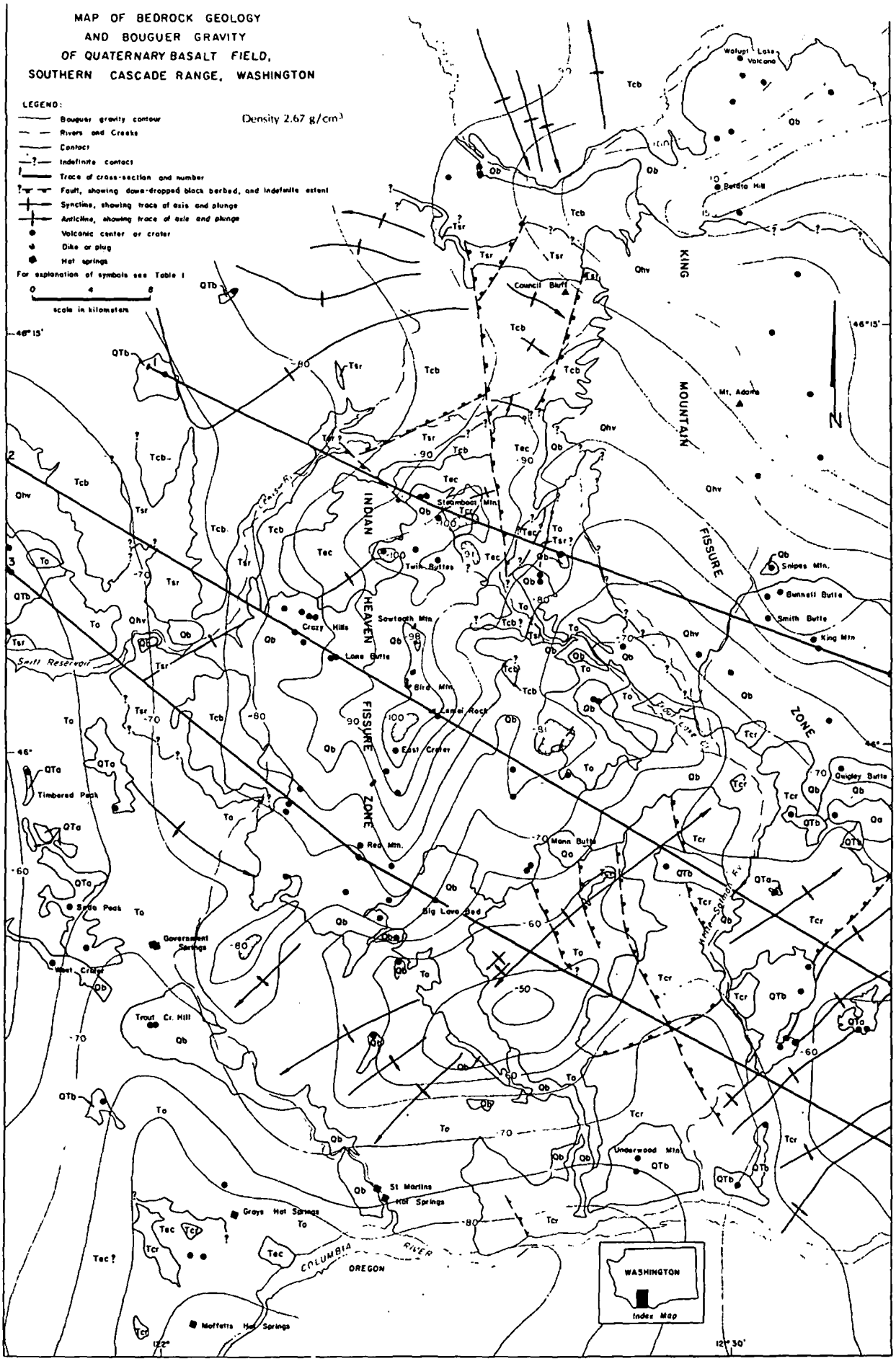

Figure 1. Map of bedrock geology and Bouguer gravity of Quaternary basalt field, southern Cascade Range, Washington.

part of the Columbia Plateau (Fig. 1). The field lies wholly within the jurisdiction of the Gifford Pinchot National Forest, with headquarters at Vancouver, Washington.

The field is accessible via paved county and Forest Service roads along Wind, Little White Salmon, and White Salmon Rivers, branching northward from State Highway 14 at the Columbia River, westward from Glenwood via the Glenwood-Trout Lake road, eastward from the Lewis River road via Forest Service roads No. N714 and No. N733, and southward from U.S. Highway 12 (Cowlitz River-White Pass highway) at Randle, via Forest Service road No. 123 and near Packwood via Forest Service road No. 1302. The area can be reached within two hours' driving from Portland, Oregon, a distance of about 112 km (70 mi).

REGIONAL GEOLOGY

General Features

The Cascade Range extends about 1000 km in length, from the Canadian border on the north, to Lassen Peak in northern California to the south, and is a narrow 120 km wide. The range has been arched and uplifted, some 1000 to 3000 m, (the greater amount occurring at the northern end) during the late Pliocene and Pleistocene, from 1 to 4 million years (m.y.) ago. Within the arch are many divergent folds and faults of Tertiary age.

The southern Cascade Range of Washington, similar to the Western Cascades of Oregon, is composed of calc-alkaline volcanic rocks of Cenozoic age. The rocks consist of predominantly pyroxene andesite, followed by basalt, rhyodacite, dacite, and rhyolite, in decreasing order. Strata are formed of lava flows and breccias, lahars (mostly breccias), fluvially deposited volcanic deposits, and tephra deposits. Several sequences of widespread diagnostic ash-flow tuff deposits or ignimbrities, for example the Stevens Ridge Formation (Table 1), form marker stratigraphic units and structural datum horizons.

The strata are intruded by many epizonal plutons ranging in size from stocks to batholiths, from 13 to 40 m.y. old (Laursen and Hammond, 1974), consisting of pyroxene and/or hornblende diorite, biotite-hornblende quartz diorite, and granodiorite, and minor amounts of hornblende-biotite quartz monzonite and biotite granite. Many dikes and plugs of porphyritic pyroxene andesite and basalt occur throughout the range. No Tertiary intrusions are shown in the map (Fig. 1).

The rocks are extensively altered and locally zeolitized to the lowest grades of metamorphism (Wise, 1959, 1961; Fiske, Hopson, and Waters, 1963; Fischer, 1971; and Hartman, 1973). Furthermore, many irregular zones of intense hydrothermal alteration, consisting predominantly of silicification and argillization with disseminated base metal sulfides (Grant, 1969) are associated with the plutons. These zones reflect older geothermal areas. Because the hydrothermal alterations affect strata of all but most recent age, geothermal activity may have been ongoing throughout the evolution of the range.

The crestal part of the range is deeply dissected by glaciation. Consequently large areas are mantled by till and glacial outwash deposits. In other areas a thick soil cover has formed.

The Quaternary volcanic pattern is superimposed upon a diverging fold-fault pattern. In the southern Cascade Range the fold axes trend predominantly northwestward but in the eastern part of the range, bordering the Columbia Plateau, the folds trend eastward. These fold trends converge in the approximate center of the range beneath the Quaternary basalt field (Fig. 1). Faults trend northwestward; many faults are as young as Quaternary.

Stratigraphy

The pre-Quaternary stratigraphic units are summarized in Table 1. References to more detailed descriptions of the units are included.

The oldest rocks exposed are part of the Ohanapecosh formation, of Eo-Oligocene age. The strata are over 4500 m thick, and consists of interstratified volcanic sediments, andesite and basalt lava flow complexes, and mudflow breccia deposits. Individual units are well stratified but discontinuous laterally. Marker or traceable strata are lacking. The Ohanapecosh is overlain unconformably by the major Tertiary marker unit, the Stevens Ridge formation, of largely ash-flow tuffs and interbedded volcanic sedimentary rocks. It is Miocene in age, having been radiometrically dated at 20 to 25 m.y. (Hartman, 1973). The Formation ranges from 90 to 600 m thick. The Stevens Ridge is, in turn, overlain conformably by the beds of Council Bluff, of pyroxene andesite lava flow complexes and volcanic sediments. The unit has a maximum thickness of 400 m.

The Ohanapecosh, Stevens Ridge, and Council Bluff formations can be traced almost continuously through the area (Fig. 1). Of the three, Ohanapecosh and Stevens Ridge are considered the least permeable, the former because of widespread zeolitization and the latter because of its compactness, zeolitization, and high clay content. Where Ohanapecosh and Stevens Ridge strata occur in fault-fracture zones, the strata could be highly permeable. The strata of Council Bluff, because of interstratified lava flows and breccias and sedimentary beds, is considered moderately permeable, yet the strata could be quite permeable in a fracture zone.

The Eagle Creek Formation is composed of volcanic sediments, conglomerate, mud flow breccia, and minor lava flows. It ranges up to 1000 m in thickness, and rests unconformably upon older strata. This formation contains permeable beds and constitutes a possible ground water reservoir beneath the Indian Heaven fissure zone of the Quaternary basalts (Figs. 1 and 2).

Columbia River basalt occurs in a small area within the Cascade Range (Fig. 1). Most occurs marginally to the Columbia Plateau but Columbia River basalt may have at one time extended across the southern Cascade Range. South and east of Mount Adams the basalt forms structural ridges, basins, and upland plateaus.

Accompanying the uplift of the Cascade Range was the deposition of early Quaternary, possibly as early as late Pliocene, olivine-hypersthene-hornblende andesite lavas, breccias, and cinder deposits. These rocks are restricted and form strata no more than 100 m thick. All lavas tested to date have reversed remanent magnetic polarity.

The main stages of late Cenozoic basaltic volcanism followed deposition of the andesites. An older group of olivine basalt lavas, breccias, and cinders, believed to be older than 690 000 years, based on their reversed remanent magnetic polarity and degree of erosional dissection, are scattered throughout the area (Fig. 1). These basalts form

Table 1. Cenozoic stratified units of southern Cascade Range, Washington.

Age	Map Symbol	Formation	References	Lithology	Thickness, m
Quaternary	Qhv	High Cascade volcanics: Mount St. Helens volcanics	Hopson (1971, 1972) Crandell and Mullineaux (1973)	Chiefly pyroxene andesite, dacite, and olivine basalt lava flows and breccia, mud flow and pyroclastic flows, and tephra deposits.	10–250
		Mount Adams volcanics	Sheppard (1967b) Hopkins (1969, 1972)	Mainly olivine, hypersthene-augite, and hornblende andesite porphyry lava flows and breccia, mud flow and pyroclastic flows, and tephra deposits.	10–200
		unconformity			
	Qb	Basalts of fissure zones (Includes basalts of Trout Creek Hill and Big Lava Bed of Wise, 1971, and Waters, 1973, Camas Prairie and White Salmon River of Sheppard, 1964)	Hammond (1973) Pedersen (1973)	Pahoehoe to blocky olivine and/or pyroxene basalt lava flows, breccia, scoria, and cinder deposits.	1–60
		unconformity			
	Qa	Andesite near Laurel (Includes brecciated rhyolite of Mann Butte)	Sheppard (1964)	Augite-hornblende andesite lava flows and breccia.	10–250
		unconformity			
Plio-Pleistocene	QTb	Basalts of Underwood Mountain and White Salmon volcanoes (Includes miscellaneous basalts of Sheppard, 1964, Newcomb, 1969, Wise, 1971, and Hopson, 1972)	Waters (1973)	Olivine basalt lava flows, breccia, scoria, cinders, and pillow-palagonite breccia.	1–100
		unconformity			
	QTa	Andesite of Soda Peak, andesite of Timbered Peak (Includes miscellaneous andesites of Sheppard, 1964)	Wise (1971)	Olivine-hypersthene-hornblende andesite lava flows, breccia, and cinder deposits.	20–100
		unconformity			
Miocene	Tcr	Columbia River basalt (Includes Ellensburg Formation of Sheppard, 1964, and Newcomb, 1969)	Sheppard (1964) Newcomb (1969) Holmgren (1969) Wise (1971) Waters (1973)	Dark-colored basalt flows and pillow-palagonite breccia; light-colored tuffaceous, diatomaceous siltstone, sandstone, and conglomerate interbeds.	100–600
		regional unconformity			
	Tec	Eagle Creek Formation	Wise (1971) Waters (1973)	Light-colored well-bedded volcanic conglomerate, mud flow breccia, sandstone, tuff; few pyroxene andesite and basalt lava flows.	80–1000
		unconformity			
	Tcb	Beds of Council Bluff	Harle (1974)	Dark-colored pyroxene andesite and basalt lava flows and breccia, mud flow, and volcanic sedimentary rocks.	<400
	Tsr	Stevens Ridge Formation	Fiske, Hopson, and Waters (1963) Hammond (1974)	Light-colored tuff, pumice, and lithic breccia; volcanic sedimentary rocks; few basalt, andesite, and silicic lava flows and breccia.	90–600
		regional unconformity			
Eo-Oligocene	To	Ohanapecosh Formation	Fiske, Hopson, and Waters (1963) Wise (1971) Waters (1973)	Interstratified dark-colored basalt and pyroxene andesite lava flows and breccia, and varicolored andesite to rhyodacite pyroclastic and volcanic sedimentary rocks.	>4500 Base not exposed.

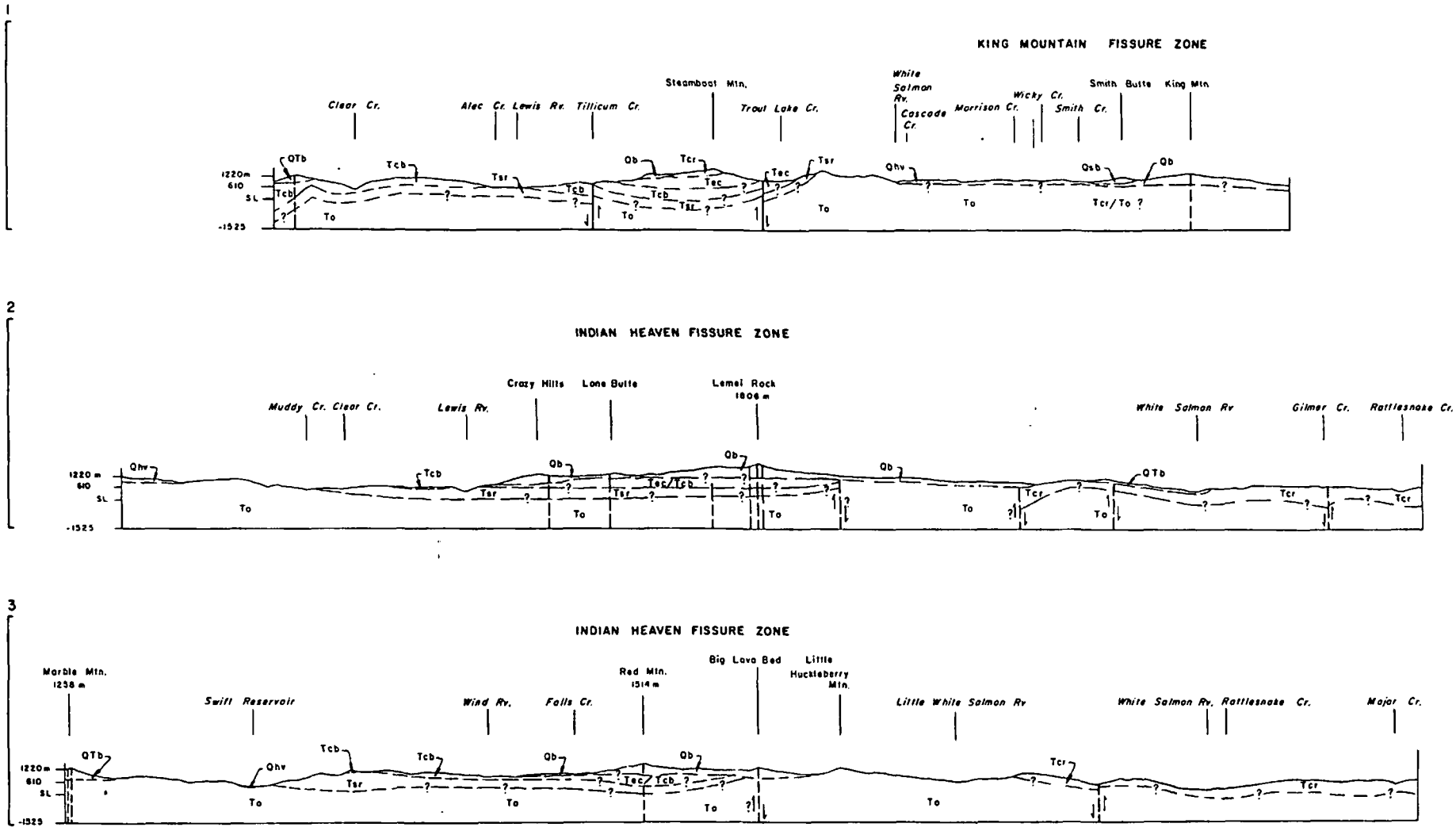

Figure 2. Cross section of Quaternary basalt field, southern Cascade Range, Washington. For explanation of symbols see Table 1.

volcanoes at Underwood Mountain, just east of the White Salmon River, along the north side of the Columbia River west of the Wind River, and near Mount St. Helens. An andesite volcano near Laurel, east of the White Salmon River, has normal remanent magnetic polarity. A younger group of olivine basalts are from 690 000 to possibly as young as 450 years based on their normal remanent magnetic polarity and interstratified relationships with dated tephra deposits of Mount St. Helens. These form the Quaternary basalts of the southern Cascade Range.

The High Cascade volcanic deposits, composed of lavas, breccias, tephra, mudflow and pyroclastic flow deposits, up to 250 m thick and younger than 690 000 years old, form the Mount St. Helens and Mount Adams volcanoes.

QUATERNARY BASALTIC FIELD

The Quaternary basalts were extruded from two parallel north-trending fissure zones lying about 25 km apart (Fig. 1). The east fissure, called the King Mountain fissure zone, extends from Quigley Butte and King Mountain northward beneath Mount Adams to Walupt Lake volcano, a distance of 48 km. At least 10 lava groups have been recognized and mapped in this zone, arising from eight centers.

The western fissure, called the Indian Heaven fissure zone, extends from Red Mountain 30 km northward to the cones on the west ridge of Steamboat Mountain. Two small intraglacial basaltic cones occur near the Cispus River about 22 km north of Steamboat Mountain along this zone. Major volcanoes are East Crater, the source of a group of lavas traceable on both flanks of the zone; and Lemei Rock, the origin of the extensive flow, which descended the White Salmon River valley. At least 14 groups of lava flows have been mapped along the Indian Heaven zone.

The lava flows from the two zones overlap only in the White Salmon River valley. The extensive flow from Lemei Rock (the olivine basalt of White Salmon River of Sheppard, 1964) fills the narrow canyon of the river which was cut into the lavas of King Mountain. These flows are shown separately in the map (Fig. 1). In addition, the Big Lava Bed flow (Wise, 1971), in its south-southeastward descent of the Little White Salmon River valley, is distinguished on the map from the underlying flows.

All volcanic centers, including those of the fissure zones, are shown in Figure 1. Note the number that are not aligned with the fissures. Some centers are sources of the most voluminous lava flows. West Crater, located west of Wind River, is of post-glacial age and indicates that recent volcanism is not confined to the fissure zones.

The fissures cannot be traced into well-defined north-trending faults or graben extending along the crest of the range; nor do the fissures align southward with the Hood River graben across the Columbia River in Oregon (Allen, 1966). Many isolated volcanoes appear to lie along northwest-trending faults. The alignment of West Crater and Trout Creek Hill volcanoes with the lower Wind River and St. Martin's Hot Springs may be evidence of another fault. The southwest-trending folds east of the Wind River cannot be traced across the Wind River valley, giving further support to the existence of a fault in the valley.

Each volcanic center consists of a shield volcano surmounted by one or more cinder cones. Where the volcanoes have been deeply glaciated, such as at Sawtooth and Bird Mountains, bedded cinders, narrow ridges of quaquaversally dipping lavas, and interlacing narrow dikes of basalt and breccia forming the skeletal framework of the volcanoes can be delineated.

The lava flows, few of which are shown separately on the map, can be mapped in the field on the basis of differences in phenocrystic minerals and stratigraphic and topographic position. Many lavas can be traced from complex broad flank sheets to intracanyon flows. Most lavas are pahoehoe and were highly fluid. Individual flows range from 1 to 50 m thick, the average being 2 m in thickness. They have vesicular to scoriaceous bases and vesicular to slab pahoehoe tops. Jointing is blocky to slabby; only in the thicker intracanyon flows is columnar jointing well developed. Contacts are rarely exposed except in postglacially incised valleys. Fluvial sedimentary interbeds form locally well-stratified to cross-bedded units up to 4 m thick. The lava sequence forms highly permeable strata.

All flow rock is colored shades of gray; some are oxidized locally to shades of brown. Most are dense, holocrystalline, and rarely inflated. Phyric olivine or olivine and pyroxene are common. Olivine content is variable. Two flows are noted for their abundant platy plagioclase phenocrysts. One flowed from East Crater into the Lewis and Little White Salmon River valleys; another flowed from Lemei Rock volcano down the White Salmon River valley (the olivine basalt of White Salmon River of Sheppard, 1964). These two flows are separated stratigraphically by a number of smaller, less extensive flows characterized by few to no phenocrysts in a dense matrix. The two flows may indicate episodic voluminous outpourings, marking the renewal of fresh fluid magma along the zone.

All lavas of the field exhibit normal remnant magnetic polarity, indicating an age younger than 690 000 years. No lavas appear to have been erupted during the Laschamp reversal event 20 000 to 30 000 years ago. Most flows are pre-Fraser Glaciation, of youngest Wisconsin, more than 25 000 years old (Crandell, 1965). Lava flows of King Mountain are radiometrically dated at 100 000 to 300 000 years old (Kienle and Newcomb, 1973) and are possibly the oldest lavas of the field. The cones of Smith and Bunnell Buttes and Snipes Mountain, north of King Mountain, are younger than Fraser Glaciation, less than 10 000 years, and older than the Trout Lake mud flow, about 5070 years old (Hopkins, 1972). To the north of Mount Adams, Potato Hill is younger than Fraser Glaciation. Walupt Lake volcano is capped by intraglacial basaltic deposits of palagonite tuff and pillow lavas and, therefore, is estimated to be between 14 500 and 20 000 years old. At the Indian Heaven fissure zone, lava of Sawtooth and Bird Mountains at the northern part of the fissure is the only rock found to be older than Salmon Springs Glaciation of early Wisconsin, 35 000 to 50 000 years ago (Crandell, 1965). Many flows of this zone postdate Salmon Springs Glaciation and are believed to be between 25 000 and 35 000 years old. The basalts of intraglacial volcanic deposits at Crazy Hills and Lone Butte are between 14 500 and 20 000 years old (Pedersen, 1973). Intraglacial deposits of similar age form cones along the west ridge of Steamboat Mountain. Twin Buttes volcanoes, between Steamboat and Sawtooth Mountains, are believed to be slightly younger than Fraser Glaciation (less than about 10 000 years), because of their minimal glacial dissection. The cinder cones at the southern base of Red Mountain and Big Lava Bed, at the southern end of the fissure, are post-Fraser Glaciation. Their cinder deposits are layered

between the "Y" and "W" tephra deposits of Mount St. Helens, between 450 and 4000 years ago (Mullineaux, Hyde, and Rubin, 1972). West of the Indian Heaven fissure zone, lavas of Trout Creek Hill volcano are interstratified between till sheets of Salmon Springs and Fraser Glaciation. The volcano is, therefore between 25 000 and 35 000 years old. Waters (1973) states that the lava is older than 35 000 years old, beyond determination by the radiocarbon method. The West Crater flows, northwest of Trout Creek Hill, are interstratified with the "J" tephra deposit of Mount St. Helens and the "O" tephra deposit of Mount Mazama (Crater Lake, Oregon) and, therefore, are between 6600 and 8000 years old (Mullineaux, Hyde, and Rubin, 1972).

The structural pattern in the vicinity of the basaltic field is not well understood. The fissures and north-trending faults, in the area west of Mount Adams, are subparallel. Gravity data reveals that the north-northeast-trending fault northwest of Mount Adams continues south-southwestward beneath the Quaternary basalts along the eastern side of the Indian Heaven zone and dies out to the south. This fault may be the conduit for the Big Lava Bed flow (cross sections Nos. 2 and 3, Fig. 2). The trace of fold axes and distribution of the younger Tertiary formations, the Eagle Creek formation and Columbia River basalt, reveal the structural lows. Most folds trend northeastward. The northern end of the Indian Heaven fissure zone transects a broad shallow synclinal basin filled with the permeable Eagle Creek formation. The southern extent of strata of Council Bluff and the Eagle Creek formation in this syncline is not known (Fig. 2, cross section Nos. 2 and 3).

One anomalous feature in the field is Mann Butte, located between the two fissures, which consists of brecciated rhyolite. The butte appears to be the erosional remnant of a plug, possibly a protrusion dome. In surficial deposits at its north base can be found a white clay layer, derived from volcanic ash and pumice, sandwiched between the Salmon Springs and Fraser Glaciation till sheets. If the ash were derived from the dome during its eruptive emplacement, Mann Butte could be as young as late Pleistocene.

THERMAL SPRINGS

Several thermal springs are located about 15 to 30 km southwest of the field near the Columbia River (Fig. 1). They are Government Mineral Springs (Iron Mike, Bubbling Mike, and Little Iron Mike) and nearby Little Soda Springs (not shown on the map), located in the Wind River valley; St. Martin's Hot Springs, located near the mouth of the Wind River; Gray's Hot Spring, to the west in Rock Creek; and Moffett's (Bonneville) Hot Spring near Bonneville Dam. Descriptions and analyses of the springs are reported in Campbell and others (1970) and Gizienski, McEuen, and Birkhahn (1975). Their data is summarized in Table 2. The structural axis of the Cascade Range passes northward through the area of the springs.

The structural setting of each spring is not known. The springs at Gray's and St. Martin's have been observed bubbling through stream waters from what appear to be multiple fractures, very likely part of a fault zone, in the bedrock. Other springs are located in alluvium or landslide deposits (Moffett's).

The temperature of the springs ranges from a low of 8°C at little Soda Springs to a high of 49°C at St. Martin's Hot Springs. The pH is variable, ranging from 6.5 to 9.5; the waters tend to be alkaline, saline, and rich in sodium chloride. The discharge is low; only that at Moffetts, 75 liters per minute, is reported (Campbell et al., 1970). It is assumed that the springs represent mixed waters; the chemistry of the waters may be at disequilibrium with the enclosing rocks. The aquifer temperatures, using the geothermometry methods of the United States Geological Survey (Gizienski, McEuen, and Birkhahn, 1975), range from 69 to 120°C for silica, conductive cooling; 102 to 139°C for Na-K; and 31 to 106°C for 4/3 Ca. The range in temperatures for silica by conductive cooling is attributed to a possible 50% analytical error for silica composition (Campbell et al., 1970).

GRAVITY STUDIES

Gravity surveys of a large part of the area (Fig. 1) were performed by Konicek (1974,1975) and Stricklin (1975), graduate students under the supervision of Z. F. Daneš, at the University of Puget Sound, Tacoma, Washington. The results of their interpretation of the regional Bouguer gravity, at a density 2.67 g/cm^3, are plotted on the map. Additional data for the southern part of the map were obtained from Daneš (1973) and for the northwestern part from Bonini, Hughes, and Daneš (1974).

The main gravity feature is a well-defined gravity low of −100 mgal coinciding with the Indian Heaven fissure zone. It presents a problem: instead of a low it should be linear gravity high, as expected where basalt intrudes less dense sedimentary rocks. Especially perplexing is the position of the maximum low, exceeding −100 mgal, centered in the outlier of Columbia River basalt at Steamboat Mountain at the northern part of the fissure. Several models have been proposed to explain the relationship but none, taken separately, is considered satisfactory. The anomaly appears to be a combination of several interpretations: 1) a thickening of the Tertiary stratigraphic section, especially the Eagle Creek formation, within the synclinal low beneath the fissure zone, a condition similar to the gravity low in the southwestern part of the map; 2) fracturing and brecciation of the pre-Quaternary rocks beneath the fissure, thus reducing their density (however, this condition is not observable beneath the King Mountain zone); 3) the possible presence of a large hydrothermally altered zone beneath the fissure, another condition not evident at the King Mountain zone; and 4) the possible presence of a fairly shallow magma chamber, possibly 1 to 2 km, beneath this part of the fissure zone. The anomaly warrants further geophysical investigations in the evaluation of geothermal resources.

A steep gravity gradient lies along the eastern side of the Indian Heaven fissure zone. It is believed to represent a fault forming part of the fissure, with the east side having dropped down a maximum of 2 1/2 km (Stricklin, 1975). The terrain between the fissure zones has a poorly defined relative gravity high. The strongest high, of about 25 mgal, is reflected in the major northeast-trending anticline located between the Big Lava Bed and White Salmon River.

No gravity low occurs beneath the King Mountain fissure zone, as might be expected in the light of the condition at the Indian Heaven zone. However, there is neither a gravity high nor a low centered beneath Mount Adams. Possibly Quaternary and Columbia River basalts underlying the volcano compensate for a mass deficiency. A major

Table 2. Thermal springs near Quaternary basalt field, southern Cascade Range, Washington.

Feature	Springs: Moffetts	St. Martins	Iron Mike	Bubbling Mike	Little Iron Mike	Little Soda Springs
Elevation, m	24	37	378	377	377	330
T°C.	32	49	10	8.5	10	8
pH	9.5	7	7	6.5	6.5	6
Approx. discharge (liters per min.)	75	un	un	un	un	un
Composition (ppm)						
Li	nd	0.2	0.4	0.3	0.8	nd
Na	126	291	211	176	404	28
K	1.5	6.2	6.2	5.1	9.6	13.6
Ca	42	104	192	154	309	46
SiO_2	un	un	40	50	un	un
Cl	151	636	318	276	561	36
CO_3	nd	nd	un	un	un	nd
SO_4	un	un	un	un	un	nd
Aquifer T°C.						
SiO_2, conductive cooling	ud	ud	69–110	77–120	ud	ud
Na-K	102	125	139	138	129	ud
Na-K-1/3 or 4/3Ca	31	106	45	43	55	ud

un = unknown, nd = none detected, ud = undetermined.

east-west-trending low of −115 mgal occurs north of Mount Adams. It is not considered to be related to the King Mountain fissure zone. Instead it probably reflects part of a Mesozoic quartz diorite batholith forming the core of a large anticline of Columbia River basalt. The batholith, mapped north of the area shown in Figure 1 by Swanson (1964, 1967), is considered to underlie this part of the western edge of the Columbia Plateau.

A small residual gravity low of about 15 mgal lies just east of Government Springs. It may represent a thickened section, within a syncline, of volcanic sedimentary strata of the Ohanapecosh Formation.

Another gravity low, a trough deepening southward towards the Columbia River and exceeding 15 mgal, lies west of the Wind River and beneath West Crater, Trout Creek Hill volcano, and the area of thermal springs.

CONCLUSION

The pertinent geologic features with respect to potential geothermal resources in the Quaternary basalt field are summarized below:

1. A Quaternary basalt field, derived from two parallel north-trending fissures, called the Indian Heaven and King Mountain fissure zones, lying west and east respectively, occur between the Mounts St. Helens and Adams volcanoes. Indian Heaven fissure zone coincides approximately with the structural axis of the southern Cascade Range. King Mountain fissure zone passes beneath Mount Adams.
2. The fissure zones are younger than 690 000 years. Most lava flows are between 25 000 and 35 000 years old. The youngest volcanic deposits are in the cinder cone at the southern base of Red Mountain and the Big Lava Bed, located adjacent to the Indian Heaven fissure zone. They are between 450 and 4000 years old. Not all young volcanic activity occurs adjacent to the fissure zones. West Crater formed between 6600 and 8000 years ago. Consequently, basaltic volcanic activity appears to have occurred sporadically yet frequently within the field, providing evidence for an almost continual source of magmatic heat at shallow depth.
3. The interlayered basalt lavas and beds of fluvial deposits, scoria, and cinders constitute an extensive highly permeable stratigraphic section which contains a very large volume of ground water. This reservoir probably extends into the underlying permeable Tertiary strata which fill a shallow synclinal basin beneath the Indian heaven fissure zone.
4. A well-defined linear gravity low of 35 mgal coincides with the Indian Heaven fissure zone. This anomaly appears to have a combination of several possible geologic interpretations: a) a thickening of the Tertiary stratigraphic section within a syncline; b) fracturing and brecciation of the underlying pre-Quaternary rocks; c) the presence of a hydrothermally altered zone; and d) the presence of a shallow magma reservoir beneath the fissure zone.
5. No thermal springs are known to occur within or adjacent to the field. The nearest springs occur near the Columbia River 15 to 30 km southwest of the field, along the approximate structural axis of the range. Temperatures and discharge of the springs are low. Chemistry of the waters indicates aquifer temperatures below 140°C. The waters are considered to be mixed and diluted by abundant meteoric water, characteristic of the Cascade Range.

ACKNOWLEDGMENTS

The field studies were largely supported by the Washington Division of Geology and Earth Resources during the 1972, 1973, and 1974 field seasons. The Research Corporation, Burlingame, California, is thanked for its partial support of the gravity studies. J. E. Schuster, state geothermal geologist, coordinated the different efforts in this investigation. The participants are thanked for their contributions and free exchange of ideas to reach an understanding of the geology and gravimetry. The Department of Earth Sciences, Portland State University, is thanked for its financial support in preparing the report. Chris Thoms did the drafting of Figures 1 and 2. The senior author (Hammond) is grateful to J. E. Schuster, Z. F. Daneš, and R. E. Thoms for their critical review and improvement of the manuscript, and accepts full responsibility for the statements herein.

REFERENCES CITED

Allen, J. E., 1966, The Cascade Range volcano-tectonic depression of Oregon, p. 21-23, *in* Transactions of the Lunar Geological Field Conference, Bend, Ore.: Oregon Dept. Geology and Mineral Industries, 98 pp.

Bonini, W. E., Hughes, D. W., and Daneš, Z. F., 1974, Complete Bouguer gravity anomaly map of Washington: Washington Div. Geology and Earth Resources, Geologic Map GM-11.

Campbell, K. V., et al., 1970, A survey of thermal springs in Washington: Northwest Science, v. 44, no. 1, p. 1-11.

Crandell, D. R., 1965, Glacial history of western Washington and Oregon, *in* Wright, H. E., Jr., And Frey, D. G., eds., Quaternary of the United States: Princeton Univ. Press, Princeton, New Jersey, 922 p.

Crandell, D. R., and Mullineaux, D. R., 1973, Pine Creek volcanic assemblage at Mount St. Helens, Washington: U.S. Geol. Survey Bull. 1383-A, 23 pp.

Daneš, Z. F., 1973, Preliminary Bouguer gravity map, south of lat. 46° and east of long. 122°, southern Cascade Range, Washington: Washington Div. Geology and Earth Resources, Olympia, Washington, open-file report.

Fischer, J. F., 1971, The geology of the White River-Carbon Ridge area, Cedar Lake quadrangle, Cascade Mountains, Washington, 200 pp. [Ph.D. thesis]: Santa Barbara, Calif., Univ. of California.

Fiske, R. S., Hopson, C. A., and Waters, A. C., 1963, Geology of Mount Rainier National Park, Washington: U.S. Geol. Survey Prof. Paper 444, 93 pp.

Gizienski, S. F., McEuen, R. B., and Birkhahn, P. C., 1975, Regional evaluation of the geothermal resource potential in central Washington State: Washington Water Power Supply System, Richland, Washington, open-file report, 113 pp.

Grant, A. R., 1969, Chemical and physical controls for base metal deposition in the Cascade Range of Washington: Washington Div. Mines and Geol., Bull. 58, 107 pp.

Hammond, P. E., 1973, Quaternary basaltic volcanism in the southern Cascade Range, Washington: Geologic Soc. America, Abs. with Programs, v. 5, no. 1, p. 49.

——, 1974, Regional extent of the Stevens Ridge formation in the southern Cascade Range, Washington (abstract): Geol. Soc. America, Abs. with Programs, v. 6, no. 3, p. 188.

Harle, D. S., 1974, Geology of Babyshoe Ridge area, southern Cascades, Washington [M.S. Thesis]: Corvallis, Oregon, Oregon State University.

Hartman, D. A., 1973, Geology and low-grade metamorphism of the Greenwater River area, central Cascade Range, Washington, 100 pp. [Ph.D. thesis]: Seattle, Univ. of Washington.

Holmgren, D. A., 1969, Columbia River Basalt patterns from central Washington to northern Oregon, 55 pp. [Ph.D. thesis]: Seattle, University of Washington.

Hopkins, K. D., 1969, Late Quaternary glaciation and volcanism on the south slope of Mount Adams, Washington: Geol. Soc. America, Abs. with Programs for 1969, Pt. 3, p. 27.

Hopson, C. A., 1971, Eruptive sequence at Mount St. Helens, Washington: Geol. Soc. America Abs. with Programs, v. 3, no. 2, p. 138.

Kienle, C. F., Jr., and Newcomb, R. C., 1973, Geologic studies of Columbia River basalt structures and age of deformation, The Dalles-Umatilla region, Washington and Oregon: Portland, Shannon and Wilson, Inc., open file report, 55 p.

Konicek, D. L., 1974, Geophysical survey in south-central Washington, 35 pp. [M.S. thesis]: Tacoma, Univ. Puget Sound.

——, 1975, Geophysical survey in south central Washington: Northwest Science, v. 49, no. 2, p. 106-117.

Laursen, J. M., and Hammond, P. E., 1974, Summary of radiometric ages of Oregon and Washington rocks, through June 1972: Isochron/West, no. 9, 32 pp.

Mullineaux, D. R., Hyde, J. H., and Rubin, Meyer, 1972, Preliminary assessment of Upper Pleistocene and Holocene pumiceous tephra from Mount St. Helens, southern Washington: Geol. Soc. America Abs. with Programs, v. 4, no. 3, p. 204-205.

Newcomb, R. C., 1969, Effect of tectonic structure on the occurrence of ground water in the basalt of the Columbia River Group of The Dalles area, Oregon and Washington: U.S. Geol. Survey Prof. Paper 383-C, 33 pp.

Pedersen, S. A., 1973, Intraglacial volcanoes of the Crazy Hills area, northern Skamania County, Washington: Geol. Soc. America, Abs. with Programs, v. 5, no. 1, p. 89.

Sheppard, R. A., 1960, Petrology of the Simcoe Mountains area, Washington, 153 pp., [Ph.D. thesis]: Baltimore, The Johns Hopkins Univ.

——, 1962, Iddingsitization and recurrent crystallization of olivine in basalts from the Simcoe Mountains, Washington: Am. Jour. Sci., v. 260, no. 1, p. 67-74.

——, 1964, Geologic map of the Husum quadrangle, Washington: U.S. Geol. Survey Mineralogical Inv. Field Studies Maps, MF-280.

——, 1967a, Geology of the Simcoe Mountains volcanic area, Washington: Washington Div. Mines and Geology, Geol. Map, GM-3.

——, 1967b, Petrology of a late Quaternary potassium-rich andesite flow from Mount Adams, Washington: U.S. Geol. Survey Prof. Paper 575-C, p. C55-C59.

Stricklin, C. R., 1975, Geophysical survey of the Lemei Rock-Steamboat Mountain area, Washington, 23 pp. [M.S. thesis]: Tacoma, Univ. Puget Sound.

Swanson, D. A., 1964, The middle and late Cenozoic volcanic rocks of the Tieton River area, south-central Washington. 329 p. [Ph.D. thesis]: Baltimore, The Johns Hopkins Univ.

——, 1967, Yakima Basalt of the Tieton River area, south-central Washington: Geol. Soc. America Bull., v. 78, no. 9, p. 1077-1110.

Waters, A. C., 1973, The Columbia River Gorge: Basalt stratigraphy, ancient lava dams and landslide dams. p. 133-162, *in* Beaulieu, J. D., Geologic field trips in northern Oregon and southern Washington: Oregon Dept. Geology and Mineral Industries, Bull. 77, 206 pp.

Wise, W. S., 1959, Occurrence of wairakite in metamorphic rocks of the Pacific Northwest: Am. Mineralogist, v. 44, p. 1099-11-1.

——, 1961, Geology of the Wind River area, Skamania County, Washington, and the stability relations of celadonite, 258 pp. [Ph.D. thesis]: Baltimore, The Johns Hopkins Univ.

——, 1971, Cenozoic volcanism of the Cascade Mountains of southern Washington: Washington Div. Mines and Geology, Bull. 60, 45 pp.